Enantioseparation of Amino Acids by Micelle-Enhanced Ultrafiltration

Experimental and Theoretical Studies of Copper(II) Amino Acid Interactions

Promotor:

Dr. E. J. R. Sudhölter

Hoogleraar in de Fysisch-Organische Chemie

Co-promotoren:

Dr. A. T. M. Marcelis

Universitair docent, verbonden aan het Laboratorium voor Organische Chemie

Dr. H. Zuilhof

Universitair docent, verbonden aan het Laboratorium voor Organische Chemie

Enantioseparation of Amino Acids by Micelle-Enhanced Ultrafiltration

Experimental and Theoretical Studies of Copper(II) Amino Acid Interactions

Theodorus J. M. de Bruin

Proefschrift

ter verkrijging van de graad van doctor op gezag van de rector magnificus van Wageningen Universiteit, dr. C. M. Karssen, in het openbaar te verdedigen op woensdag 28 juni 2000 des namiddags te vier uur in de Aula.

The research described in this thesis has been performed in the Laboratory of Organic Chemistry, Wageningen University, The Netherlands, and was funded by the Dutch Technology Foundation (Contract Grant Number: WCH.3380), AKZO-Nobel and DSM.

ISBN 90-5808-240-7

Stellingen

1. De gemeten resolutie met een (D)-penicillamine ligand-exchange 5 cm HPLC kolom voor diverse enantiomere aminozuren geeft een goede indicatie voor de te meten operationele enantioselectiviteit van die aminozuren met MEUF.
   Dit proefschrift.

2. De parametrisatie van Cu^{II}-complexen voor moleculaire mechanica berekeningen leidt, in tegenstelling tot de situatie voor Cu^{I}-complexen, tot grote problemen.
   F. Hæffner, T. Brinck, M. Haeberlein, C. Moberg, *J. Mol. Struct. (Theochem)* **1997**, *397*, 39-50.
   Dit proefschrift.

3. Het door Bérces *et al.* berekende energieverschil tussen equatoriale en axiale binding van watermoleculen aan het Cu^{II} ion is te hoog.
   A. Bérces, T. Nukada, P. Margl, T. Ziegler, *J. Phys. Chem. A* **1999**, *103*, 9693-9701.

4. De ene basisset is de andere niet.
   A. C. Scheiner, J. Baker, J. W. Andzelm, *J. Comp. Chem.* **1997**, *18*, 775-795. Dit proefschrift.

5. De toekenning door George en Das van de smectisch A vloeibaar kristallijne fase van hun verbindingen waarin azobenzeen is gekoppeld aan cholesterol is onjuist.
   M. George, S. Das, *Chem. Lett.* **1999**, 1081-1082.

6. De bandbreedte voor elektronisch dataverkeer is voorlopig niet breed genoeg.

7. De beslissing van de stichting Collectieve Propaganda voor het Nederlandse Boek om het boekenweekgeschenk voor 2001 te betrekken van de Engelstalige auteur Salman Rushdie is paradoxaal.
   NRC Handelsblad, 22 april 2000.

8. De muziek van de (joodse) Oostenrijker Mahler leent zich eigenlijk beter voor achtergrondmuziek in documentaires over de Tweede Wereldoorlog dan de daarvoor veel vaker gebruikte muziek van de Duitser Wagner.

9. Gezien het toenemende aantal RSI klachten zou het instellen van een keur- of kwaliteitsmerk voor muizen en toetsenborden een goede zaak zijn.

Stellingen behorende bij het proefschrift:

Enantioseparation of Amino Acids by Micelle-Enhanced Ultrafiltration. Experimental and Theoretical Studies of Copper(II) Amino Acid Interactions

Wageningen, 28 juni 2000 — Theodorus J. M. de Bruin

Voorwoord

Voor u ligt het resultaat van ruim 4 jaar promotieonderzoek. Dit onderzoek heb ik natuurlijk niet alleen uitgevoerd, en bij deze wil ik een ieder bedanken die op zijn of haar wijze een steentje heeft bijgedragen. Een aantal mensen wil ik echter graag even bij naam noemen.

Allereerst wil ik mijn promotor Prof. dr. E. J. R. Sudhölter bedanken. Beste Ernst, de mogelijkheid om dit onderzoek uit te voeren en jouw stimulans waren van groot belang voor de totstandkoming van dit proefschrift.

Daarnaast wil ik mijn beide co-promotoren Dr. A. T. M. Marcelis en Dr. H. Zuilhof bedanken. Beste Ton, Ave Han, ik heb met jullie beide op een hele prettige manier samengewerkt. Vrijwel altijd kon ik bij jullie binnenlopen voor uitleg, tips en suggesties. En natuurlijk ben ik jullie ook dankbaar voor het razendsnel en kritisch corrigeren van de diverse manuscripten.

Pieter Overdevest, Albert van der Padt, Klaas van 't Riet en Remko Boom van de Sectie Proceskunde wil ik bedanken voor de vele waardevolle discussies, de gebruikmaking van diverse apparatuur, *etc.*, wat allemaal van groot belang voor dit onderzoek is geweest. Pieter, jou wil ik speciaal bedanken, omdat ik altijd bij jou terecht kon wanneer ik je nodig had.

Mijn beide studenten, Lisette Rodenburg en Jules Roelofs, wil ik bedanken voor hun inzet en hulp. Van het werk dat jullie hebben verricht is, in expliciete zin, niet zo veel terug te vinden in dit boekje. Desalniettemin, wat jullie gesynthetiseerd en gemeten hebben, is van groot belang geweest voor het gehele onderzoek waar ik jullie erg dankbaar voor ben.

Arie Koudijs wil ik ook graag even een aparte vermelding geven. Hoewel er in dit boekje niet zo veel syntheses zijn beschreven, waren jouw tips & trucs op dit gebied vaak hard nodig; bedankt hiervoor!

Frank Vergeldt ben ik veel dank verschuldigd voor de vele "kleine" unix probleempjes die moesten worden opgelost en de compilaties die altijd even snel tussendoor gedaan moesten worden. Ook Robert Schrijvers en Jasper Aukes wil ik bedanken voor de gebruikmaking van hun unix-kennis.

I would like to thank Dr. U. Ryde and Ms. E. Sigfridsson for the fruitful discussions concerning the calculation of ESP-charges.

Ten aanzien van de diverse analyses wil ik Elbert van der Klift, Beb van Veldhuizen, Hugo Jongejan en Rien van Dijk en in het bijzonder Harm Niederländer bedanken; Ronald de Bruin

en Pleun van Lelieveld voor de chemicaliënvoorziening; en de dames van het secretariaat (incl. Ien!) wil ik bedanken voor alle administratieve zaken.
De leden van STW-begeleidingscommissie en ook de leden van de promotiecommissie: Prof. dr. W. J. Briels, Prof. dr. Æ. de Groot en Prof. dr. J. Reedijk wil ik bedanken voor hun inzet en hun geleverde inspanningen.
Alle collega (ex-)AIO/OIO's, post-docs, alle andere (wetenschappelijke) medewerkers, en mijn kamergenoten: Robert Schrijvers, Alex Sieval en Herman Verheij wil ik bedanken voor de goede tijd. De mensen die geregeld de Loburg-borrels bijwoonden, Dennis, Gert Jan, Frans, Henk, Jan, Tommi, Marcel, Cindy, Peter en Matthew en alle anderen, jullie waren een goede uitlaatklep na een week hard werken.
Steven Rijsdijk en Michel Verhoef. Ik wil jullie bedanken voor het feit dat jullie mijn paranimfen willen zijn, voor jullie steun en jullie belangstelling in mij en mijn onderzoek.
Mijn familie, met name mijn ouders, Ton & Yvonne, en Jacqueline & Hugo. Bedankt voor jullie onvoorwaardelijke steun, hoewel jullie niet altijd hebben begrepen waar ik nou precies mee bezig was. Lieve Papa & Mama, zonder jullie was dit boekje er zelfs nooit gekomen. Jullie voortdurende stimulans, vertrouwen en vrijheid die ik heb gekregen, zijn van onschatbare waarde.
Als laatste wil ik Béatrice bedanken. Ma chère Béa, je veux te dire que je veux être pour toi la personne que tu as été pour moi l'année dernière, donc tu comprendras ce que tu signifies pour moi. Merci pour ton amour, pour ta confiance, pour tout.

Theo de Bruin

Contents

Voor mijn ouders

en Béa

Chapter

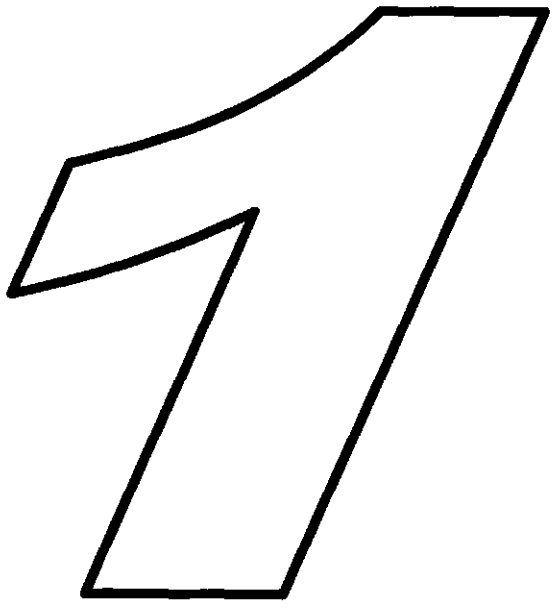

General Introduction

1.1 Introduction

The part of chemistry that deals with structure in three dimensions is called stereochemistry. An important aspect of stereochemistry is that stereoisomers have the same atomic connectivity but differ in the way the atoms are oriented in space. The history of stereochemical aspects in organic chemistry starts at the beginning of the 19th century, when Biot performed some polarized light experiments.[1,2] In 1848 Pasteur discovered that sodium ammonium tartrate can be separated in two types of crystals.[3] Each type had properties identical to tartaric acid (density, melting point, solubility, *etc.*) except that one of the components rotated the polarized light clockwise, while the other component rotated the polarized light by the same amount counterclockwise. The two forms of tartaric acid that Pasteur found were enantiomers, *i.e.*, non-superimposable mirror image structures.

Although enantiomers possess identical physical properties – except for the direction of rotation of polarized light – they can exhibit distinct chemical behavior when subjected to a chiral environment. Many pharmaceuticals, flavor compounds and agrochemicals are chiral compounds and their physiological or biological activity is often only caused by one of the two enantiomers. Consequently, use of only the enantiomer with the correct activity is preferred, since the other one can either have no effect, undesired effects or even harmful effects.

In 1992, the US Food & Drug Administration (FDA) issued guidelines for the development of chiral drugs.[4] Drug companies worldwide have taken these guidelines seriously, and at present, most research departments study the pharmaceutical properties of both isomers separately. Furthermore, methods needed to be developed to obtain both isomers in an enantio-pure form. Table 1-I shows some figures about single-isomer chiral drugs sales in 1997 and 1998. It is expected that the worldwide annual sales of enantiomeric drugs surpasses the € 100 billion mark in the year 2000![5]

The most obvious source for optically pure compounds is the chiral pool.[6] The chiral pool customarily refers to relatively inexpensive and readily available optically active natural products, however, the largely unrecognized and unexploited source of new optically active materials should be included as well.[7] Unfortunately, the number of readily available compounds in this pool is limited, and in order to obtain the desired compounds, stereoselective synthetic methods need to be applied. Synthesis of racemic mixtures using racemic or non-chiral substrates – which are often much less expensive – followed by a chiral resolution, is often a good alternative. In fact, the dominant method to produce chiral compounds during multistep syntheses remains resolution of racemates.[5]

Table 1-I. Chiral drug sales surge (in € millions).[5]

	1997	1998	Annual change
Antibiotics	21,031	23,250	11%
Cardiovascular	19,551	21,145	8%
Hormones	9,903	11,585	17%
Central nervous system	7,573	7,805	3%
Cancer	6,913	7,605	10%
Antiviral	4,893	6,220	27%
Hematology	5,923	6,185	4%
Respiratory	3,159	4,255	35%
Gastrointestinal	1,314	1,420	8%
Other	6,535	6,910	6%
TOTAL	**86,795**	**96,380**	**11%**

Resolution can also be accomplished by enzymatic methods, but in many cases an appropriate route has to be developed for each compound due to substrate specificity, which can lead to considerable costs and increased development time.[8] If there is a market for both enantiomers, or if multi-step asymmetric syntheses result in very low yields, the symmetric synthesis followed by a separation step becomes a more attractive route. Furthermore, resolution provides both enantiomers, and both can be used for study as a part of satisfying the FDA regulations on the properties of each, even if only one is developed as a drug.[5] The separation of enantiomers is, however, not straightforward, since the physical properties of a pair of enantiomers only differ in chiral media. Although numerous techniques are available for the resolution of racemic mixtures on an analytical scale, the conventional method for large-scale production is frequently a batchwise operation based on fractional crystallization, kinetic enzymatic resolution technology, or a microbiological method.[9,10] Due to the generally low enantioselectivities, multiprocessing is needed, which is relatively inflexible[11] and can also lead to significant product losses.

An alternative process makes use of membranes in order to accomplish resolution. Membrane separations can be continuously operated at ambient temperatures. This, in combination with an easy scale-up, makes membrane separations attractive and cost-efficient. Two types of membrane processes for enantiomer separations are often employed: (a) separations with enantioselective membranes and (b) separations with non-chiral membranes. Examples of the first type are membranes containing proteins,[12,13] chiral polymers,[14,15]

molecularly imprinted membranes,[9,16-18] or emulsion liquid membranes.[19-21] In the separations with non-chiral membranes, the membranes are only used to retain one phase, or two (im)miscible phases of which at least one is enantioselective.[11,22] For example, Kellner *et al.* have performed liquid-liquid extractions to study the enantioselective transport of chiral *N*-protected amino acids derivatives from an aqueous solution into an organic phase employing highly lipophilic carbamoylated quinine as chiral selector and phase transfer carrier.

1.2 Micelle-Enhanced Ultrafiltration

Another example of separations with non-chiral membranes is the concept of Micelle-Enhanced UltraFiltration (MEUF). In MEUF the pore size of the membrane is small enough to reject micelles, but large enough to allow all other low-weight monomers to pass. After filtration, the retentate is enriched with the micelles including the compounds that are solubilized in the micelles (Figure 1.1).

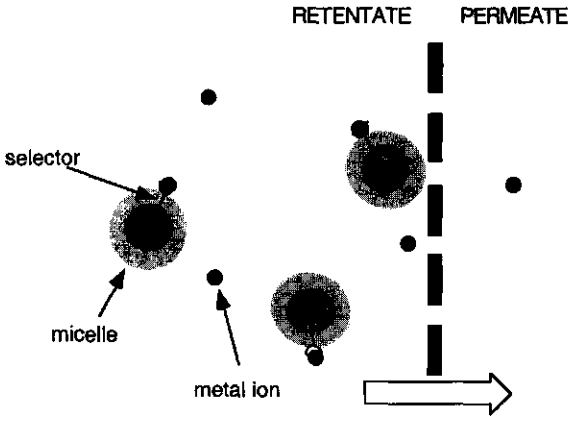

Figure 1.1 Schematic representation of the Micelle-Enhanced UltraFiltration (MEUF) system to selectively separate metal ions (see text).

Depending on the affinity of a compound for the micelle, compounds can be separated from aqueous streams. MEUF can be used for the separation of (small) organic compounds from aqueous waste water streams,[23-26] *e.g.*, phenols[27] and 1-naphthol.[28] Sometimes a complexing agent is added to the micelle to improve the affinity, or to selectively remove a

metal ion such as Cu^{II} (Figure 1.2).[29-32] Other examples include Co^{II}, Ni^{II} and Au^{III},[33] and U^{VI}.[34]

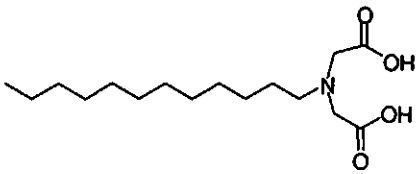

Figure 1.2. *N*-n-dodecyl iminodiacetic acid used to specially bind Cu^{II} ions.[32]

The possibilities of the application of MEUF can be extended by the use of chiral selectors that selectively bind one of the enantiomers present in the aqueous bulk and thus MEUF can be used to separate racemic mixtures. In 1996 Creagh *et al.* were the first to successfully apply MEUF for the separation of enantiomers.[35] They obtained an operational enantioselectivity of 4.2 for the separation of the enantiomers of the amino acid phenylalanine with cholesteryl glutamate as a chiral selector.

The operational enantioselectivity (α_{op}) was defined as the distribution of the D-enantiomer over micellar phase and bulk, divided by the distribution of the L-enantiomer.

$$\alpha_{op} = \frac{D_D}{D_L} = \frac{C_D^{micelle} / C_D^{bulk}}{C_L^{micelle} / C_L^{bulk}} \qquad (1\text{-}1)$$

The study of Creagh *et al.* provoked a number of detailed mechanistic and process-related questions: can the applied selector be used for the separation of other amino acids? What is the effect of the chiral glutamate headgroup and the chiral cholesteryl part on the enantioselectivity? How does the chiral recognition precisely take place? Is there an influence on the enantioselectivity of the microhetereogeneous medium (in this case the micelles)? Is the process applicable on an industrial scale, *etc.*? The research described in this dissertation tries to answer some of these questions.

1.2.1 Components of the Micelle-Enhanced Ultrafiltration system

i) Chiral selector. In the MEUF system chiral recognition must occur via the chirality in the micelles. This can be accomplished either by the use of chiral surfactants only,[36,37] or by use of a non-chiral surfactant in which the chiral selector is solubilized. In the latter case, the selector preferentially needs to have an amphiphilic character, whereas in the first case the

selector also has to have the property to self-assembly into micelles or vesicles. The use of a non-selective surfactant thus puts fewer restrictions on the choice of the selector. Creagh *et al.* have used cholesteryl L-glutamate as chiral selector (Figure 1.3), and since this selector fails to form micelles spontaneously a co-surfactant was needed. The combination of an amino acid derivative and Cu^{II} ions as a chiral selector shows a large resemblance with Chiral Ligand Exchange Chromatography (CLEC). CLEC is probably the most widely used technique for the separation for α-amino acids and α-hydroxy acids.[38] However, CLEC is an HPLC technique that is only used on an analytical or on a small preparative scale that is difficult and costly to scale up, whereas MEUF has the potential to be applied on a large, industrial scale.

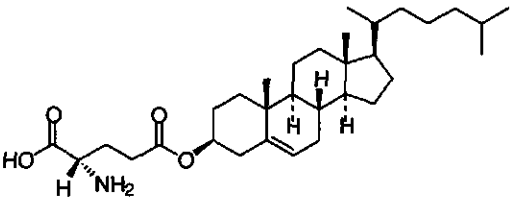

Figure 1.3. Cholesteryl L-glutamate.

CLEC is based on the reversible formation of diastereomeric complexes between metal ions, and chiral ligands either in the stationary or in the mobile phases. The major requirement for complex-forming ions in ligand-exchange chromatography is the formation of kinetically labile sorption complexes. This requirement is satisfied by many metal ions including Fe^{II}, Co^{II}, Ni^{II}, Cu^{II}, Zn^{II}, and Cd^{II}.[39] For the separations of amino acids and derivatives frequently Cu^{II} ions are used,[21,40-50] since Cu^{II} ions yield the most stable complexes of the first row transition metal ions.[51-53] In principle, each chiral selector that is used for chiral separations in HPLC can be implemented in the MEUF system.

ii) Substrate. α-Amino acids are involved in many important biological processes and find numerous applications in pharmaceutical and food industries. Their biological activity is strictly related to the absolute configuration. The less abundant D-amino acids[1] are of growing importance. For example, replacement of an L-amino acid by its mirror image in an enzyme or receptor binding agent may provide a required inhibitory, or antagonist activity.

[1] The word 'unnatural' is not appropriate, since D-amino acids occur in bacteria. Furthermore, it was recently found that D-serine is synthesized in mammals' brains and acts as there as a neurotransmitter (H. Wolosker, S. Blackshaw, S. H. Snyder, *Proc. Natl. Acad. Sci. USA* **1999**, *96*, 13409-13414).

Alternatively, D-amino acids may improve properties such as resistance to metabolic degradation, may themselves be versatile synthetic intermediates, or have potential use as chiral auxiliaries.[7,54]

iii) Microheterogeneous medium. Although the name "micelle-enhanced ultrafiltration" (MEUF) suggests that only micelles can be used, also other molecular aggregates can be applied as long as the aggregates or molecules are larger in size than the pore-diameter of the membrane. Thus, apart from micelles and polymerized micelles,[55] also vesicles,[56,57] dendrimers,[58,59] polymers, *etc.* can be used. However the applicability of the MEUF system on an industrial scale can become limited if the microhetereogeneous medium is relatively expensive, such as some of the above-mentioned aggregates. Surfactants that are cheap, readily available and biodegradable are much more preferred.

Surfactants can be divided into two classes: surfactants without charge (non-ionic), and charged surfactants (cationic, anionic or zwitterionic). The non-ionic surfactants have two important advantages in the MEUF system since they generally have a lower critical micelle concentration than charged surfactants,[60] and thus the loss of surfactant after each filtration step is smaller. Secondly, non-ionic surfactants have no electrostatic charge-charge interactions with the charged chiral selector, substrate or chelating Cu^{II} ion. Therefore, only non-ionic surfactants have been used in this research.

1.3 Techniques used to investigate diastereomeric complex formation

Knowledge of the properties and the behavior of the diastereomeric complex is essential to optimize the separation process. In this case, the diastereomeric complex is formed by an amino acid derivative (selector), a Cu^{II} ion, and one of the enantiomers of the racemic amino acid. Cu^{II} ions generally yield the best enantioselectivities as compared to other transition metal ions. However, a complicating property of Cu^{II} is the tendency to change its coordination upon changing the nature or size of its ligand. A wide variety of coordination complexes for this metal ion has been observed: the coordination number can vary from 2 to 7,[61] and even for a given coordination number the geometry is variable.[62] This so-called plasticity of the Cu^{II} ion makes it difficult to build a theoretical model to explain the observed enantioselectivities. Davankov and Rogozhin have set up a theoretical model for the key process leading to enantiomeric separation of α-amino acids with CLEC.[63-65] In this model, apart from the chiral interactions between the (racemic) amino acid, Cu^{II} ion and chiral

selector, the interactions of either the hydrophobic or hydrophilic stationary phase also play an important role. In many cases the order of elution of the enantiomer is predicted rather well,[66,67] although exceptions have also been reported.[68] Taking into account that in micelles both hydrophobic and hydrophilic regions are present, it becomes difficult to transfer the model of Davankov and Rogozhin to the MEUF system. Therefore, the formation of diastereomeric complexes is studied from an experimental point of view using isothermal titration calorimetry, and from a theoretical approach applying sophisticated quantum mechanical methods.

1.3.1 Isothermal Titration Calorimetry

The thermodynamics of the formation of the diastereomeric complex is an important parameter to investigate. Isothermal titration calorimetry (ITC) is a sensitive technique to investigate the thermodynamics of several kinds of processes. This technique has been used to obtain information about changes in Gibbs free energy (ΔG), enthalpy (ΔH) and entropy (ΔS) of reactions such as the binding between enzyme and substrate,[69-73] other host-guest complexation reactions,[74,75] the binding of ions,[76-78] critical micelle concentrations,[79,80] or the interaction of solutes with vesicles.[81-85] Furthermore, ITC experiments have been used to investigate stereoselectivity aspects of mixed-ligand complexes with Cu^{II} and histidine.[86,87] With ITC the most important thermodynamic data of the complexation reaction of each enantiomer to the chiral metal complex can be obtained: the stoichiometry (n), the binding constant (K), ΔG, ΔH and ΔS. Consequently, ITC cannot only give additional information on the binding of the amino acid to the selector, but can also be used as a tool to quickly measure enantioselectivities, since the enantioselectivity can be expressed as the ratio of the equilibrium constants (K_D/K_L).

The titration microcalorimeter used in this research consists of two identical coin-shaped cells that are enclosed in an adiabatic jacket: a reference cell and a sample cell (Figure 1.4).[88] During an experiment the reference cell is heated by a very small constant power, the reference offset. The temperature difference between the two cells is constantly measured and a proportional power is increased or reduced to the sample cell by the cell feedback system to minimize the temperature difference.

An injection that results in the evolution of heat within the sample cell causes a peak downward in the cell feedback power, since the heat evolved provides heat that the cell feedback no longer has to supply. The opposite is true for endothermic reactions. Since the

cell feedback has units of power ($\mu cal \cdot s^{-1}$), integration of this signal over time yields the overall change in thermal energy.

From the heat evolved or absorbed of a chemical reaction, the molar heat of binding ($\Delta H°$), binding constant K, and the stoichiometry (n) of the reaction can be determined.[89] From these data, ΔG and ΔS can be calculated.

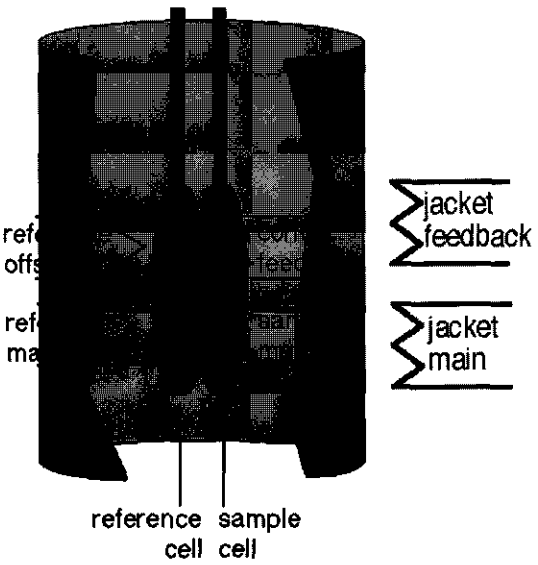

Figure 1.4. Schematic representation of an isothermal titration calorimeter.

1.3.2 Theoretical approach

In order to gain a better understanding of the geometry and the electronic structure of the Cu^{II} complexes formed between substrate and selector, an accurate model is needed to quantitatively describe the interactions between Cu^{II} and (amino acid) ligands. With such a model a better understanding can be obtained of the interactions that play a significant role in the chiral recognition process (Figure 1.5).

Experimental techniques can be used to obtain information about the geometry around bis(amino acid)Cu^{II} complexes, but these techniques can have some serious disadvantages. For example, recently an X-ray absorption study was performed on Cu^{II}-glycinate complexes in aqueous solutions, but the applied EXAFS technique could not give conclusive information whether the *cis* or *trans* isomers of the bis(glycinato)$Cu^{II} \cdot 2\ H_2O$ complex was present.[90]

Computational approaches provide an attractive alternative to obtain information about the geometry and electronic structures of such Cu^{II} systems.[91-98]

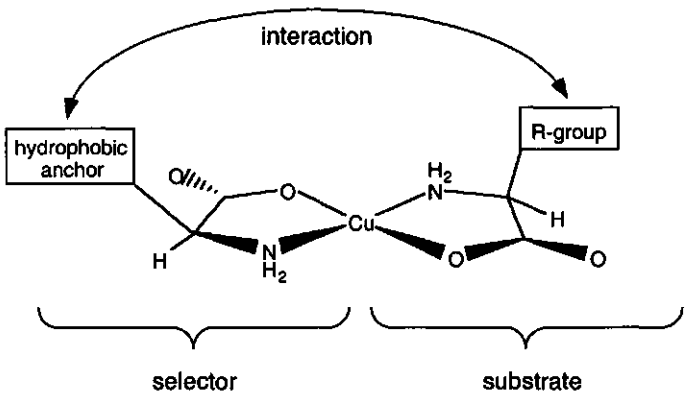

Figure 1.5. *Schematic description of the proposed formed ternary diastereomeric complex.*

To describe large transition metal complexes, molecular mechanics is an appealing tool, since it is relatively fast and numerous force fields for transition metal complexes have therefore been developed.[99-105] However, the number of investigations on Cu^{II} amino acid complexes is surprisingly small.[106] This is due to the problem of deriving a set of parameters to accurately describe the wide variety of experimentally observed Cu^{II} complexes. This is exemplified by the increasing amounts of X-ray and quantum mechanical data that are used for the parameterizations to describe the relatively small bis(amino acid)Cu^{II} complexes.[107] Important features that are difficult to describe with empirical methods are: (i) the wide variety of copper coordination geometries, (ii) the facile ligand exchange, and (iii) the accommodation of electronic effects (*e.g.*, *trans* and *cis* configurations, Jahn-Teller distortions).[108]

To avoid the problems related to the description of Cu^{II} ions with molecular mechanics, the only alternative seems to be the use of *ab initio* methods. However, a complete diastereomeric complex is at present too large to be routinely described by quantum mechanical methods, and a simplification is therefore needed. Bis(glycinato)Cu^{II} is a good model since it can give insight in the geometrical and electronic features of the diastereomeric complexes, and its size – *i.e.*, the number of electrons – allows the use of methods in which the electron correlation is sufficiently well described.

The quality of the quantum mechanical computation is mainly determined by two factors: the method to account for electron correlation and the basis set. There are several levels of theory

for electron correlation. From the 'basic' Hartree Fock theory, through Møller-Plesset (MP)[109] perturbation series (*e.g.*, MP2[110] or MP4[111]) to configuration interactions methods such as QCISD(T) and CCSD(T)[112] and Full CI.[112,113] An impression of the quality of these methods and their computational costs is given in Figure 1.6. Another method, based on density functional theory[2] (DFT) has gained much in popularity.[114] Functionals like Becke's three-parameter hybrid exchange functional (B3)[115] in combination with the correlation functional of Lee-Yang-Parr (LYP),[116] known as the B3LYP functional, achieve significantly much better results than the Hartree-Fock theory at only a modest increase in cost.

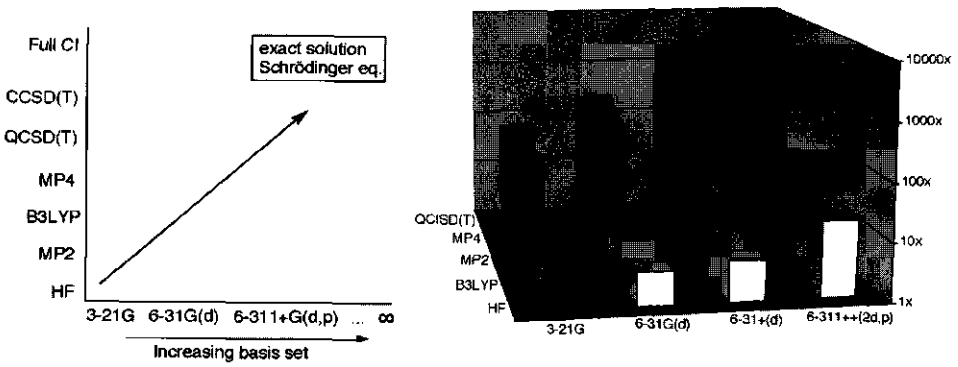

Figure 1.6. Qualitative comparison of several theories to account for electron correlation (left). Relative comparison computation time of several electron correlation methods and different basis sets (computation time of HF/3-21G set to 1.0; note that the vertical scale is logarithmic (right)).[117]

The practical use of DFT is relatively new. Although DFT methods are often superior to Hartree-Fock results when compared to experimental values for the main group compounds,[115,118,119] the question must be raised whether DFT methods are likewise suitable for transition metal systems. These systems are more complex and often have an open-shell electronic structure, *i.e.*, they have an unpaired electron. Therefore, several studies have lately been reported in which DFT methods were compared with other methods, and it was found that DFT calculations generally give better and more reliable descriptions of geometries and relative energies for transition metal systems than either HF or MP2 methods.[91,120-128]

Another important factor that determines the accuracy of a quantum mechanical calculation is the basis set[3] that is used in combination with the method to calculate the electronic

[2] For a brief historical overview and description of density functional theory see Chapter 4, Appendix I.
[3] For a brief description of basis sets see Chapter 4, Appendix II.

correlation. If a very accurate method for electron correlation is chosen in combination with a basis set that is too small, the results of the calculations will be unreliable. On the other hand, if the basis set is very large, but the method is poor, the quality of the results of the computation will be limited as well. Moreover, the size of the basis set required for precise calculations can differ from system to system. For example, anions and electronegative elements generally need larger basis sets than electropositive elements. From Figure 1.6 it can be seen that also the size of the basis set has a large influence on the overall CPU-time. Consequently, it is important to find the right balance between accuracy and computation time.

Although the B3LYP functional has proven to be an accurate method for transition metal complexes, there is less clarity which basis set should be used to describe systems like bis(glycinato)Cu^{II}. Therefore, first a basis set study is required before a comparative study of the geometric and electronic structures of such complexes can be performed.

1.4 Process Engineering Aspects

As mentioned before, MEUF has the potential to be used on a large scale and to be competitive with other separation processes, since it can be operated continuously at ambient temperatures. Moreover, MEUF opens up the possibility to perform continuous multi-step or multi-stage cascaded separations, if the efficiency of one separation step is not sufficient to reach a 99+% purity of the desired enantiomer. A successful application of the MEUF system in large scale chiral separation is determined by a number of factors: (i) is it possible to linearly scale up from laboratory to pilot plant scale; (ii) if the efficiency of a separation of an enantiomer is low, how many additional separation steps are needed to obtain the desired purity. In other words is it possible to develop a multi-stage process, in which the number of stages is minimized, *e.g.*, by using counter-current flows. Additionally, is it possible to build a model that describes the concentrations of the enantiomer in each separation step, and thus can predict how many stages are needed for the separation of a certain compound with a given operational enantioselectivity; (iii) is it possible to regenerate the chiral selector after a separation step, for the next separation step. Related to this problem is the decomplexation of the (desired) enantiomer from the chiral selector.

These and other factors concerning the scale-up of the MEUF system from a laboratory to a pilot plant scale have been investigated by Overdevest,[129] who worked as a Ph.D. student on the same project but with a process engineering point of view.

1.5 Scope of this thesis

The aim of the research described in this thesis is to investigate the interactions that take place between amino acids and Cu^{II} ions relevant to chiral separations, and to obtain a better understanding of the parameters that are of importance to improve the separation capability of the MEUF system. Chapter 2 describes the synthesis of the chiral selectors that are used in the MEUF system to systematically investigate the influence of the chiral selectors on the operational enantioselectivity. Furthermore, it describes the results of the MEUF experiments in which cholesteryl L-glutamate is applied for the separation of the enantiomers of several amino acids. In Chapter 3 the formation of the diastereomeric complex is approached from a thermodynamic point of view. It describes isothermal titration calorimetry experiments in which several amino acids are titrated to cholesteryl L-glutamate, and phenylalanine is titrated to several chiral selectors. The measured enantioselectivities with ITC are compared to those found with MEUF. In the second part of the thesis, Chapters 4 and 5, the diastereomeric complex is approached from a theoretical point of view. In Chapter 4 first an extensive basis set study is performed to find out which basis set gives the best accuracy/efficiency ratio to describe bis(amino acid)Cu^{II} complexes in combination with the B3LYP density functional. For that purpose the model compound bis(glycinato)$Cu^{II}\cdot 2\ H_2O$ was used. In the second theoretical chapter, Chapter 5, the basis set that was found to be the best according to the criteria set in the previous chapter is applied to investigate the *cis* and *trans* isomerism of bis(glycinato)Cu^{II} complexes and the preferential sites of complexation of coordinating water molecules. Of these complexes both the geometric and electronic structure were investigated, to find out whether it is possible to derive a set of atomic charges that can be used for the parameterization in molecular mechanics and molecular dynamics calculations. In the concluding Chapter 6, the results of this research are discussed, and recommendations are given for further investigations.

References

[1] J. B. Biot, *Bull. Soc. Philomath. Paris* **1815**, 190.

[2] E. L. Eliel, S. H. Wilen, L. N. Mander. In *Stereochemistry of Organic Compounds*; J. Wiley & Sons: New York, 1994, pp 2.

[3] L. Pasteur, *Ann. Chim. Phys.* **1842**, *24*, 442.

[4] *Chirality* **1992**, *4*, 338-340.

[5] S. C. Stinson, *Chemical & Engineering News* **1999**, *77(41)*, October 11, 101-120.

[6] R. A. Sheldon. In *Chirotechnology: Industrial Synthesis of Optically Active Compounds*; Marcel Dekker: New York, 1993, pp 143-171.

[7] J. Crosby, *Tetrahedron* **1991**, *47*, 4789-4846.

[8] J. T. F. Keurentjes, L. J. W. M. Nabuurs, E. A. Vegter, *J. Membr. Sci.* **1996**, *113*, 351-360.

[9] M. Yoshikawa, J.-i. Izumi, T. Kitao, S. Sakamoto, *Macromolecules* **1996**, *29*, 8197-8203.

[10] J. T. F. Keurentjes, F. J. M. Voermans. Membrane Separations in the Production of Optically Pure Compounds. In *Chirality in Industry II: Developments in the Commercial Manufacture and Applications of Optically Active Compounds*; A. N. Collins, G. N. Sheldrake, J. Crosby, Eds.; J. Wiley & Sons: Chichester, 1997; pp 157-180.

[11] P. E. M. Overdevest, J. T. F. Keurentjes, A. Van der Padt, K. Van 't Riet. Resolution of Enantiomers Using Enantioselective Micelles in Ultrafiltration Systems. In *Surfactant-Based Separations: Science and Technology*; J. F. Scamehorn, J. H. Harwell, Eds.; Oxford University Press: Washington, D.C., 1999; pp 123-138.

[12] A. Higuchi, T. Hashimoto, M. Yonehara, N. Kubota, K. Watanabe, S. Uemiya, T. Kojima, M. Hara, *J. Membr. Sci.* **1997**, *130*, 31-39.

[13] B. B. Lakshmi, C. R. Martin, *Nature* **1997**, *388*, 758-760.

[14] T. Aoki, M. Ohshima, K. I. Shinohara, T. Kaneko, E. Oikawa, *Polymer* **1997**, *38*, 235-238.

[15] S. Tone, T. Masawaki, K. Eguchi, *J. Membr. Sci.* **1996**, *118*, 31-40.

[16] M. Yoshikawa, J. I. Izumi, T. Kitao, *Polym. J.* **1997**, *29*, 205-210.

[17] C. J. Allender, K. R. Brain, C. M. Heard, *Chirality* **1997**, *9*, 233-237.

[18] A. Dzgoev, K. Haupt, *Chirality* **1999**, *11*, 465-469.

[19] P. J. Pickering, J. B. Chaudhuri, *J. Membr. Sci.* **1997**, *127*, 115-130.

[20] P. J. Pickering, J. B. Chaudhuri, *Chirality* **1997**, *9*, 261-267.

[21] P. J. Pickering, J. B. Chaudhuri, *Chirality* **1999**, *11*, 241-248.

[22] K.-H. Kellner, A. Blasch, H. Chmiel, M. Lämmerhofer, W. Lindner, *Chirality* **1997**, *9*, 268-273.

[23] R. O. Dunn, J. F. Scamehorn, S. D. Christian, *Sep. Sci. Technol.* **1985**, *20*, 257-284.

[24] P. J. M. Lebens, J. T. F. Keurentjes, *Ind. Eng. Chem. Res.* **1996**, *35*, 3415-3421.

[25] J. F. Scamehorn, S. D. Christian, R. T. Ellington. Surfactant-Based Separation Processes. In *Surfactant Science Series*; J. F. Scamehorn, J. H. Harwell, Eds.; Marcel Dekker: New York, 1989; Vol. 33.

[26] M. Abe, Y. Kondo, *Chemtech* **1999**, *29(3)*, March, 33-42.

[27] H. Adamczak, K. Materna, R. Urbanski, J. Szymanowski, *J. Colloid Interface Sci.* **1999**, *218*, 359-368.

[28] Y. K. Choi, S. B. Lee, D. J. Lee, Y. Ishigami, T. Kajiuchi, *J. Membr. Sci.* **1998**, *148*, 185-194.

[29] C. Tondre, M. Hebrant, M. Perdicakis, J. Bessiere, *Langmuir* **1997**, *13*, 1446-1450.

[30] B. R. Fillipi, J. F. Scamehorn, S. D. Christian, R. W. Taylor, *J. Membr. Sci.* **1998**, *145*, 27-44.

[31] M. Hebrant, N. Francois, C. Tondre, *Colloids Surf., A* **1998**, *143*, 77-88.

[32] J. Klepac, D. L. Simmons, R. W. Taylor, J. F. Scamehorn, S. D. Christian, *Sep. Sci. Technol.* **1991**, *26*, 165-173.

[33] S. Akita, L. P. Castillo, S. Nii, K. Takahashi, H. Takeuchi, *J. Membr. Sci.* **1999**, *162*, 111-117.

[34] E. Pramauro, A. B. Prevot, V. Zelano, M. Gulmini, G. Viscardi, *Analyst* **1996**, *121*, 1401-1405.

[35] A. L. Creagh, B. B. E. Hasenack, A. Van der Padt, E. J. R. Sudhölter, K. Van 't Riet, *Biotechnol. Bioeng.* **1994**, *44*, 690-698.

[36] T. Imae, Y. Takahasi, H. Muramatsu, *J. Am. Chem. Soc.* **1992**, *114*, 3414-3419.

[37] V. De Biasi, J. Senior, J. A. Zukowski, R. C. Haltiwanger, D. S. Eggleston, P. Camilleri, *J. Chem. Soc. Chem. Commun.* **1995**, 1575-1576.

[38] Z. Chilmonczyk, H. Ksycinska, J. Cybulski, M. Rydzewski, A. Les, *Chirality* **1998**, *10*, 821-830.

[39] V. A. Davankov, A. V. Semechkin, *J. Chromatogr.* **1977**, *141*, 313-353.

[40] E. Armani, L. Barazzoni, A. Dossena, R. Marchelli, *J. Chromatogr. A* **1988**, *441*, 287-298.

[41] R. P. Bonomo, V. Cucinotta, F. D'Alessandro, G. Impellizzeri, G. Maccarrone, E. Rizzarelli, G. Vecchio, L. Carima, R. Corradini, G. Sartor, R. Marchelli, *Chirality* **1997**, *9*, 341-349.

[42] R. Corradini, A. Dossena, G. Impellizzeri, G. Maccarrone, R. Marchelli, E. Rizzarelli, G. Sartor, G. Vecchio, *J. Am. Chem. Soc.* **1994**, *116*, 10267-10274.

[43] F. Dallavalle, G. Folesani, R. Marchelli, G. Galaverna, *Helv. Chim. Acta* **1994**, *77*, 1623-1630.

[44] G. Galaverna, R. Corradini, A. Dossena, E. Chiavaro, R. Marchelli, F. Dallavalle, G. Folesani, *J. Chromatogr. A* **1998**, *829*, 101-113.

[45] R. Marchelli, R. Corradini, T. Bertuzzi, G. Galaverna, A. Dossena, F. Gasparrini, B. Galli, C. Villani, D. Misiti, *Chirality* **1996**, *8*, 452-461.

[46] M. Remelli, P. Fornasari, F. Pulidori, *J. Chromatogr. A* **1997**, *761*, 79-89.

[47] M. Sliwka, M. Slebioda, A. M. Kolodziejczyk, *J. Chromatogr. A* **1998**, *824*, 7-14.

[48] T. Takeuchi, R. Horikawa, T. Tanimura, *Anal. Chem.* **1984**, *56*, 1152-1155.

[49] W. A. Tao, D. X. Zhang, F. Wang, P. D. Thomas, R. G. Cooks, *Anal. Chem.* **1999**, *71*, 4427-4429.

[50] Z. B. Yuan, L. L. Yang, S. S. Zhang, *Electrophoresis* **1999**, *20*, 1842-1845.

[51] H. Irving, R. J. P. Williams, *Nature* **1948**, *162*, 746-747.

[52] H. Irving, R. J. P. Williams, *J. Chem. Soc.* **1953**, 3192-3210.

[53] H. Sigel, D. B. McCormick, *Acc. Chem. Res.* **1970**, *3*, 201-208.

[54] R. McCague, S. J. C. Taylor. Integration of Acylase Biotransformation with Process Chemistry: A One-Pot Synthesis of N-boc-L-3-(4-thiazolyl) Alanine and Related Amino Acids. In *Chirality in Industry II: Developments in the Commercial Manufacture and Applications of Optically Active Compounds*; A. N. Collins, G. N. Sheldrake, J. Crosby, Eds.; J. Wiley & Sons: Chichester, 1997; pp 194-206.

[55] E. M. Landau, S. G. Wolf, M. Levanon, L. Leiserowitz, M. Lahav, J. Sagiv, *J. Am. Chem. Soc.* **1989**, *111*, 1436-1445.

[56] M. Abe, Y. Kondo. Organic Componds Removal by Vesicle-Enhanced Ultrafiltration. In *Surfactant-Based Separations: Science and Technology*; J. F. Scamehorn, J. H. Harwell, Eds.; Oxford University Press: Washington, D.C., 1999; pp 201-227.

[57] M. Hebrant, P. Tecilla, P. Scrimin, C. Tondre, *Langmuir* **1997**, *13*, 5539-5543.

[58] J. M. J. Fréchet, *Science* **1994**, *263*, 1710-1715.

[59] C. W. Thomas, Y. Tor, *Chirality* **1998**, *10*, 53-59.

[60] D. Myers. In *Surfactant Science and Technology*, 2 ed.; VCH: New York, 1992, pp 81-127.

[61] R. F. Jameson. Coordination Chemistry of Copper with Regard to Biological Systems. In *Metal Ions in Biological Systems*; H. Sigel, A. Sigel, Eds.; Dekker: New York, 1981; Vol. 12; pp 1-30.

[62] For a list of examples see in F. Wiesemann, S. Teipel, B. Krebs and U. Höweler, *Inorg. Chem.*, 1994, **33**, 1891-1898 ref. 15.

[63] S. V. Rogozhin, V. A. Davankov, Germany Patent: 1932190, 1970.

[64] S. V. Rogozhin, V. A. Davankov, *J. Chem. Soc. Chem. Commun.* **1971**, 490-490.

[65] V. A. Davankov, *J. Chromatogr. A* **1994**, *666*, 55-76.

[66] G. Gübitz, S. Mihellyes, G. Kobinger, A. Wutte, *J. Chromatogr. A* **1994**, *666*, 91-97.

[67] Y. Yuki, K. Saigo, H. Kimoto, K. Tachibana, M. Hasegawa, *J. Chromatogr.* **1987**, *400*, 65-75.

[68] G. Gübitz, F. Juffmann, W. Jellenz, *Chromatographia* **1982**, *16*, 103-106.

[69] B. B. Kragelund, K. Poulsen, K. V. Andersen, T. Baldursson, J. B. Kroll, T. B. Neergard, J. Jepsen, P. Roepstorff, K. Kristiansen, F. M. Poulsen, J. Knudsen, *Biochemistry* **1999**, *38*, 2386-2394.

[70] C. C. DiRusso, V. Tsvetnitsky, P. Hojrup, J. Knudsen, *J. Biol. Chem.* **1998**, *273*, 33652-33659.

[71] S. S. Hegde, A. R. Kumar, K. N. Ganesh, C. P. Swaminathan, M. I. Khan, *Biochim. Biophys. Acta* **1998**, *14*, 93-100.

[72] L. Qin, D. K. Srivastava, *Biochemistry* **1998**, *37*, 3499-3508.

[73] A. Farooq, O. Plotnikova, L. Zeng, M. M. Zhou, *J. Biol. Chem.* **1999**, *274*, 6114-6121.

[74] P. L. Irwin, J. N. Brouillette, S. F. Osman, K. B. Hicks, *Carbohydr. Res.* **1998**, *311*, 37-49.

[75] Y. F. Liu, J. M. Sturtevant, *Biophys. Chem.* **1997**, *64*, 121-126.

[76] F. Y. Lin, W. Y. Chen, L. C. Sang, *J. Colloid Interface Sci.* **1999**, *214*, 373-379.

[77] M. Prorok, F. J. Castellino, *J. Biol. Chem.* **1998**, *273*, 19573-19578.

[78] P. M. Wang, R. M. Izatt, S. E. Gillespie, J. L. Oscarson, X. X. Zhang, C. Wang, J. D. Lamb, *J. Chem. Soc. Faraday Trans.* **1995**, *91*, 4207-4213.

[79] M. J. Blandamer, P. M. Cullis, J. B. F. N. Engberts, *Pure Appl. Chem.* **1996**, *68*, 1577-1582.

[80] K. Bijma, J. B. F. N. Engberts, G. Haandrikman, N. M. van Os, M. J. Blandamer, M. D. Butt, P. M. Cullis, *Langmuir* **1994**, *10*, 2578-2582.

[81] H. H. Heerklotz, H. Binder, R. M. Epand, *Biophys. J.* **1999**, *76*, 2606-2613.

[82] P. J. Koch, J. Frank, J. Schuler, C. Kahle, H. Bradaczek, *J. Colloid Interface Sci.* **1999**, *213*, 557-564.

[83] M. Suurkuusk, S. K. Singh, *Chem. Phys. Lipids* **1998**, *94*, 119-138.

[84] F. Zhang, E. S. Rowe, *Biochemistry* **1992**, *31*, 2005-2011.

[85] G. J. Fox, D. M. Bloor, J. F. Holzwarth, E. Wyn-Jones, *Langmuir* **1998**, *14*, 1026-1030.

[86] G. Borghesani, F. Pulidori, M. Remelli, R. Purrello, E. Rizzarelli, *J. Chem. Soc. Dalton Trans.* **1990**, 2095-2100.

[87] G. Arena, C. Conato, A. Contino, F. Pulidori, R. Purrello, M. Remelli, G. Tabbi, *Annali di Chimica* **1998**, *88*, 1-12.

[88] Manual Omega Titration Calorimeter, Northampton, MA, USA, 1993.

[89] T. Wiseman, S. Williston, J. F. Brandts, L.-N. Lin, *Anal. Biochem.* **1989**, *179*, 131-137.

[90] P. D. Angelo, E. Bottari, M. R. Festa, H. F. Nolting, N. V. Pavel, *Inorg. Chem.* **1998**, *102*, 3114-3122.

[91] J. Bertrán, L. Rodríguez-Santiago, M. Sodupe, *J. Phys. Chem. B* **1999**, *103*, 2310-2317.

[92] T. Lind, P. E. M. Siegbahn, R. H. Crabtree, *J. Phys. Chem. B* **1999**, *103*, 1193-1202.

[93] C. L. Gatlin, F. Turecek, T. Vaiser, *J. Mass Spectrom.* **1995**, *30*, 1605-1616.

[94] K. Pierloot, J. O. A. De Kerpel, U. Ryde, B. O. Roos, *J. Am. Chem. Soc.* **1997**, *119*, 218-226.

[95] J. O. A. De Kerpel, K. Pierloot, U. Ryde, B. O. Roos, *J. Phys. Chem. B* **1998**, *102*, 4638-4647.

[96] A. Bérces, *Inorg. Chem.* **1997**, *36*, 4831-4837.

[97] K. Tanaka, H. Johansen, *Int. J. Quantum Chem.* **1997**, *64*, 453-458.

[98] C. J. Calzado, J. F. Sanz, *J. Am. Chem. Soc.* **1998**, *120*, 1051-1061.

[99] M. Zimmer, *Chem. Rev.* **1995**, *95*, 2629-2649.

[100] J. Savolovic, K. Rasmussen, *Inorg. Chem.* **1995**, *34*, 1221-1232.

[101] V. J. Burton, R. J. Deeth, C. M. Kemp, P. J. Gilbert, *J. Am. Chem. Soc.* **1995**, *117*, 8407-8415.

[102] B. P. Hay, *Coord. Chem. Rev.* **1993**, *126*, 177-236.

[103] P. V. Bernardt, P. Comba, *Inorg. Chem.* **1992**, *31*, 2638-2644.

[104] F. Wiesemann, S. Teipel, B. Krebs, U. Höweler, *Inorg. Chem.* **1994**, *33*, 1891-1898.

[105] P. Comba, T. W. Hambley. In *Molecular Modeling of Inorganic Compounds*; VCH: Weinheim, 1995, pp 188-191.

[106] P. Comba, T. W. Hambley. In *Molecular Modeling of Inorganic Compounds*; VCH: Weinheim, 1995, pp 124.

[107] J. Sabolovic, K. R. Liedl, *Inorg. Chem.* **1999**, *38*, 2764-2774.

[108] C. R. Landis, D. M. Root, T. Cleveland. Molecular Mechanics Force Fields for Modeling Inorganic and Organometallic Compounds; VCH: New York, 1995; Vol. VI; pp 73-148.

[109] C. Møller, M. S. Plesset, *Phys. Rev.* **1934**, *46*, 618-622.

[110] J. S. Binkley, J. A. Pople, *Int. J. Quantum Chem.* **1975**, *9*, 229-236.

[111] R. Krishnan, J. A. Pople, *Int. J. Quantum Chem.* **1978**, *14*, 91-100.

[112] J. A. Pople, M. Head-Gordon, K. Raghavachari, *J. Chem. Phys.* **1987**, *87*, 5968-5975.

[113] J. A. Pople, R. Krishnan, H. B. Schlegel, J. S. Binkley, *Int. J. Quantum Chem.* **1978**, *14*, 545-560.

[114] R. G. Parr, W. Yang. In *Density Functional Theory of Atoms and Molecules*; Oxford University Press: Oxford, 1989.

[115] A. D. Becke, *J. Chem. Phys.* **1993**, *98*, 5648-5652.

[116] C. Lee, W. Yang, R. G. Parr, *Phys. Rev. B* **1988**, *37*, 785-789.

[117] J. B. Foresman, Æ. Frisch. In *Exploring Chemistry with Electronic Structure Methods*; Gaussian, Inc.: Pittsburgh, PA, 1996, pp 111-140.

[118] T. Ziegler, *Chem. Rev.* **1991**, *91*, 651-667.

[119] J. P. Perdew, J. A. Chevary, S. H. Vosko, K. A. Jackson, M. R. Pederson, D. J. Singh, C. Fiolhais, *Phys. Rev. B* **1992**, *46*, 6671-6687.

[120] M. C. Holthausen, M. Mohr, W. Koch, *Chem. Phys. Lett.* **1995**, *240*, 245-252.

[121] M. C. Holthausen, C. Heinemann, H. H. Cornehl, W. Koch, H. Schwarz, *J. Chem. Phys.* **1995**, *102*, 4931-4941.

[122] S. Niu, M. B. Hall, *J. Phys. Chem. A* **1997**, *101*, 1360-1365.

[123] I. Cacelli, D. W. Keogh, R. Poli, A. Rizzo, *J. Phys. Chem. A* **1997**, *101*, 9801-9812.

[124] M. N. Glukhovtsev, B. R. D., C. J. Nagel, *J. Phys. Chem. A* **1997**, *101*, 316-323.

[125] C. Adamo, F. Lelj, *J. Chem. Phys.* **1995**, *103*, 10605-10613.

[126] K. Pierloot, J. O. A. De Kerpel, U. Ryde, M. H. M. Olsson, B. O. Roos, *J. Am. Chem. Soc.* **1998**, *120*, 13156-13166.

[127] A. Bérces, T. Nukada, P. Margl, T. Ziegler, *J. Phys. Chem. A* **1999**, *103*, 9693-9701.

[128] S. Niu, M. B. Hall, *Chem. Rev.* **2000**, *100*, 353-406.

[129] P. E. M. Overdevest, *Ph.D. Thesis*, Wageningen University, Wageningen, 2000.

Chapter

Ultrafiltration Experiments

A slightly modified version of this chapter has been accepted for publication in Chirality

Abstract

A Micelle-Enhanced UltraFiltration (MEUF) separation process is investigated that can potentially be used for large-scale enantioseparations. Copper(II)-amino acid-derivatives dissolved in non-ionic surfactant micelles were used as chiral selectors for the separation of dilute racemic amino acids solutions. For the α-amino acids phenylalanine, phenylglycine, O-methyltyrosine, isoleucine and leucine good separation was obtained using cholesteryl L-glutamate and Cu^{II} ions as chiral selector, with an operational enantioselectivity (α_{op}) up to 14.5 for phenylglycine. From a wide set of substrates, including four β-amino acids, it was concluded that the performance of this system is determined by two factors: the hydrophobicity of the racemic amino acid, which results in a partitioning of the racemic amino acid over micelle and aqueous solution, and the stability of the diastereomeric complex formed upon binding of the amino acid with the chiral selector. The chiral hydrophobic cholesteryl anchor of the chiral selector also plays an active role in the recognition process, since inversion of the chirality of the glutamate does not yield the reciprocal enantioselectivities. However, if the cholesteryl group is replaced by a non-chiral alkyl chain, reciprocal operational enantioselectivities are found with enantiomeric glutamate selectors.

2.1 Introduction

The need for the production of enantio-pure compounds was put under the attention again, when the FDA issued guidelines for the marketing of chiral drugs in May 1992.[1] The most obvious source for enantio-pure compounds is the chiral pool.[2] Unfortunately, the number of compounds in this pool is limited, and in order to obtain the desired compounds, stereoselective synthetic methods need to be applied. Synthesis of racemic mixtures using racemic or non-chiral substrates – which are often much less expensive – followed by a resolution, is often a good alternative. Although numerous techniques are available for the resolution of racemic mixtures on an analytical scale, generally feasible methods for large-scale production are frequently based on diastereomeric salt formation.[3] This technique often involves many processing steps, which can lead to significant product losses.

An alternative process makes use of membranes in order to accomplish resolution. Membrane separations can be continuously operated at ambient temperatures. This, in combination with an easy scale-up, makes membrane separations attractive and cost-efficient. Two types of membrane processes for enantiomer separations are often employed: (a) separations with enantioselective membranes and (b) separations with non-chiral membranes. Examples of the first type are membranes containing proteins,[4,5] chiral polymers,[6,7] molecularly imprinted membranes,[8-10] or emulsion liquid membranes.[11-13] In the second type of membrane processes, the membranes are used to retain one phase or two (im)miscible phases of which at least one is enantioselective.[14,15] For example, Kellner *et al.* have studied the enantioselective transport of chiral *N*-protected amino acids derivatives from an aqueous solution into an organic phase employing highly lipophilic carbamoylated quinine as chiral selector and phase transfer carrier.

Recently, a novel method for separation of racemic mixtures was developed, based on Micelle-Enhanced UltraFiltration (MEUF).[16] This method makes use of an amphiphilic chiral selector that is dissolved in a micelle and preferentially binds one of the enantiomers of a racemic mixture. The pore size of the ultrafiltration membrane is small enough to reject the micelles, but is large enough for all other unbound aqueous solutes to pass. Resolution is accomplished by the filtration of the solution through an ultrafiltration membrane: the micelles, including the diastereomeric complex formed between selector and substrate are retained (Figure 2.1). The permeate is now enriched with the enantiomer that forms the least stable diastereomeric complex; the retentate is enriched with the other enantiomer.

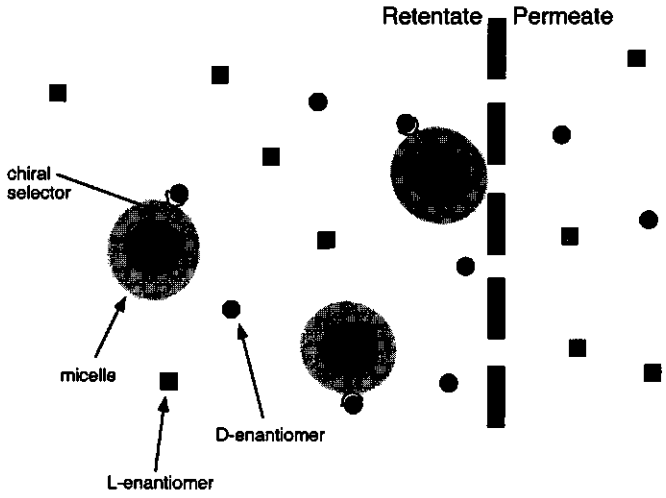

Figure 2.1 Schematic representation of the Micelle-Enhanced UltraFiltration (MEUF) system.

The chiral selector that is used in the ultrafiltration system is an L-glutamic acid derivative, which is esterified at the 5-position with a large hydrophobic alcohol, *e.g.*, cholesterol (Figure 2.2). Since cholesteryl glutamate cannot spontaneously self-assemble into micelles, a non-ionic surfactant was added to promote micelle formation. In the micellar system, the hydrophobic anchor is buried in the core of the micelle, whereas the hydrophilic glutamate headgroup will be present at the surface region of the micelle. The amino acid headgroup can easily bind a copper(II) ion, and this chiral metal complex can form diastereomeric complexes with the enantiomers of the racemic mixtures. Due to the chiral environment, one of the two enantiomers in the racemic mixture binds stronger to the chiral selector than the other enantiomer. This separation technique is closely related to chiral ligand exchange chromatography (CLEC) in which amino acid derivatives are used as chiral selectors and are chemically bound or physically adsorbed to the stationary phase.[17] Many examples can be found in the literature that make use of amino acid derivatives and copper(II) ions in the stationary phase,[18-22] or in the mobile phase[23,24] to separate racemic mixtures of amino acids. However, to the best of our knowledge, these separation systems were only used for analytical or small scale preparative purposes, whereas the MEUF system can potentially be used to separate enantiomers on a large scale.

In our laboratories Creagh *et al.* already performed some very promising experiments on the separation of phenylalanine enantiomers with cholesteryl L-glutamate as selector.[16] This initial success prompted us to investigate the use of this type of chiral selector in MEUF

separations more thoroughly, and test it also for the resolution of other racemic mixtures of amino acids.

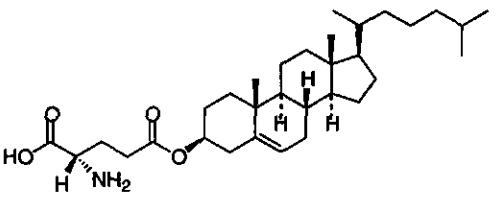

Figure 2.2 Cholesteryl L-glutamate.

In this chapter the syntheses of several selectors with different hydrophobic anchors (cholesterol, dihydrocholesterol and *n*-dodecyl) are described, and the results of ultrafiltration experiments with various racemic α-amino acids and β-amino acids are presented and discussed.

2.2 Materials and methods

2.2.1 Measurements

^{1}H NMR spectra were recorded on a Bruker AC 200 spectrometer. Chemical shifts are given in ppm values with $CHCl_3$ as reference (set at 7.24 ppm). Abbreviations: TFA trifluoroacetic acid, m multiplet, t triplet, d doublet, and s singlet. Melting points were determined by a Mettler FP 82 HT hot stage in combination with an Olympus BH-2 polarization microscope. Optical rotations were measured on a Perkin Elmer 241 polarimeter.

2.2.2 Materials.

All chemicals were purchased from Acros Organics unless mentioned otherwise. The nonionic surfactant Serdox nonyl-phenyl polyoxyethylene E10 ether (NNP-10) was purchased form Servo Delden, The Netherlands. Phenylhydrazine was purchased from Aldrich. The ethanol, which is present in chloroform (~0.1%) was removed by washing the chloroform three times with water, and the chloroform was subsequently dried with Na_2SO_4.

The glutamate chiral selectors were synthesized following the reactions in Scheme 2.1.

Scheme 2.1

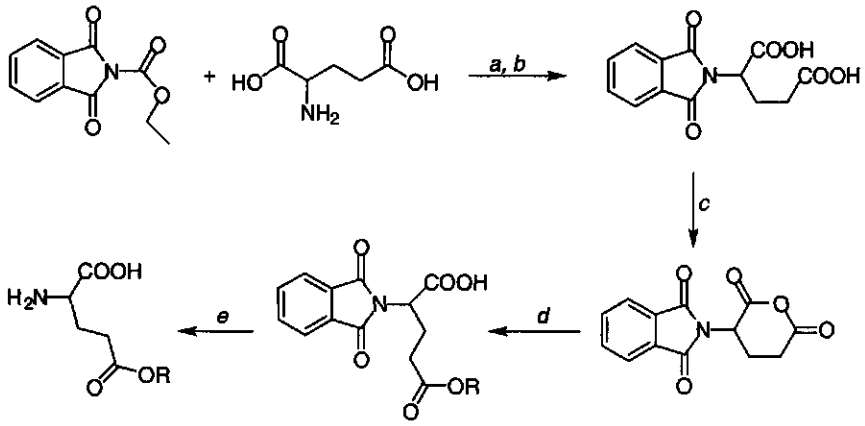

a) Na_2CO_3/H_2O b) 6 N HCl; c) Ac_2O, 70°C; d) (dihydro)cholesterol or *n*-dodecanol, $CHCl_3$, reflux; e) phenylhydrazine, Et_3N, EtOH.

***N*-Phthaloyl L-glutamic acid**[25] L-Glutamic acid, 9.60 g (65.9 mmol), was dissolved in a solution of 20.0 g (189 mmol) of sodium carbonate in 80 ml water. After cooling the mixture to 0°C, 20.0 g (91.2 mmol) well-ground *N*-carbethoxyphthalimide was added and the white suspension was stirred for 5 min at 0°C, and 40 min at room temperature and then filtered. The filtrate was acidified to pH 2.5 with 6 M HCl. The colorless oil that separated slowly crystallized upon cooling. The crystals were collected after 48 h at 7°C. Yield: 11.7 g (42.2 mmol; 64%); m.p. 160°C (lit.: 160°C).[25] ^{1}H NMR ($CDCl_3$ + ~5% TFA): δ 2.40 – 2.80 (m, 4H, CH_2-CH_2); 5.05 – 5.18 (m, 1H, *CH*); 7.75 – 7.95 (m, 4H, phthaloyl).

***N*-Phthaloyl L-glutamic anhydride**[26] 11.7 g (42.2 mmol) *N*-phthaloyl L-glutamic acid was suspended in 75 ml acetic anhydride and heated at 70°C until a clear solution was obtained (about 15 min). After cooling to room temperature a colorless powder precipitated. The mixture was concentrated by evaporation of the solvent under reduced pressure. The white residue was washed three times with dry diethyl ether. Yield: 10.9 g (42.0 mmol; 99%); m.p. 197°C); $[\alpha]_D^{295}$ = -43.0 (*c* = 1.1 in dioxane); lit.: 196-198°C; $[\alpha]_D^{295}$ = -43.1 (*c* = 1.75 in dioxane).[27] IR (KBr) ν: 2923 (CH_2); 1816, 1778, 1714 (C=O) cm^{-1}.

***N*-Phthaloyl 5-cholesteryl L-glutamate** A mixture of 7.9 g (30.5 mmol) *N*-Phthaloyl L-glutamic anhydride and 12.8 g (33.0 mmol) cholesterol (Sigma) in 60 ml of ethanol-free $CHCl_3$ was heated at reflux and a clear solution was slowly obtained. After 48 h the solvent was removed under reduced pressure and a viscous, light yellow oil remained which slowly became solid. The solid material was washed with cold methanol (25 ml) to yield 19.0 g (29.5 mmol; 97%) of a white powder. ^{1}H NMR ($CDCl_3$): δ 0.60 – 2.08 (m, 41H, cholesteryl

moiety); 2.08 – 2.67 (m, 6H, cholesteryl moiety (2H) and CH_2-CH_2 glutamic acid residue); 4.42 – 4.70 (m, 1H, C(O)-O-C*H*-); 4.88 – 5.03 (m, 1H, C*H*-COOH); 5.21 – 5.39 (m, 1H, CH=C cholesteryl); 7.62 – 7.92 (m, 4H, phthaloyl).

5-Cholesteryl L-glutamate[28] A mixture of 19.0 g (29.4 mmol) *N*-phthaloyl 5-cholesteryl L-glutamate, 6.36 g (58.8 mmol) phenylhydrazine and 2.97 g (29.4 mmol) triethylamine was refluxed in 250 ml ethanol (abs.) for 4 h. After about 15 min a clear solution was obtained and 30 min later a white precipitate formed. The mixture was cooled to room temperature, filtered and the white solid was washed extensively with ethanol. Yield: 6.07 g (11.8 mmol; 40%); m.p. 196°C dec. (heating rate 20°/min); $[\alpha]_D^{295}$ = -29 (*c* = 1.05, 3% TFA in $CHCl_3$). ^{1}H NMR ($CDCl_3$ + ~5% TFA): δ 0.61 – 2.10 (m, 41H, cholesteryl moiety); 2.10 – 2.48 (m, 4H, cholesteryl moiety (2H) and NH_2-CH-CH_2-CH_2); 2.71 (t, 2H, NH_2-CH-CH_2-CH_2); 4.23 (broad s, 1H, NH_2-C*H*); 4.50 – 4.71 (m, 1H, C(O)-O-C*H*-); 5.30 – 5.43 (m, 1H, CH=C cholesteryl). Analysis: cholesteryl L-glutamate: calculated ($C_{32}H_{53}NO_4$): C: 74.52; H: 10.36; N: 2.72; found: C: 74.57; H: 10.82; N: 2.48.

Cholesteryl DL-glutamate, cholesteryl D-glutamate and dihydrocholesteryl L-glutamate. These compounds were synthesized according to the same procedure as described above: cholesteryl DL-glutamate $[\alpha]_D^{295}$ = -33 (*c* = 1.05, 3% TFA in $CHCl_3$), which is equal to a 1:1 mixture of cholesteryl L-glutamate and cholesteryl D-glutamate; cholesteryl D-glutamate $[\alpha]_D^{295}$ = -38 (*c* = 1.05, 3% TFA in $CHCl_3$); dihydrocholesteryl L-glutamate $[\alpha]_D^{295}$ = +20 (*c* = 1.29, 3% TFA in $CHCl_3$). Analysis: dihydrocholesteryl L-glutamate ($C_{32}H_{55}NO_4$)·0.5 H_2O calculated: C: 72.96; H: 10.71; N: 2.66; found: C: 72.73; H: 10.85; N: 2.54.

***N*-Phthaloyl 5-dodecyl D-glutamate.** A mixture of 0.80 g (3.1 mmol) *N*-phthaloyl D-glutamic anhydride and 0.96 g (5.2 mmol) *n*-dodecanol in 10 ml of ethanol-free $CHCl_3$ was heated at reflux and a clear solution was slowly obtained. After 48 h the solvent was removed under reduced pressure to yield 1.30 g (2.9 mmol; 97%) of a white solid. ^{1}H NMR ($CDCl_3$): δ 0.85 (t, 3H, CH_3, *J* = 6.7); 1.08 – 1.41 (m, 18H, (CH_2)$_9$-CH_3); 1.53 (t, 2H, CH_2-$(CH_2)_9$-CH_3, *J* = 6.1); 2.28 – 2.70 (m, 4H, CH-CH_2-CH_2-); 3.96 (t, 3H, C(O)-O-CH_2, *J* = 6.7); 4.85 – 5.0 (m, 1H, C*H*); 7.65 – 7.90 (m, 4H, phthaloyl).

5-Dodecyl D-glutamate. A mixture of 1.30 g (2.9 mmol) *N*-phthaloyl 5-dodecyl D-glutamate, 0.67 g (6.2 mmol) phenylhydrazine and 0.31 g (3.1 mmol) triethylamine was refluxed in 10 ml ethanol (abs.) for 4 h. The mixture was cooled to room temperature, filtered and the white solid was washed extensively with butanone. Yield: 0.35 g (1.11 mmol; 35%); m.p.: 178 – 179°C; (lit.: 177.2 – 179.2).[29] ^{1}H NMR ($CDCl_3$): δ 0.85 (t, 3H, CH_3, *J* = 6.7); 1.12 – 1.45 (m, 18H, (CH_2)$_9$-CH_3); 1.63 (t, 2H, CH_2-$(CH_2)_9$-CH_3 *J* = 6.4); 2.10 – 2.49 (m, 2H, CH-CH_2-

CH_2); 2.75 (t, 2H, CH-CH_2-CH_2, J = 6.0); 4.11 (t, 2H, C(O)-O-CH_2, J = 6.7); 4.15 – 4.35 (m, 1H, C*H*). $[\alpha]_D^{295}$ = -15 (c = 1.02, 3% TFA in $CHCl_3$).

5-Dodecyl L-glutamate. This compound was synthesized according to the same procedure as 5-dodecyl D-glutamate. $[\alpha]_D^{295}$ = +18 (c = 1.42, 3% TFA in $CHCl_3$).

***N*-Acetyl-*O*-methoxy-DL-tyrosine**[30,31] To a suspension of 5.01 g (27.7 mmol) of D L-tyrosine in 30 ml of water at 95°C was slowly added 22 ml of acetic anhydride (25 min). The mixture was stirred for 5 min at 90°C, and after slowly cooling down to room temperature a clear solution was obtained. The solvent was removed under reduced pressure and a yellow gum of *N*-acetyl-DL-tyrosine was obtained. Yield: 5.92 g (26.6 mmol; 96%). ^{1}H NMR (D_2O) δ 1.98 (s, 3H, C(O)C*H*$_3$); 2.72 – 3.15 (m, 2H, C*H*$_2$); 4.46 (m, 1H, C*H*); 6.76 (d, 2H, Ar (C*H*)$_2$-C-CH_2, J = 8.2); 7.05 (d, 2H, Ar (C*H*)$_2$-C-OH, J = 8.2).

The gum was dissolved in a solution of 30 g NaOH in 140 ml water. Then 4.5 ml of dimethylsulfate was added dropwise with stirring over a period of about 15 min. The yellow solution was stirred at 90°C for 15 min and then cooled to room temperature. After the solution was acidified with 6 N HCl a white solid material precipitated, which was extracted with $CHCl_3$. After evaporation of the solvent under reduced pressure, an oil was obtained which crystallized from a solution of 10 ml $CHCl_3$ and 30 ml diethyl ether at -35°C. Yield: 4.64 g (19.6 mmol; 74%). ^{1}H NMR ($CDCl_3$) δ 1.92 (s, 3H, C(O)C*H*$_3$); 2.85 – 3.23 (m, 2H, C*H*$_2$); 3.78 (s, 3H, CH_3-O); 4.62 – 4.82 (m, 1H, C*H*); 6.85 (d, 2H, Ar (C*H*)$_2$-C-CH_2, J = 6.6); 7.19 (d, 2H, Ar (C*H*)$_2$-C-OH, J = 6.6)

***O*-Methoxy-DL-tyrosine**[31] A solution of 4.64 g (19.6 mmol) of *N*-Acetyl-*O*-methoxy-DL-tyrosine in 25 ml 6 N HCl was refluxed for 2 h, and subsequently stored at -35°C for 30 min. The resulting crystals were collected, and dissolved in 30 ml water. The pH of the solution was increased by dropwise addition of a 25% NH_3 solution in water. The amino acid separated as shining plates and was washed with water to yield (2.20 g; 11.3 mmol; 57%) of colorless crystals. M.p. 225°C dec. (heating rate 15°/min). ^{1}H NMR ($CDCl_3$ +~5% TFA): δ 3.00 – 3.25 (m, 1H, C*H*$_2$); 3.28 – 3.49 (m, 1H, C*H*$_2$); 3.80 (s, 3H, O-C*H*$_3$); 4.37 (broad s, 1H, C*H*); 6.88 (d, 2H, Ar (C*H*)$_2$-C-CH_2, J = 8.6); 7.10 (d, 2H, Ar (C*H*)$_2$-C-OH, J = 8.6). Analysis: calculated ($C_{10}H_{13}NO_3$): C: 61.52; H: 6.71; N: 7.18; found: C: 61.25; H: 6.75; N: 7.16.

2.2.4 Methods

Ultrafiltration: preparation of the samples. All solutions were made with ultrapure water (Millipore filtration system) and 50 ml sample solutions were prepared to contain the following compounds: chiral selector (0.3 mM), $CuCl_2$ (0.3 mM), racemic amino acid (0.15

mM), $Na_2B_4O_7 \cdot 10\ H_2O$ (0.025 M), KCl (0.1 M) and NNP-10 (0.5% w/w). The solutions were prepared as follows. First, the chiral selector was dispersed in the NNP-10 surfactant and about 10 ml water was added. This mixture was stirred overnight, and after dilution with water to 40 ml a clear solution was obtained. However, for the dodecyl glutamate selectors no completely clear solution could be obtained, even after additional ultrasonic treatment. Subsequently, 5 ml of a stock solution of KCl (1.0 M) and $CuCl_2$ (3.0 mM) was added. After about 15 min, 5 ml of a lukewarm buffered solution of the racemic amino acid (1.5 mM) and 0.25 M $Na_2B_4O_7 \cdot 10\ H_2O$ (pH 9.0) was added, and immediately a light blue solution was obtained. Creagh *et al.* found that the enantioselectivity increased upon increasing the pH from 5.5 to 11.[16] However, we frequently observed some precipitation of copper hydroxyde salts at pH 11, whereas if the pH was lowered to pH 9 always clear solutions were obtained. The resulting solution was stirred overnight and used for ultrafiltration experiments the next morning.

Ultrafiltration: experimental setup. The sample solution (50 ml) was placed in an Amicon 300 ml cell equipped with a Millipore PLCC regenerated cellulose membrane (44 cm^2) with an approximate molecular-weight cut-off of $5 \cdot 10^3$ Daltons. The pure water flux of the membrane was ~130 $ml/min \cdot m^2 \cdot bar$. During the filtration the stirring speed (300 rpm), the overpressure (3 bar N_2) and the temperature (298 K) were held constant. After 5 min (~10 ml), 3 samples of 1 ml of the permeate were collected for analysis.

In a previous study it was verified that the micelles are retained, since the concentration of the NNP-10 surfactant in the permeate was not larger than the critical micelle concentration (0.003% w/w).[16] Furthermore, dynamic light scattering experiments have shown that the micelles are about 10 nm in size, whereas the pore-size of the membrane is estimated to be 5 nm.

Ultrafiltration: analysis of the samples. The concentrations of the racemic amino acids in the permeate were analyzed by HPLC using a Chirex® 3126 (D)-penicillamine ligand exchange type column (Phenomenex, Torrance, Ca, USA). For serine, homoserine and threonine a 250 × 4.6 mm column was used, and for all other amino acids a 50 × 3.2 mm column; particle size 5 μm. As mobile phase a solution of 2 mM $CuSO_4$ in ultrapure water mixed with methanol (HPLC grade, LabScan) or acetonitrile (HPLC grade, LabScan) was used, depending on the hydrophobicity of the analyzed amino acid. When the 250 × 4.6 mm column was applied, the mobile phase needed to be adjusted by adding $Na_2B_4O_7 \cdot 10\ H_2O$ (0.025 M) to match the composition of the samples as good as possible; the pH was reduced to 5.3. Furthermore, the samples analyzed on this column needed to be acidified by mixing

0.9 ml of the permeate solution and 0.1 ml 1 M HCl solution. Injection volumes of 100 µl were used and a flow of 0.5 ml/min. The peaks were detected by UV at 254 nm and the concentrations were determined using a 5 point calibration based on peak area.

Ultrafiltration: operational enantioselectivity. The operational enantioselectivity (α_{op}) is defined as the distribution of the D-enantiomer over micelle and aqueous bulk divided by the distribution of the L-enantiomer over micelle and aqueous bulk:

$$\alpha_{op} = \frac{C_D^{micelle} / C_D^{bulk}}{C_L^{micelle} / C_L^{bulk}} = \frac{C_D^o - C_D^p}{C_D^p} \times \frac{C_L^p}{C_L^o - C_L^p} \tag{2.1}$$

in which C^o is the initial concentration of enantiomer D or L, and C^p is the concentration of the enantiomer in the permeate. From Equation 2.1 it follows that if $\alpha_{op} = 1$, there is no enantioselectivity; if $0 < \alpha_{op} < 1$, there is a preference for binding the L-enantiomers to the selector; and if $\alpha_{op} > 1$, more D-enantiomers are bound.

Two aspects of the MEUF system need to be distinguished: the enantioselectivity of the selector for the enantiomers, and the affinity of the selector for the enantiomers. The affinity is characterized by the equilibrium constant K of the reaction between the chiral selector and the enantiomer to form a diastereomeric complex, for example:

$$K_D = \frac{C_{diastereomeric\ complex}}{C_D \times C_{selector}} = \frac{C_D^{micelle}}{C_D^p \times C_{selector}} \tag{2.2}$$

Overdevest *et al.* have validated that the binding of the phenylalanine to cholesteryl L-glutamate in NNP-10 micelles can be described with multi-component Langmuir isotherms.[1] Consequently, the intrinsic enantioselectivity α (= K_D/K_L) is equal to the operational enantioselectivity.

$$\alpha = \frac{K_D}{K_L} = \frac{\dfrac{C_D^{micelle}}{C_D^p \times C_{selector}}}{\dfrac{C_L^{micelle}}{C_L^p \times C_{selector}}} = \frac{\dfrac{C_D^{micelle}}{C_D^p}}{\dfrac{C_L^{micelle}}{C_L^p}} = \frac{C_D^{micelle} / C_D^{bulk}}{C_L^{micelle} / C_L^{bulk}} = \frac{D_D}{D_L} = \alpha_{op} \tag{2.3}$$

[1] This implies that every binding site of the chiral selector is equivalent and the ability of an enantiomer to bind there is independent whether or not nearby sites are already occupied.

2.3 Results and Discussion

2.3.1 Substrate variation: α-amino acids.

Phenylglycine, phenylalanine and homophenylalanine. The initial success that Creagh *et al.* obtained with phenylalanine prompted us to first test amino acids with a phenyl ring in the R-group of the amino acid. A mixture of D- and L-phenylalanine can be separated very well by MEUF as can be seen from the high enantioselectivity that is measured: $\alpha_{op} = 8.3$ (Table 2-I, entry 2), and corresponds to an enantiomeric excess in the permeate (ee_p) of 69% and an enantiomeric excess in the micellar phase (ee_m) of 11%. Such an enantioselectivity is high as compared to maximum enantioselectivity (2.4) of Pickering *et al.* obtained with an emulsion liquid membrane.[12]

Table 2-I. Binding percentages, operational enantioselectivities of MEUF experiments with cholesteryl L-glutamate as chiral selector, and hydrophobic parameters of several α-amino acids.

Entry	Substrate	R-Group	Γ_D [a] (%)	Γ_L [a] (%)	α_{op} [b]	π [c]
1	Phenylglycine	$-C_6H_5$	98	78	14.5 ± 2.5	1.22
2	Phenylalanine	$-CH_2-C_6H_5$	96	78	8.3 ± 2.3	1.63
3	Homophenyl-alanine	$-CH_2-CH_2-C_6H_5$	100	100	-	2.04
4	Tryptophan	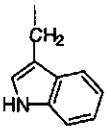	47	46	1.0 ± 0.1	1.84
5	Tyrosine	$-CH_2-C_6H_4-OH$	0	0	-	0.36[d]
6	*O*-Methyltyrosine	$-CH_2-C_6H_4-O-CH_3$	76	33	7.2 ± 1.6	1.87
7	Leucine	$-CH_2-CH(CH_3)_2$	94	74	5.1 ± 1.0	1.64
8	Isoleucine	$-CH(CH_3)-CH_2-CH_3$	17	15	1.3 ± 0.2	1.55
9	Valine	$-CH(CH_3)CH_3$	0	0	-	1.18
10	Serine	$-CH_2-OH$	0	0	-	-0.08
11	Homoserine	$-CH_2-CH_2-OH$	0	0	-	0.37
12	Threonine	$-CH(OH)-CH_3$	0	0	-	0.33

[a] Percentage bound substrate to the selector; [b] The enantiomeric excess can be calculated from the Γ values: $ee_m = (\Gamma_D-\Gamma_L)/(\Gamma_D+\Gamma_L)*100\%$ and ee_p $[100-\Gamma_D)-(100-\Gamma_L)]/[100-\Gamma_D)+(100-\Gamma_L)]*100\%$; [c] $\pi = \log P_{OW}$ (amino acid) – $\log P_{OW}$(glycine); [d] π-value of phenolate anion.

The chiral selector also shows a high affinity for phenylalanine as can be concluded from the high percentages substrate bound to the selector (Γ): the amount of bound D-enantiomer (Γ_D) is 96% and bound L-enantiomer (Γ_L) is 78% (Table 2-I). The selection process probably involves a ternary complex between selector, Cu^{II} and phenylalanine.[32,33] The effect of the rotational freedom of the benzyl group was studied by also analyzing phenylglycine, which lacks a CH_2 spacer, and homophenylalanine, which has an extra CH_2 group. In case of phenylglycine, the chiral selector is even more selective than for phenylalanine: slightly more of the D-enantiomer and the same amount of the L-enantiomer is bound. This is reflected in a large increase in α from 8.3 to 14.5. Therefore, it was expected that for homophenylalanine a smaller enantioselectivity would be found. However, with HPLC neither of the enantiomers of homophenylalanine could be found in the permeate. This absence can be explained by the hydrophobicity of the substrate. In Table 2-I (last column) the π-values of the investigated amino acids are displayed. This π-value is a measure for the hydrophobicity and is defined as: $\pi = \log P_{OW}(\text{amino acid}) - \log P_{OW}(\text{glycine})$. A larger π-value consequently means a more hydrophobic amino acid. It is seen that homophenylalanine (π = 2.04) is much more hydrophobic than phenylalanine (π = 1.63).

Two distinct processes thus take place in the ultrafiltration system: a) the chemical binding of the substrate to the selector, and b) the physical partitioning of the substrate over solution and micelle, which is referred to as a partitioning effect. It can be concluded that homophenylalanine is too hydrophobic to be separated into its enantiomers in this UF-system. This is additionally supported by ultrafiltration experiments in which there was no chiral selector present in the micelle, and again no homophenylalanine could be detected in the permeate by HPLC. From these experiments it can be concluded that cholesteryl L-glutamate is highly selective for these amino acids with an unsubstituted phenyl ring in the R-group. However, if the substrate is too hydrophobic the partitioning effect becomes a dominant factor.

Tryptophan, tyrosine, and O-methyltyrosine. Other aromatic amino acids were tested as well and the results are presented in Table 2-I, entries 4 – 6. Tyrosine, which has a phenolic group, is partly present as its phenolate anion under the ultrafiltration conditions of pH 9 (pK_a = 10.46).[34] This ionization makes this amino acid more hydrophilic (π-value = 0.36) and explains the fact that only negligible amounts are bound to the selector. This undesirable effect can be eliminated by methylation of the hydroxyl group. *O*-Methyltyrosine, which is thus much more hydrophobic than tyrosine (π-value = 1.87), is bound to the selector in larger quantities (76% and 33% for the D- and L-enantiomers, respectively). This results in α_{op} = 7.2, which is comparable to the enantioselectivity of phenylalanine.

The π-values of tryptophan and *O*-methyltyrosine are almost equal, 1.84 and 1.87 respectively. However, tryptophan is bound to a smaller degree than *O*-methyltyrosine. Furthermore, the chiral selector does not show any selectivity ($\alpha = 1.0$) for tryptophan. The lower binding percentages and the absence of enantioselectivity suggest that binding of the substrate is different as compared to *O*-methyltyrosine or phenylalanine. The indole group of tryptophan has excellent π-electron donating properties.[35] Consequently, the indole moiety may be competitively involved in binding to Cu^{II} ions. Since the indole functionality is relatively far away from the chiral center of the amino acid, the selector cannot distinguish between the two enantiomers. Additionally, the above-mentioned non-enantioselective partitioning effect can also contribute to the absence of enantioselectivity.

Leucine, isoleucine, valine. The effect of the length of the alkyl chains and the type of branching is studied by using leucine, isoleucine and valine. The branching of the alkyl chain at the α-carbon makes isoleucine a little more hydrophilic than its isomer leucine, although this is not very pronounced in the π-values of 1.55 and 1.64, respectively. However, leucine is much better bound to the selector than isoleucine (Table 2-I, entries: 7 and 8). The branching at the β-carbon (isoleucine) seems to have a dramatic negative effect on the affinity. This can also be concluded from the fact that valine is hardly bound to the selector. This amino acid is more hydrophilic than (iso)leucine, but this cannot solely explain the small Γ-value. The π-value of valine is nearly identical to that of phenylglycine ($\pi_{PheGly} = 1.22$ and $\pi_{Val} = 1.18$) but phenylglycine binds very well to the selector. Consequently, it can be concluded that branching at the β-carbon has a negative influence on the performance of the system.

Apart from the fact that there is a lower affinity for isoleucine as compared to leucine, isoleucine also has a lower operational enantioselectivity: $\alpha_{op} = 1.3$ as compared to $\alpha_{op} = 5.1$ for leucine. This contrasts with the CLEC data of Davankov *et al.* who have found higher selectivities for isoleucine than for leucine.[36] They state that branching at the β-carbon atom (isoleucine) is more favorable for the enantioselectivity than branching at the γ-position (leucine), while branching at the α-carbon has an adverse effect.

Serine, threonine and homoserine. The operational enantioselectivity for amino acids with a hydroxyl group, namely serine, threonine and homoserine was also tested. These amino acids differ in the branching and length of the R-group. As seen from the π-values, these amino acids are too hydrophilic, which results in very low binding percentages ($\Gamma \approx 0\%$). Consequently, none of these amino acids could be separated.

It is noteworthy that all racemic mixtures of amino acids that could be separated in the MEUF

system, also gave a good resolution using a 5 cm Chirex 3126 (D)-penicillamine ligand exchange type HPLC column, except homophenylalanine, which gave good resolution, but no separation in the MEUF system. Tryptophan, which could not be separated in the MEUF system, was also poorly separated on this Chirex column. The resolution for isoleucine is also much smaller than for leucine, similar to the ultrafiltration experiments. The more hydrophilic amino acids (valine, serine, threonine, homoserine and tyrosine) gave a (very) poor resolution on this Chirex column and also gave no separation in the MEUF system. From the large resemblance between the MEUF system and this Chirex column, it can be deduced that this HPLC column can be used to predict which enantiomers can be separated in the MEUF system.

2.3.2 Substrate variation: β-amino acids.

In addition to α-amino acids, some β-amino acids were tested as well in the MEUF system. Four compounds were tested, namely 3-amino-3-phenylpropanoic acid, 3-amino-4,4,4-trifluorobutanoic acid, 3-amino-butanoic acid, and 3-amino-4-methylpentanoic acid (Scheme 2.2).

Scheme 2.2

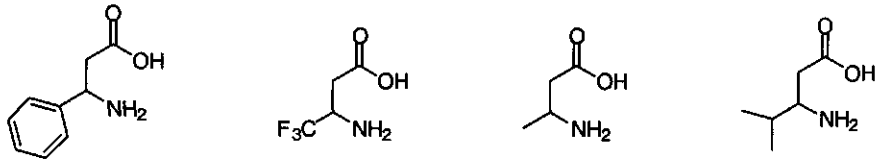

(a) 3-amino-3-phenylpropanoic acid; (b) 3-amino-4,4,4-trifluorobutanoic acid; (c) 3-amino-butanoic acid; (d) 3-amino-4-methylpentanoic acid.

None of these amino acids could be separated. The lack of selectivity can be explained by the fact that instead of a five-membered chelate ring, now a more flexible six-membered chelate ring is formed with Cu^{II}.[36] This flexibility probably reduces the energetic differences between the ternary complexes formed with the L- and D-enantiomer, respectively, which results in diminished discrimination.

2.3.4 Chiral selector variation

The mechanism of the chiral selection process was studied in more detail by a slight modification of the chiral selector. Therefore, six different chiral selectors were used, and in all cases phenylalanine was used as racemic substrate, since this amino acid is well bound by the chiral selectors and non-selective partitioning plays only a minor role (Table 2-II).

First it was investigated whether there is a contribution to the chiral recognition of the (chiral) cholesteryl part of the selector. If recognition solely takes place at the glutamate headgroup, a reciprocal operational enantioselectivity would be expected for cholesteryl D-glutamate (CDG) as compared to the results obtained with cholesteryl L-glutamate (CLG), *i.e.*, α_{op} = 1/8.3 = 0.12 is expected. However, for CDG α_{op} = 0.45 is measured. In combination with the lower binding percentages obtained with CDG (Table 2-II, entries 3 *vs.* 1), this strongly suggests that the chiral hydrophobic anchor contributes to the enantioselectivity in such a way that it has a negative influence on the binding of L-phenylalanine. This conclusion is supported by UF-experiments in which cholesteryl DL-glutamate is used as chiral selector. If there is no influence of the cholesteryl anchor, absence of enantioselectivity is expected (α_{op} = 1). However, the measured operational enantioselectivity is 1.6. From these measurements it can be concluded that chiral recognition does not exclusively take place at the glutamate headgroup and that the cholesteryl group plays an additional role in the recognition process. The role of the cholesteryl anchor in this recognition process is currently investigated in more detail.

Table 2-II. Binding percentages, operational enantioselectivities of MEUF experiments with different chiral selectors, and DL-phenylalanine as racemic substrate.

Selector	Γ_D (%)	Γ_L (%)	α_{op}
Cholesteryl L-glutamate	96	78	8.3 ± 2.3
Cholesteryl DL-glutamate	82	75	1.6 ± 0.2
Cholesteryl D-glutamate	31	50	0.45 ± 0.07
Dihydrocholesteryl L-glutamate	98	88	7.1 ± 3.2
n-Dodecyl L-glutamate	57	49	1.5 ± 0.4
n-Dodecyl D-glutamate	44	51	0.77 ± 0.1

Another trend can be seen in the amount of bound phenylalanine to the selector. It is obvious that CDG better binds L-Phe than D-Phe, like D-Phe is better bound by CLG than L-Phe. In other words, the heterochiral complex is more stable than the homochiral complex. This

could probably be the result of steric hindrance as schematically depicted in Figure 2.3. The carbonyl group of the ester linkage of cholesteryl glutamate can be axially coordinated to the Cu^{II} ion, thereby blocking one site.[37] Since the phenyl ring of phenylalanine can also coordinate axially to the Cu^{II} ion,[38,39] one of the two enantiomers is sterically hindered. This can partly account for the measured difference in enantioselectivities. Remarkably, the affinities of both D and L-Phe for CDG are lower than for CLG. How the chirality of the hydrophobic cholesteryl anchor exactly influences the affinity and the enantioselectivity is not clear at present. Perhaps it is caused by differences in aggregation of the selector in the non-ionic micelle, *i.e.*, a supramolecular effect.

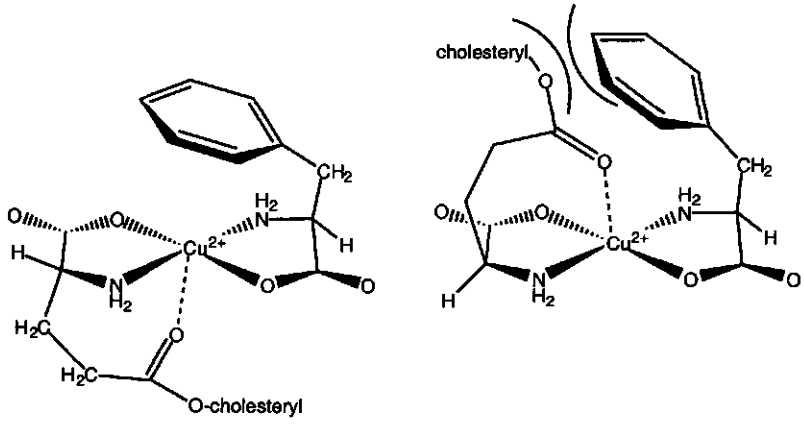

Figure 2.3. Model to explain the different binding of L-Phe to a) CDG-Cu^{II} and b) CLG-Cu^{II} selectors.

Dihydrocholesteryl L-glutamate yields similar enantioselectivities and affinities as cholesteryl L-glutamate. The amounts of bound D-Phe and L-Phe are slightly larger, 98% and 88%, respectively, which results in a slightly smaller operational enantioselectivity of $\alpha_{op} = 7.1$, as compared to 8.3 for cholesteryl L-glutamate.

The effects of chiral centers in the hydrophobic anchor on the operational enantioselectivity can be eliminated by using achiral alkyl chains, *e.g.*, *n*-dodecyl chains. The measured enantioselectivities for *n*-dodecyl-L-glutamate (DLG) and *n*-dodecyl-D-glutamate (DDG) deviate substantially from the cholesteryl glutamate selectors. For the separation of phenylalanine with the chiral selectors DLG and DDG operational enantioselectivities of $\alpha_{op} = 1.5$ and 0.77, respectively are found, which are reciprocal values within the margins of experimental error. Additionally, the affinities of both enantiomers for dodecyl L-glutamate are lower than for cholesteryl L-glutamate (Table 2-II). This could be the result of the fact that for these chiral selectors, using the 'standard' solution preparation, not an entirely clear

selector solution could be obtained, and therefore not all the chiral selectors are available for binding enantiomers.

From the experiments described above, it is apparent that the measured operational enantioselectivity is sensitive to a number of different factors, including the chirality of the hydrophobic anchor, the solubility of the chiral selector in the micellar environment, and the nature of the microhetereogeneous medium.[40,41] Since for different amino acid substrates different enantioselectivities are found, it is very likely that the geometry around Cu^{II} in such complexes is highly dependent on the type and size of the substrate. To obtain more information about the geometrical structure, and thus the interactions that are taking place in the complex, a start has been made to approach this problem also from a computational point of view, using high-level quantum mechanical calculations.[42,43]

To obtain both enantiomers enantio-pure (99^{+}%), the described batch processes should, and can be implemented in countercurrent, cascaded ultrafiltration systems.[14] This cascaded ultrafiltration system enables enantiomer separation in systems that are essentially aqueous, which may prove to be advantageous for the development of new, relatively environment-friendly separation processes.

2.4 Conclusions

A Micelle-Enhanced UltraFiltration system using Cu^{II}-amino acid-derivatives as chiral selectors, was used for testing the chiral separation of dilute, racemic amino acid solutions. Racemic mixtures of several α-amino acids like phenylalanine, phenylglycine, *O*-methyltyrosine, isoleucine and leucine showed good enantioselectivity using cholesteryl L-glutamate and Cu^{II} as chiral selector. The measured operational enantioselectivities, up to 14.5, are the result of two processes: (i) the chemical binding of the substrate to selector and (ii) a non-selective partitioning of the substrate over hydrophobic micelle and aqueous water phase. It is found that the chemically bound substrates containing a phenyl ring yield higher enantioselectivities, as compared to the ones containing a more flexible alkyl chain; branching at the β-carbon atom of the alkyl chain further diminishes the enantioselectivity. For the amino acids that are too hydrophobic (π-value $\geq$ 2.0) or too hydrophilic (π-value $\leq$ 1.2) the non-selective partitioning becomes a dominant factor, which results in absence of enantioselectivity. Furthermore, the presence of additional coordinating groups in the amino acids can also annihilate the enantioselectivity. The cholesteryl L-glutamate Cu^{II} selector did

not show enantioselectivity for β-amino acids, probably because the formation of more flexible 6-membered chelate rings, as compared to 5-membered rings for α-amino acids, negatively influences the selectivity.

It was shown that the cholesteryl anchor plays an important role in the recognition process, since use of cholesteryl D-glutamate does not yield the reciprocal enantioselectivity of cholesteryl L-glutamate. Replacing the chiral cholesteryl anchor by a non-chiral alkyl chain, yields near reciprocal enantioselectivities. Chiral ligand exchange chromatography appears to be not only a good method for analysis of amino acid concentrations, but can also be used to predict which enantiomers could be separated using the MEUF system.

References

[1] *Chirality* **1992**, *4*, 338-340.

[2] R. A. Sheldon. In *Chirotechnology: Industrial Synthesis of Optically Active Compounds*; Marcel Dekker: New York, 1993, pp 143-171.

[3] J. T. F. Keurentjes, F. J. M. Voermans. Membrane Separations in the Production of Optically Pure Compounds. In *Chirality in Industry II: Developments in the Commercial Manufacture and Applications of Optically Active Compounds*; A. N. Collins, G. N. Sheldrake, J. Crosby, Eds.; J. Wiley & Sons: Chichester, 1997; pp 157-180.

[4] A. Higuchi, T. Hashimoto, M. Yonehara, N. Kubota, K. Watanabe, S. Uemiya, T. Kojima, M. Hara, *J. Membr. Sci.* **1997**, *130*, 31-39.

[5] B. B. Lakshmi, C. R. Martin, *Nature* **1997**, *388*, 758-760.

[6] T. Aoki, M. Ohshima, K. I. Shinohara, T. Kaneko, E. Oikawa, *Polymer* **1997**, *38*, 235-238.

[7] S. Tone, T. Masawaki, K. Eguchi, *J. Membr. Sci.* **1996**, *118*, 31-40.

[8] A. Dzgoev, K. Haupt, *Chirality* **1999**, *11*, 465-469.

[9] M. Yoshikawa, J. I. Izumi, T. Kitao, *Polym. J.* **1997**, *29*, 205-210.

[10] C. J. Allender, K. R. Brain, C. M. Heard, *Chirality* **1997**, *9*, 233-237.

[11] P. J. Pickering, J. B. Chaudhuri, *J. Membr. Sci.* **1997**, *127*, 115-130.

[12] P. J. Pickering, J. B. Chaudhuri, *Chirality* **1997**, *9*, 261-267.

[13] P. J. Pickering, J. B. Chaudhuri, *Chirality* **1999**, *11*, 241-248.

[14] P. E. M. Overdevest, J. T. F. Keurentjes, A. Van der Padt, K. Van 't Riet. Resolution of Enantiomers Using Enantioselective Micelles in Ultrafiltration Systems. In *Surfactant-Based Separations: Science and Technology*; J. F. Scamehorn, J. H. Harwell, Eds.; Oxford University Press: Washington, D.C., 1999; pp 123-138.

[15] K.-H. Kellner, A. Blasch, H. Chmiel, M. Lämmerhofer, W. Lindner, *Chirality* **1997**, *9*, 268-273.

[16] A. L. Creagh, B. B. E. Hasenack, A. Van der Padt, E. J. R. Sudhölter, K. Van 't Riet, *Biotechnol. Bioeng.* **1994**, *44*, 690-698.

[17] V. A. Davankov, J. D. Navratil, H. F. Walton. In *Ligand exchange chromatography*; CRC Press: Boca Raton, FL, 1988, pp

[18] V. A. Davankov, *J. Chromatogr. A* **1994**, *666*, 55-76.

[19] R. Marchelli, R. Corradini, T. Bertuzzi, G. Galaverna, A. Dossena, F. Gasparrini, B. Galli, C. Villani, D. Misiti, *Chirality* **1996**, *8*, 452-461.

[20] M. Sliwka, M. Slebioda, A. M. Kolodziejczyk, *J. Chromatogr. A* **1998**, *824*, 7-14.

[21] M. Remelli, P. Fornasari, F. Pulidori, *J. Chromatogr. A* **1997**, *761*, 79-89.

[22] Q.-H. Wan, P. N. Shaw, M. C. Davies, D. A. Barrett, *J. Chromatogr. A* **1997**, *765*, 187-200.

[23] E. Gil-Av, A. Tishbee, P. E. Hare, *J. Am. Chem. Soc.* **1980**, *102*, 5115-5117.

[24] S. Weinstein, M. H. Engel, P. E. Hare, *Anal. Biochem.* **1982**, *121*, 370-377.

[25] G. H. L. Nefkens, G. L. Tesser, R. J. F. Nivard, *Recl. Trav. Chim. Pays-Bas* **1960**, *79*, 688-698.

[26] F. E. King, D. A. A. Kidd, *J. Chem. Soc.* **1949**, 3315-3319.

[27] R. S. Tipson, *J. Org. Chem.* **1956**, *1956*, 1353-1357.

[28] I. Schumann, R. A. Boissonnas, *Helv. Chim. Acta* **1952**, *35*, 2235-2237.

[29] M. De Lourdes de Araujo Silva, E. De Castro Antunes Felício, *Bull. Soc. Chim. Fr.* **1997**, *134*, 645-651.

[30] L. D. Behr, H. T. Clarke, *J. Am. Chem. Soc.* **1932**, *54*, 1630-1634.

[31] B. R. Baker, J. P. Joseph, J. H. Williams, *J. Am. Chem. Soc.* **1955**, 1-7.

[32] D. Van der Helm, M. B. Lawson, E. L. Enwall, *Acta Crystallogr., Sect. B: Struct. Crystallogr. Cryst. Chem.* **1971**, *27*, 2411-2418.

[33] R. P. Martin, M. M. Petit-Ramel, J. P. Scharff. Mixed-Ligand Metal Ion Complexes of Amino Acids and Peptides. In *Metal ions in biological systems*; H. Sigel, Ed.; Dekker: New York, 1973; Vol. 2; pp 1-61.

[34] D. Voet, J. G. Voet. In *Biochemistry*, 2 ed.; J. Wiley & Sons: New York, 1995, pp 58-59.

[35] K. Aoki, H. Yamazaki, *J. Chem. Soc. Dalton Trans.* **1987**, 2017-2021.

[36] V. A. Davankov, Y. A. Zolotarev, *J. Chromatogr.* **1978**, *155*, 285-293.

[37] W. Chen, M.-C. Lim, *Acta Crystallogr., Sect. C: Cryst. Struct. Commun.* **1997**, *53*, 539-543.

[38] D. Van der Helm, C. E. Tatsch, *Acta Crystallogr., Sect. B: Struct. Crystallogr. Cryst. Chem.* **1972**, *28*, 2307.

[39] H. Muhonen, R. Hamalainen, *Finn. Chem. Lett.* **1983**, 120-124.

[40] P. E. M. Overdevest, A. Van der Padt, *Chemtech* **1999**, *29(12)*, December, 17-27.

[41] T. J. M. de Bruin, A. Koudijs, A. T. M. Marcelis, H. Zuilhof, E. J. R. Sudhölter, Unpublished Results.

[42] T. J. M. De Bruin, A. T. M. Marcelis, H. Zuilhof, E. J. R. Sudhölter, *Phys. Chem. Chem. Phys.* **1999**, *1*, 4157-4163 (Chapter 4).

[43] T. J. M. De Bruin, A. T. M. Marcelis, H. Zuilhof, E. J. R. Sudhölter, *J. Phys. Chem. A* - submitted (Chapter 5).

Chapter

Isothermal Titration Calorimetry and Enantioselectivity

A slightly modified version of this chapter has been submitted for publication in Langmuir

Abstract

Enantioselectivity experiments for the binding to chiral Cu^{II} complexes have been performed for several α-amino acids using isothermal titration calorimetry. To a system containing non-ionic micelles, Cu^{II} ions and cholesteryl glutamate as chiral selector, either the D- *or* L-*amino acid was titrated. The highest enantioselectivities (K_D/K_L) were measured for the amino acids with relatively bulky R-groups: phenylalanine (1.24) and phenylglycine (1.26), while an increase in enantioselectivity from 1.00 to 1.21 was measured upon increasing the size of the R-group in the amino acids alanine to leucine. For serine no enantioselectivity was measured. Reciprocal enantioselectivities have been measured with phenylalanine upon inversion of the chirality of the glutamate headgroup of the chiral selector. Finally, it was found that the binding of the amino acid to the chiral-metal selector is an entropically driven process.*

3.1 Introduction

Isothermal titration calorimetry (ITC) is a sensitive technique to investigate the thermodynamics of several kinds of processes. This technique has been used to obtain information about changes in Gibbs free energy, enthalpy and entropy of phenomena such as the binding between enzymes and substrates,[1-5] and host-guest complexation reactions.[6,7] In addition, with this technique critical micelle concentrations have been measured,[8,9] and information has been obtained about the interaction of solutes with vesicles.[10-14] ITC has also been used to investigate the binding of metal ions to crown ethers,[15] the binding of Ca^{II}, Mg^{II} and Zn^{II} to neuroactive peptides,[16] and the interactions of lysozyme with immobilized Cu^{II} and Fe^{III} ions.[17] Furthermore, studies have been reported in which titration calorimetry experiments in combination with potentiometry have been used to investigate the complexation of Cu^{II} ions with diastereomeric dipeptides,[18] or to study stereoselective aspects of mixed-ligand complexes with Cu^{II} ions and the aromatic amino acid histidine.[19] More recently, a similar study on Cu^{II}-L-glutamine and Cu^{II}-L-asparagine binary complexes has been published.[20] These latter two studies have shown that non-covalent interactions, like π-stacking and hydrogen bonds between side chains of the amino acids play an important role in the stereoselective recognition of Cu^{II} amino acid complexes. If such complexes are formed in aggregates such as micelles, it is expected that this will have an influence on the formation and also on the stereoselectivity of bis(amino acid)Cu^{II} complexes in the micelle-enhanced ultrafiltration system.

In chapter 2 it is described that the performance of this separation system, measured by the operational enantioselectivity α_{op}, is equal to the ratio of the equilibrium constants (K_D/K_L) of the formation of both diastereomeric complexes. The equilibrium constant is related to the change in Gibbs free energy ($\Delta G^\circ = -RT \ln K$), and thus the enantioselectivity (α) can be expressed in terms of the Gibbs free energy (Equation 3.1).

$$\alpha = \exp[(\Delta G^\circ_D/RT - \Delta G^\circ_L/RT)] = \exp(\delta\Delta G^\circ/RT) \qquad (3.1)$$

For example, an operational enantioselectivity of 1.1 corresponds to a free energy difference ($\delta\Delta G$) of about 0.26 $kJ \cdot mol^{-1}$ between the two diastereomeric complexes. Such energy differences can be measured with modern isothermal titration calorimeters, and ITC can thus be used to measure enantioselectivities.

With ITC the most important thermodynamic data of the reaction of each enantiomer to the chiral metal complex can be determined: the binding constant (K), the stoichiometry (n) and change in enthalpy (ΔH) are measured directly, and from these the change in Gibbs free

energy (ΔG) and change in entropy (ΔS) can be calculated.[21] Consequently, ITC can not only be used as a tool to quickly measure enantioselectivities (K_D/K_L), but can also give additional information on the binding of the amino acid to the selector. In order to determine which thermodynamic parameters play an important role in the separation process and to be able to predict enantioselectivity, ITC experiments were performed in which either D- or L-amino acids are titrated to the chiral Cu^{II}-selector complex dissolved in micelles under conditions that are similar to those used in the MEUF system.

3.2 Experimental Section

Materials. The synthesis of the chiral selectors is described elsewhere.[22] Gly (Fluka, 99%), L-Ala (Fluka, p.a.), D-Ala (Acros, 99+%), L-Val (Janssen, 99%), D-Val (Aldrich, 98+%), L-Leu (Janssen, 99%), D-Leu (Aldrich), L-Phenylglycine (Acros, 99%), D-Phenylglycine (Acros, 98%), L-Phe (Aldrich, 99%), D-Phe (Merck, 99+%), L-Ser (Fluka, p.a.), D-Ser (Acros, 98%), $(CH_3COO)_2Cu{\cdot}1H_2O$ (Merck, extra pure), sodium acetate (Acros, p.a.) and Serdox nonyl-phenyl-polyoxyethylene-E10-ether (NNP-10; Servo Delden, The Netherlands) were used without further purification.

Methods. All solutions were made in a 0.1 M sodium acetate solution of pH 7.0 using ultrapure water (Millipore filtration system). A 100 ml chiral selector solution containing either cholesteryl L-glutamate or cholesteryl D-glutamate (3.0 mM) and the surfactant NNP-10 (1% w/w) was prepared as follows. The selector (154.8 mg) was dispersed in NNP-10 (1.00 g) and about 10 ml of the acetate solution was added. This mixture was stirred overnight, and was afterwards diluted with the acetate solution to obtain the final volume of 100 ml. For each titration experiment, a fresh mixture of 5.0 ml of this selector solution and 5.0 ml of 3.0 mM $(CH_3COO)_2Cu{\cdot}1\ H_2O$ solution was prepared. For the experiments with cholesteryl DL-glutamate equal amounts (2.5 ml) of the cholesteryl L-glutamate and cholesteryl D-glutamate containing solutions were mixed. The concentration of the amino acid solutions used for titration was 25.0 mM.

Experimental setup. The calorimetric experiments were performed with an Omega Titration Calorimeter (MicroCal, Northampton, MA, USA). The experimental temperature was set at 25 °C and the temperature of the (external) water bath at 20 °C. The reference cell was filled with the acetate solution; the reaction cell (1.353 ml) was filled with the Cu^{II}-selector solution. For each experiment, there was an initial delay of 60 sec and at least 25 injections

of 9.0 μl (injection duration 22.63 sec) were made, with a waiting time of 300 sec between each injection. The stirring speed was set at 410 rpm.

3.3 Results and Discussion

The stoichiometry (n), the binding constant (K), and the change in enthalpy (ΔH) of the complexation reactions of several α-amino acids with the cholesteryl glutamate selectors were derived from the titration S-curves such as depicted in Figure 3.1. These curves were obtained using the "1 set of sides" model as implemented in the MicroCal Origin software.[23] First, these thermodynamic parameters together with the change in ΔG and ΔS will be discussed, and subsequently, the enantioselectivities, derived from the K values, will be presented and discussed.

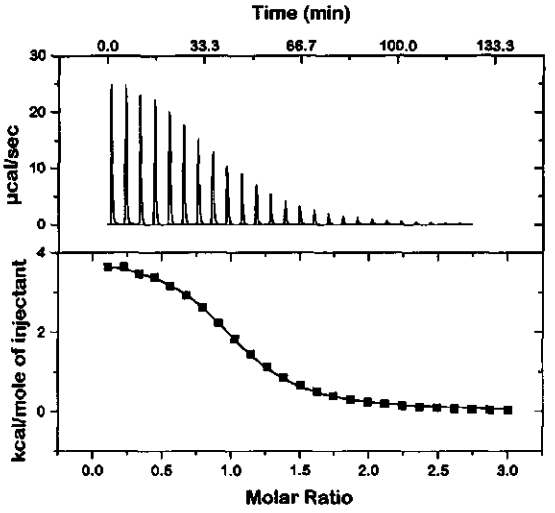

Figure 3.1. Typical plot of the titration complexation of D-phenylalanine to the cholesteryl DL-glutamate: calorimetric signals at 298 K (top) and the integration of the peaks (bottom) yield an S-shaped curve from which the thermodynamic data are calculated.

3.3.1 Thermodynamic properties

The thermodynamic parameters (n, K, ΔH, ΔG and ΔS) of the complexation reaction of cholesteryl-L-glutamate with several α-amino acids are presented in Table 3-I.

Table 3-I. Thermodynamic properties n, K ($l \cdot mol^{-1}$), ΔH ($kJ \cdot mol^{-1}$), ΔG ($kJ \cdot mol^{-1}$) and ΔS ($J \cdot mol^{-1} \cdot K^{-1}$) and hydrophobicity parameter π of several α-amino acids for the binding with cholesteryl L-glutamate at 298 K and pH 7.

Titrant	n	K	ΔH	ΔG	ΔS	π [a]
Gly	0.96 ±0.02	$2.59 \cdot 10^3$ ±160	16.1 ±0.4	-19.4 ±0.2	119 ±3	0
D-Ala	0.90 ±0.03	$1.74 \cdot 10^3$ ±130	22.8 ±1.0	-18.5 ±0.2	139 ±4	0.40
L-Ala	0.79 ±0.03	$1.74 \cdot 10^3$ ±130	23.8 ±1.2	-18.5 ±0.2	142 ±5	0.40
D-Val	0.96 ±0.02	$2.41 \cdot 10^3$ ±130	20.2 ±0.5	-19.3 ±0.1	133 ±2	1.18
L-Val	0.94 ±0.04	$2.27 \cdot 10^3$ ±120	20.9 ±0.6	-19.1 ±0.1	134 ±3	1.18
D-Leu	0.74 ±0.04	$3.47 \cdot 10^3$ ±240	19.3 ±0.3	-20.2 ±0.2	133 ±2	1.64
L-Leu	0.72 ±0.08	$2.87 \cdot 10^3$ ±220	20.8 ±0.7	-19.7 ±0.2	135 ±3	1.64
D-PheGly	0.90 ±0.02	$3.64 \cdot 10^3$ ±260	18.8 ±0.4	-20.3 ±0.2	131 ±2	1.22
L-PheGly	0.96 ±0.04	$2.90 \cdot 10^3$ ±130	19.3 ±0.3	-19.8 ±0.1	131 ±2	1.22
D-Phe	1.07 ±0.02	$9.10 \cdot 10^3$ ±380	16.7 ±0.1	-22.5 ±0.1	132 ±1	1.63
L-Phe	1.06 ±0.01	$7.31 \cdot 10^3$ ±250	17.3 ±0.1	-22.0 ±0.1	132 ±1	1.63
D-Ser	1.01 ±0.03	$3.89 \cdot 10^3$ ±220	15.8 ±0.4	-20.5 ±0.1	122 ±2	-0.08
L-Ser	1.02 ±0.06	$3.99 \cdot 10^3$ ±180	15.7 ±0.2	-20.5 ±0.1	121 ±1	-0.08

[a] $\pi = \log P_{ow}$ (amino acid) – $\log P_{ow}$(glycine).[24]

For all the complexation reactions (except for leucine) the stoichiometry (n) is close to 1.0, which means that all available chiral metal-selectors bind a substrate, suggesting that ternary complexes of the form selector:Cu^{II}:substrate are formed. In contrast to earlier studies[19,20] the formation of the complexes in this work is only entropically driven, and not both enthalpically and entropically favored, as can be seen from the measured positive ΔS and positive ΔH values. For the tested amino acids (AA) the changes in entropy vary from 119 $J \cdot mol^{-1} \cdot K^{-1}$ for glycine, to 142 $J \cdot mol^{-1} \cdot K^{-1}$ for alanine. These values are of the same order of magnitude as the ΔS values found for the reaction $2\ AA^- + Cu^{2+} \leftrightarrows Cu(AA)_2$, which range from ~110 to ~130 $J \cdot mol^{-1} \cdot K^{-1}$ in a non-micellar aqueous system. However, they are clearly larger than those of the reaction $AA^- + Cu^{2+} \leftrightarrows [Cu(AA)]^+$, which range from ~70 to ~80 $J \cdot mol^{-1} \cdot K^{-1}$.[19,20] Remarkably, the measured ΔS values in the micellar system that correspond to the reaction $[Cu(AA)]^+ + AA^- \leftrightarrows Cu(AA)_2$, are much larger than the expected 40 to 50 $J \cdot mol^{-1} \cdot K^{-1}$ (calculated from the difference between $2\ AA^- + Cu^{2+} \leftrightarrows Cu(AA)_2$ and $AA^- + Cu^{2+} \leftrightarrows [Cu(AA)]^+$).

The increase in entropy can be explained by the water molecules that were initially coordinated to the cholesteryl L-glutamate-Cu^{II} selector (CLG:Cu^{II}) and titrated amino acid, but are released upon binding of the substrate to the selector:

$$CLG{:}Cu^{II}{:}(H_2O)_n + AA{:}(H_2O)_m \quad \leftrightarrows \quad CLG{:}Cu^{II}{:}AA(H_2O)_x + y\,H_2O$$

The larger ΔS values measured for the "micellar system" as compared to those of the "aqueous bulk system" suggest that in the micellar system more water molecules are released and that this is caused by the micelles. It can be speculated that upon binding of the amino acid to the CLG:Cu^{II}:$(H_2O)_n$ complex, the complex becomes more hydrophobic. In the micellar system, this could result in a shift of the diastereomeric complex towards the hydrophobic core of the micelle. Such a repositioning is unfavorable for the water molecules coordinated to the complex, and this could result in an extra release of coordinated water molecules, making the complex even more hydrophobic.

The different substituents of the amino acids also influence ΔS to some degree, as the measured variation in change of entropy for the different amino acids is slightly outside the experimental error. However, no obvious correlation could be found between the size or functionalities in the R-group of the amino acid and the change in entropy. For example, a hydrophilic hydroxyl group (as in serine) and a relatively hydrophobic benzyl group (as in phenylalanine), will stabilize a different number of coordinated water molecules around the amino acid. Therefore, the number of water molecules that will be released upon binding to the selector will likely be different. The hydrophobicity of amino acids can be quantified with the hydrophobicity parameter π, which is defined as: π = log P_{ow} (amino acid) – log P_{ow}(glycine).[24] A larger π value therefore means a more hydrophobic amino acid (Table 3-I, column 7). It can be seen that the two most hydrophilic amino acids that were investigated, serine (π = -0.08) and glycine (π = 0.00), have ΔS values that are significantly smaller than those measured for the other more hydrophobic amino acids. This could suggest that a smaller number of water molecules is released upon binding, because serine and glycine are relatively more hydrophilic. However, the highest ΔS is measured for alanine, whereas this amino acid is significantly less hydrophobic than *e.g.*, phenylalanine for which a smaller ΔS is measured.

There are remarkable differences between the K, ΔH and ΔG values found in this work and those of the previous mentioned reactions $AA^- + Cu^{2+} \leftrightarrows [Cu(AA)]^+$ and $2\ AA^- + Cu^{2+} \leftrightarrows Cu(AA)_2$ in the non-micellar system.[19,20] The latter two reactions are exothermic and typical

values of ΔH are -25 kJ·mol^{-1} and -50 kJ·mol^{-1}, respectively, whereas in this study all reactions are endothermic (see Table 3-I, column 4). These differences in ΔH between this work and the other two studies strongly suggest an influence of the micelle on the complex formation. In line with the model that the increase in entropy can be interpreted as the release of coordinated water molecules upon binding of the amino acid to the complex, also the overall measured change in enthalpy can be understood in this way. Initially, the titrated amino acid is completely hydrated. However, upon going from the aqueous bulk into the more hydrophobic micelle, the amino acid will lose some of its coordinated water molecules. This dehydrating process has an endothermic effect,[25] and it is not unlikely that due the total number of released water molecules, this process can eventually even dominate the overall ΔH.

The K values, and thus also the ΔG values, are much larger in the previously mentioned studies.[19,20] Typical ΔG values for the binding of one amino acid to Cu^{II} are -50 kJ·mol^{-1} and for two amino acids to Cu^{II} -85 kJ·mol^{-1}, whereas in this work ΔG values are measured between -18.5 and -22.5 kJ·mol^{-1} (Table 3-I, column 5). It can be hypothesized that the smaller K values are also the results of the micelles. Since the chiral cholesteryl:Cu^{II} complex is solubilized in the micelle, it is more shielded from the reacting amino acid, as compared to a cholesteryl:Cu^{II} complex dissolved in an aqueous bulk system.

From Table 3-I it can be seen that K is also clearly dependent on the nature of the R-group of the amino acid. Especially, the values for DL-phenylalanine are significantly larger than measured for all other amino acids, and this may suggest that the binding of this amino acid is different from the other amino acids. It is expected that all amino acids bind with the nitrogen atom of the amino group and an oxygen atom of the carboxylate to the Cu^{II} ion.[26] Furthermore, it is known that the phenyl ring of phenylalanine can yield a third, aromatic ring-Cu^{II}, interaction.[27] Such an extra interaction would also lower the (positive) ΔH value, however, this is not observed; for serine and glycine even smaller ΔH values are measured. In addition, this interaction would also affect $\delta\Delta H_{DL}$ and this is also absent. Consequently, it seems not very likely that there is an extra aromatic-Cu^{II} interaction. It seems more probable that the larger K values of phenylalanine, and to a smaller extent those of phenylglycine, have a non-chiral origin. Since the used surfactant contains a phenyl ring, π-stacking between an aromatic amino acid and the surfactant is possible, and this could account for the substantially larger K values for the aromatic amino acids phenylalanine and phenylglycine. The fact that phenylalanine has an extra methylene group as compared to phenylglycine, gives phenylalanine the possibility to have a more optimized π-π interaction, which results in the

larger K values. Likewise, the relatively large K values for serine suggest non-selective hydrogen bonding in which the hydroxyl of serine is involved.

From the data of the ITC measurements performed in this study it can be seen that it is difficult to observe a trend or a correlation between the different types of amino acids tested and the binding constants, changes in enthalpy or changes in entropy. On the other hand, upon using enantiomeric amino acids, or changing the chirality in the headgroup of the chiral selector, comparisons can be made much easier, since effects like (de)hydration are expected to be much smaller between two enantiomeric amino acids, than between different types of amino acids.

3.4.2 Enantioselectivity measurements

From Table 3-I is can be seen that the stoichiometry of each couple of amino acid enantiomers is the same within the experimental errors, except for alanine. For the amino acids with relatively bulky R-groups, *i.e.*, leucine, phenylglycine and phenylalanine, the D-enantiomer is bound more strongly. This can be seen from the less positive (or less endothermic) ΔH value for the D-enantiomer, and also from the larger K value. The entropy changes are similar for the two enantiomers, from which follows that the R-group itself is not involved in an extra binding to the Cu^{II} ion. If this were the case, one of the enantiomers would have been better bound to the Cu^{II}, since its R-group is spatially closer the Cu^{II} ion. This would then result in a decrease of degrees of (rotational) freedom, which in turn should be reflected in ΔS.

As indicated earlier, the quotient of the binding constants of two enantiomers (K_D/K_L) yields the enantioselectivity, and these are presented in Table 3-II.

In the series of aliphatic amino acids it is seen that with increasing size of the alkyl chain there is a concomitant increase in enantioselectivity. For alanine, which has a methyl substituent, there is no enantioselectivity (1.00) and the error is relatively large. The enantioselectivity for valine, which contains an isopropyl substituent, is already more pronounced: $\alpha = 1.06$. The largest selectivity is measured for leucine, with an isobutyl group: $\alpha = 1.21$. Apparently, the chiral selector can better distinguish between the D- and L-enantiomers with increasing size of the substituent, which results in higher enantioselectivities. For serine, which has a relatively small R-group (CH_2-OH), but is slightly larger than the methyl group of alanine, no enantioselectivity is observed. This may suggest that the hydroxyl functionality has no or even an opposite effect on the

enantioselectivity as compared to the influence of the size of the R-group on the enantioselectivity.

Table 3-II. Comparison of enantioselectivities measured with isothermal titration calorimetry and micelle-enhanced ultrafiltration.

Substrate	Chiral Selector	Enantioselectivity ITC	Enantioselectivity MEUF
Ala	cholesteryl-L-glutamate	$1.16 \geq \mathbf{1.00} \geq 0.86$	1.0
Val	cholesteryl-L-glutamate	$1.19 \geq \mathbf{1.06} \geq 0.95$	1.0
Leu	cholesteryl-L-glutamate	$1.40 \geq \mathbf{1.21} \geq 1.05$	5.2
Ser	cholesteryl-L-glutamate	$1.08 \geq \mathbf{0.98} \geq 0.88$	1.0
PheGly	cholesteryl-L-glutamate	$1.41 \geq \mathbf{1.26} \geq 1.12$	14.5
Phe	cholesteryl-L-glutamate	$1.34 \geq \mathbf{1.24} \geq 1.15$	8.2
Phe	cholesteryl-D-glutamate	$0.96 \geq \mathbf{0.83} \geq 0.70$	0.5
Phe	cholesteryl-DL-glutamate	$1.16 \geq \mathbf{1.07} \geq 0.99$	1.6

The two aromatic amino acids, phenylalanine and phenylglycine, both have relatively bulky substituents. The phenyl and benzyl group are of similar size as the isobutyl group of leucine, and for these three amino acids similar enantioselectivities are measured: α = 1.24 (phenylalanine), α = 1.26 (phenylglycine) and α = 1.21 (leucine). From these results it can be concluded that the larger the R-group, the better the selector can discriminate between the two enantiomers. Following the reasoning mentioned above that the R-group is not involved in an extra interaction with the Cu^{II} ion, it can be concluded that the enantioselectivity probably originates from a destabilization effect due to steric hindrance that is present in a larger extent in the homochiral complex than in the heterochiral complex.

The thermodynamic properties for the titration experiments in which the chirality of the selector has been altered (cholesteryl L-glutamate, cholesteryl DL-glutamate and cholesteryl D-glutamate) are shown in Table 3-III. For these titrations D- and L-phenylalanine were used as substrate, since phenylalanine gives the highest binding constants of the amino acids tested. The stoichiometry of the complexation reaction (n) is close to 1.0 in all cases, which is expected for the formed ternary complexes, although the values of n for cholesteryl D-glutamate are relatively large. When the K values of cholesteryl D-glutamate (CDG) and cholesteryl L-glutamate (CLG) are compared, it is seen that D-Phe is better bound by the L-glutamate selector, and L-Phe by the D-glutamate selector. This is also reflected in the

enthalpy change: the stronger-bound enantiomer has a lower, less endothermic, ΔH value (+16.7 and +16.5 kcal·mol^{-1}) than the poorer bound enantiomer (+17.3 and +17.2 kcal·mol^{-1}).

Table 3-III. Thermodynamic properties n, K (l·mol^{-1}), ΔH (kJ·mol^{-1}), ΔG (kJ·mol^{-1}) and ΔS (J·mol^{-1}·K^{-1}) of D/L-phenylalanine with several chiral selectors at 298 K and pH 7.

Selector	Titrant	n	K	ΔH	ΔG	ΔS
Chol. L-glutamate	D-Phe	1.07 ±0.02	$9.10 \cdot 10^3$ ±380	16.7 ±0.1	-22.5 ±0.1	132 ±1
	L-Phe	1.06 ±0.01	$7.31 \cdot 10^3$ ±250	17.3 ±0.1	-22.0 ±0.1	132 ±1
Chol. D-glutamate	D-Phe	1.12 ±0.02	$7.94 \cdot 10^3$ ±900	17.2 ±0.2	-22.2 ±0.3	132 ±2
	L-Phe	1.13 ±0.01	$9.61 \cdot 10^3$ ±410	16.5 ±0.1	-22.9 ±0.1	132 ±1
Chol. DL-glutamate	D-Phe	1.03 ±0.02	$9.05 \cdot 10^3$ ±310	16.6 ±0.1	-22.6 ±0.1	131 ±1
	L-Phe	1.05 ±0.01	$8.45 \cdot 10^3$ ±360	16.8 ±0.2	-22.4 ±0.1	132 ±1

If the chiral recognition solely takes places at the glutamate head group of the chiral selector, it is expected that the enantioselectivity changes to the reciprocal value upon changing the chirality of the headgroup of the selector from L-glutamate to D-glutamate, and there is no enantioselectivity with cholesteryl DL-glutamate. From Table 3-II it can be seen that for cholesteryl L-glutamate an enantioselectivity of 1.24 is measured, and for cholesteryl D-glutamate $\alpha = 0.83$. These reciprocal enantioselectivities suggest no influence of the cholesteryl group. However, for cholesteryl DL-glutamate an intermediate enantioselectivity is found ($\alpha = 1.07$). This could indicate a small contribution of the chiral cholesteryl anchor to the selectivity. However, due to the large errors in K, such a contribution could very well be absent, *i.e.*, α could also be 1.0. From these experiments it can be concluded, that the chiral recognition predominantly takes place at the glutamate head group, and there seems to be no or only a small contribution to the observed enantioselectivity from the chiral cholesteryl anchor of the selector.

3.3.4 Comparison of ITC with MEUF enantioselectivities.

The measured operational enantioselectivities obtained with micelle-enhanced ultrafiltration (MEUF) are also presented in Table 3-II. For alanine, valine and serine both techniques show an almost complete absence of enantioselectivity. For the other amino acids, phenylglycine, phenylalanine and leucine with both techniques an enantioselectivity is observed that is significantly larger than 1.0. Qualitatively, the enantioselectivities measured with ITC closely

follow those obtained with MEUF, *i.e.*, for the α's obtained with ITC the order is PheGly > Phe > Leu > Val ≥ Ala ≥ Ser and the order obtained with MEUF is PheGly > Phe > Leu > Val ≈ Ala ≈ Ser. However, the operational enantioselectivities measured with MEUF are much larger.[22] Furthermore, upon inversion of the chirality of the glutamate headgroup of the chiral selector, no reciprocal enantioselectivities are measured, as is the case with ITC. Additionally, the operational enantioselectivity obtained with MEUF is clearly larger than 1.0 when cholesteryl DL-glutamate is used, whereas with ITC the enantioselectivity is 1.07. These observations suggest that in the MEUF and ITC experiments different processes contribute to the measured values of α. The most important difference between the MEUF and ITC experiments lies in the large difference in time scale that exists between the two types of experiments: ITC experiments take place on the time scale of seconds to minutes, whereas for the MEUF experiments it is ~24 h. Therefore, it is possible that apart from a fast binding process that occurs in both experiments, there is also a slower process that is only apparent in the MEUF experiments.

To explain the above-mentioned results the following model is proposed. Initially, the substrate (titrant) binds to the Cu^{II} ion, which is already bound to the glutamate headgroup of the chiral selector. The chirality of the glutamate headgroup determines which enantiomer of the substrate is bound preferentially, resulting in an enantioselectivity. This type of enantioselectivity is measured with ITC, and also takes place in MEUF experiments. However, once the diastereomeric complex is formed, it is likely that it will rearrange in the micelle, as a consequence of changes in hydrophobicity due to binding of the substrate. The time scale on which this 'supra-molecular' effect takes place, is too large to be measured with ITC, which can only measure changes in heat that occur almost instantaneously. In this so-called supra-molecular effect the cholesteryl anchor of the selector can also play an active role. This can for example be concluded from the MEUF experiments where a clear operational enantioselectivity (α = 1.6) is measured when cholesteryl DL-glutamate is used. The precise role of cholesteryl anchor in the enantioselectivity process is however yet unclear, and further research on this is needed.

3.4 Conclusions

In this work it is shown that enantioselectivities can be measured using isothermal titration calorimetry, as exemplified for the complexation of D- and L-amino acids to micellar chiral Cu^{II} complexes. In a system that contains non-ionic micelles, Cu^{II} ions and cholesteryl

glutamate as chiral selector the binding of several titrated amino acid is investigated. It is found that for all amino acids the binding to the selector, which is present in the micelles, is an entropically driven process. This has been interpreted as the release of coordinated water molecules when the titrated amino acid is going from the hydrophilic aqueous bulk into the hydrophobic micelle to bind to the chiral complex. This dehydration is an energy consuming process, and the release of water molecules results in the overall measured endothermic effect. The differences in K, ΔH and ΔS are understood for the pairs of enantiomers, but not between amino acids themselves. The result that one enantiomer is better bound by the selector is explained by steric hindrance, *i.e.*, an increasing enantioselectivity was measured with increasing size of the substituent of the titrated amino acid. Upon inversion of the chirality of the glutamate headgroup of the selector, reciprocal enantioselectivities are measured for phenylalanine. From the measurements with cholesteryl DL-glutamate selector it is found that there might be a small contribution of the cholesteryl anchor in the overall chiral recognition process. The results of the ITC experiments closely follow those of the MEUF experiments in a qualitatively way, only in the MEUF experiments the enantioselectivities are significantly more pronounced. Therefore a chiral recognition model has been proposed, which states that recognition initially takes place at the glutamate headgroup. On a larger time scale, which cannot be measured with ITC, the influence of a supramolecular rearrangement of the chiral complex in the micellar environment becomes more pronounced, resulting in larger enantioselectivities.

References

[1] B. B. Kragelund, K. Poulsen, K. V. Andersen, T. Baldursson, J. B. Kroll, T. B. Neergard, J. Jepsen, P. Roepstorff, K. Kristiansen, F. M. Poulsen, J. Knudsen, *Biochemistry* **1999**, *38*, 2386-2394.

[2] C. C. DiRusso, V. Tsvetnitsky, P. Hojrup, J. Knudsen, *J. Biol. Chem.* **1998**, *273*, 33652-33659.

[3] S. S. Hegde, A. R. Kumar, K. N. Ganesh, C. P. Swaminathan, M. I. Khan, *Biochim. Biophys. Acta* **1998**, *14*, 93-100.

[4] L. Qin, D. K. Srivastava, *Biochemistry* **1998**, *37*, 3499-3508.

[5] A. Farooq, O. Plotnikova, L. Zeng, M. M. Zhou, *J. Biol. Chem.* **1999**, *274*, 6114-6121.

[6] P. L. Irwin, J. N. Brouillette, S. F. Osman, K. B. Hicks, *Carbohydr. Res.* **1998**, *311*, 37-49.

[7] Y. F. Liu, J. M. Sturtevant, *Biophys. Chem.* **1997**, *64*, 121-126.

[8] M. J. Blandamer, P. M. Cullis, J. B. F. N. Engberts, *Pure Appl. Chem.* **1996**, *68*, 1577-1582.

[9] K. Bijma, J. B. F. N. Engberts, G. Haandrikman, N. M. van Os, M. J. Blandamer, M. D. Butt, P. M. Cullis, *Langmuir* **1994**, *10*, 2578-2582.

[10] H. H. Heerklotz, H. Binder, R. M. Epand, *Biophys. J.* **1999**, *76*, 2606-2613.

[11] P. J. Koch, J. Frank, J. Schuler, C. Kahle, H. Bradaczek, *J. Colloid Interface Sci.* **1999**, *213*, 557-564.

[12] M. Suurkuusk, S. K. Singh, *Chem. Phys. Lipids* **1998**, *94*, 119-138.

[13] F. Zhang, E. S. Rowe, *Biochemistry* **1992**, *31*, 2005-2011.

[14] G. J. Fox, D. M. Bloor, J. F. Holzwarth, E. Wyn-Jones, *Langmuir* **1998**, *14*, 1026-1030.

[15] P. M. Wang, R. M. Izatt, S. E. Gillespie, J. L. Oscarson, X. X. Zhang, C. Wang, J. D. Lamb, *J. Chem. Soc. Faraday Trans.* **1995**, *91*, 4207-4213.

[16] M. Prorok, F. J. Castellino, *J. Biol. Chem.* **1998**, *273*, 19573-19578.

[17] F. Y. Lin, W. Y. Chen, L. C. Sang, *J. Colloid Interface Sci.* **1999**, *214*, 373-379.

[18] R. P. Bonomo, R. Cali, V. Cucinotta, G. Impellizzeri, E. Rizzarelli, *Inorg. Chem.* **1986**, *25*, 1641-1646.

[19] G. Borghesani, F. Pulidori, M. Remelli, R. Purrello, E. Rizzarelli, *J. Chem. Soc. Dalton Trans.* **1990**, 2095-2100.

[20] G. Arena, C. Conato, A. Contino, F. Pulidori, R. Purrello, M. Remelli, G. Tabbi, *Annali di Chimica* **1998**, *88*, 1-12.

[21] T. Wiseman, S. Williston, J. F. Brandts, L.-N. Lin, *Anal. Biochem.* **1989**, *179*, 131-137.

[22] T. J. M. De Bruin, A. T. M. Marcelis, H. Zuilhof, L. M. Rodenburg, H. A. G. Niederländer, A. Koudijs, P. E. M. Overdevest, A. Van der Padt, E. J. R. Sudhölter, *Chirality* - submitted (Chapter 2).

[23] MicroCal Origin, 2.9, MicroCal Software, Inc., Northampton, MA, USA, 1991-1993.

[24] V. Pliska, M. Schmidt, J.-L. Fauchère, *J. Chromatogr.* **1981**, *216*, 79-92.

[25] T. J. M. De Bruin, A. T. M. Marcelis, H. Zuilhof, E. J. R. Sudhölter, *J. Phys. Chem. A* - submitted (Chapter 5).

[26] T. J. M. De Bruin, A. T. M. Marcelis, H. Zuilhof, E. J. R. Sudhölter, *Phys. Chem. Chem. Phys.* **1999**, *1*, 4157-4163 (Chapter 4).

[27] O. Yamauchi, A. Odani, *J. Am. Chem. Soc.* **1985**, *107*, 5938-5945.

Chapter

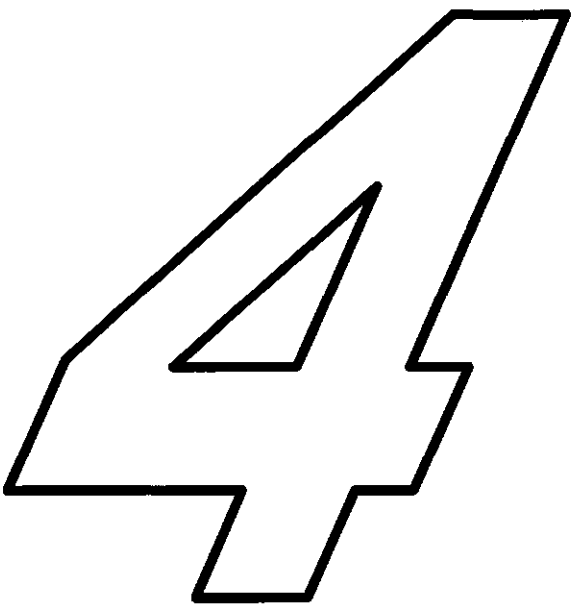

Geometry and Electronic Structure of Bis(glycinato)Cu^{II} ·2 H_2O Complexes as studied by the B3LYP Functional. A basis set study

A slightly modified version of this chapter has been published in Physical Chemistry Chemical Physics, 1999, 1, 4157-4163.

Abstract

Geometry optimizations using the density functional method B3LYP with a variety of basis sets were performed on bis(glycinato)copper(II) · 2 H_2O complexes. The geometry and electronic structure were probed with various basis sets and Natural Population Analysis. Geometry optimizations should at least be performed with the all-electron basis set 6-311+G(d,p) or with C, H, N, O = 6-311+G(d,p) and an effective core potential for Cu; spurious minima were found with smaller basis sets. Two real minima were found on these potential energy surfaces: a trans configurated complex of C_i symmetry, and a cis configurated complex with C_1 symmetry. In vacuo the trans structure is more stable by 18 kcal·mol^{-1}, which reduces to 10 kcal·mol^{-1} in a dielectric medium representing water. The final geometries strongly depend on the number of hydrogen bonds formed between the coordinating water molecules and the amino and carboxylate functionalities, as formation of such hydrogen bonds competes with axial $Cu^{II}\cdots OH_2$ interactions.

4.1 Introduction

From chapter 2 it can be seen that the measured enantioselectivities in the MEUF system vary over a wide range, and that this might point to differences in the coordination geometry and amino acid-amino acid intramolecular interactions in the complex. The coordination geometry of the Cu^{II} ion is dictated by the nature and size of the ligands, which explains the wide variety of observed coordination complexes for this metal ion: the coordination number can vary from 2 to 7 and even for a given coordination number the geometry is variable.[1] Recently, it was observed that the interactions of lysine peptides with the copper blue protein plastocyanin also lead to subtle geometrical changes.[2] This suggests that the geometry around Cu^{II} in such complexes is highly dependent on the type and size of the ligands, and thus crucial for the measured enantioselectivities. Hence, a transparent model is needed that clearly describes the interactions between Cu^{II} and (amino acid) ligands, which determine the geometry around copper in experimental systems.

X-ray crystallography may give inconclusive results on the geometry of such complexes because of the problems of correlating several different interatomic distances with short, long, or non-existent bonds.[3] Moreover, the geometry and the detailed electronic structure of the solid state complex does not need to be identical to the structure of the complex in solution due to the difference between crystal lattice and solute-solvent interactions. Recently, an X-ray absorption study was performed on Cu^{II}-glycinate complexes in aqueous solutions, but the applied EXAFS technique could not give conclusive information about the presence of the *cis* or *trans* isomers of the bis(glycinato)$Cu^{II} \cdot 2\ H_2O$ complex.[4]

Therefore, both the geometrical and electronic structures of bis(glycinato)Cu^{II} complexes are investigated by computational means. Although a lot of work has been done on copper species using molecular mechanics,[5-11] important features are difficult to describe with empirical methods: (i) the wide variety of copper coordination geometries, (ii) the facile ligand exchange, and (iii) the accommodation of electronic effects (*e.g.*, *trans* and *cis* configurations, Jahn-Teller distortions).[12] The problems related to describe the interactions between the Cu^{II} ion and amino acid ligands, and of the plasticity of Cu^{II} complexes with molecular modeling, prompted us to describe these complexes with density functional theory (DFT)[1]. Various DFT methods have recently been used to obtain structural information about transition metal complexes, and are found to yield results that are at least as good as those obtained with correlated structure methods.[13-20] Within the family of DFT methods, B3LYP has been found to represent certain aspects of Cu^{II} chemistry significantly better than

[1] For a brief historical overview and description of density functional theory see Chapter 4, Appendix 4.1.

BLYP,[21] and this method is therefore chosen in all our computations. However, there is less clarity about the size of the basis set[2] that should be used to describe these Cu^{II} complexes accurately. Recently, Scheiner *et al.* have performed a variety of DFT computations for a large number of small elements (up to 3rd row elements) to investigate the basis set dependence of the Kohn-Sham equations, and concluded that for an accurate description of geometries, basis sets of at least triple-ζ quality augmented with polarization functions are needed.[22]

Up till now only a few, for this research relevant, *ab initio* studies of bis(amino acid)Cu^{II} complexes studies have been published. A series of α-amino alkyl [Cu-bipyridyl]$^{+}$ complexes was studied in which unrestricted Hartree-Fock computations were performed with the STO-3G* basis set that was augmented with a single set of *d* polarization functions on Cu.[23] Geometry optimizations on models of blue copper proteins were performed by Ryde *et al.*[24,25] and Pierloot *et al.*[26] using the B3LYP method and the double-ζ copper basis of Schäfer,[27] enhanced with diffuse *p*, *d* and *f* functions and 6-31G* basis sets for the other atoms. More recently, Flock *et al.* used the same basis sets for their theoretical study on the interconversion of O_2-binding dicopper complexes.[28]

In this chapter the first part of high level theoretical investigations of both the geometry and electronic structures of bis(amino acid)Cu^{II} complexes are presented. Unrestricted density functional B3LYP calculations with a systematically varied series of basis sets are performed on the *cis* and *trans* isomers of bis(glycinato)$Cu^{II} \cdot 2\ H_2O$ (Figure 4.1). In addition to various all-electron basis sets, the influence of effective core potentials (ECPs) for copper is investigated as well, since this type of computation can substantially reduce the CPU time per calculation. Considering the fact that relativistic effects become more important for the heavier elements, next to a non-relativistic ECP, an ECP that includes relativistic effects is investigated as well. Although these effects are generally rather small for elements such as copper, Hertwig *et al.* concluded on their study of Cu^{I}-ethylene complexes that relativistic effects do have a notable effect on the geometry.[29]

Since the different C_α-substituents in amino acids hardly affect the electron density directly, except for C_α-substituents that can coordinate to Cu^{II}, study of these bis(glycinato)$Cu^{II} \cdot 2\ H_2O$ complexes can therefore illuminate the characteristic geometric and electronic features of this class of compounds.

---

[2] For a brief description of basis sets see Chapter 4, Appendix 4.2.

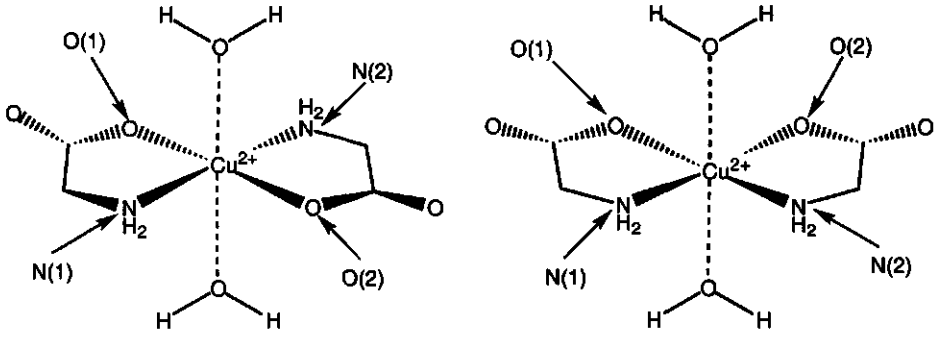

Figure 4.1. Schematic representation of *trans*-$Cu^{II}(gly)_2(H_2O)_2$ (left) and *cis*-$Cu^{II}(gly)_2(H_2O)_2$ with nomenclature N(1), N(2), O(1) and O(2) to designate specific atoms (see text).

4.2 Theoretical Methods

All computations were performed using the Gaussian 94 suite of programs,[30] with the unrestricted B3LYP method as implemented in there.[31-33] The expectation value of $\langle S^2 \rangle$ for the complexes under study was smaller than 0.755 in all cases, in very good agreement with the theoretical value of 0.75 expected for a doublet system. All basis sets used are available in Gaussian 94, apart from Bauschlicher's Atomic Natural Orbital basis for Cu, which was downloaded from the EMSL website.[34] The 6-311G notation for Cu refers to the Wachters-Hay all-electron basis set for first-row transition elements.

Since especially the coordination around copper is crucial for the amino acid-amino acid interactions, large basis sets to describe copper were used. First, a triple-ζ basis set for Cu was used (6-311G), which was augmented with either one set of polarization *f* functions, or one set of polarization *f* functions plus one *s*, one *p* and one *d* diffuse function, or 3 sets of polarization *f* functions and 1 set of polarization *g* functions.[35] Since the charge distribution within the complex places different charges on the different atoms, the use of one and the same basis set for all atoms in the complex would be ideal, *i.e.*, the inclusion of both many polarization functions for the optimal description of Cu^{II}, inclusion of diffuse functions for the description of the partially negative oxygen and nitrogen atoms, and inclusion of polarization functions on hydrogen atoms for the formation of hydrogen bonds. However, use of such basis sets would currently make geometry optimization completely unpractical. Therefore, apart from three uniform basis sets [3-21G(d,p); 6-311G(d,p); 6-311+G(d,p)], also three tailor-made basis sets were used: mixed basis set **I**: H, C, N, O = 6-31G(d,p) and Cu = 6-311G(f); subsequently denoted as Mixed **I**; mixed basis set **II**: [C, H = 6-31G(d,p); N, O = 6-311+G(d,p) and Cu = 6-311G(3fg)]; denoted as Mixed **II**; mixed basis set **III**: [C, H =

6-31G(d,p), N, O = 6-311+G(d,p) and Cu = Bauschlicher ANO]; denoted as Mixed **III**. The possibility to use ECPs was investigated with two ECPs for Cu: the non-relativistic LanL2DZ[36] and the relativistic compact effective potential (RCEP) of Stevens *et al.*[37] In combination with the 6-311+G(d,p) for C, H, N, O these tailor-made basis sets are denoted as Mixed **IV**: [C, H, N, O = 6-311+G(d,p) and Cu = LanL2DZ)]; and Mixed **V**: [C, H, N, O = 6-311+G(d,p) and Cu = RCEP], respectively. This leads to the following number of basis functions [in square brackets] for the basis sets used: 3-21G(d,p) [197]; Mixed **I** [274]; 6-311G(d,p) [334]; Mixed **IV** [358]; Mixed **II** [361]; Mixed **V** [367]; Mixed **III** [376]; and 6-311+G(d,p) [394].

The optimizations were performed in a stepwise manner using an increasing number of basis functions, *i.e.*, starting with the default guess for the smallest basis set [3-21G(d,p)]; the resulting electron density and geometry were used as starting point in the next calculation with a larger basis set. However, for the ECP calculations with LanL2DZ for Cu the starting geometry of *trans*-bis(glycinato)Cu^{II} ·2 H_2O was obtained from the optimized geometry using 3-21G(d,p); for *cis*-bis(glycinato)Cu^{II} ·2 H_2O the (Mixed **I**)–optimized geometries were used as starting structures. For the calculations using the relativistic Mixed **V** basis set, the non-relativistic Mixed **IV**-optimized geometries were used as starting geometries.

Single point computations with diffuse functions were performed with the G94 keyword SCF = tight. Vibrational frequency calculations were performed on every optimized geometry: all structures represent a minimum on the potential energy surface unless mentioned otherwise.

Single point calculations were performed to simulate the dielectric effects of an aqueous environment using the SCIPCM reaction field method,[38] with the dielectric constant ε set at 78.3, and the solute cavity defined by the isodensity surface set at 0.000400 au.

The electronic structure of each of the optimized structures was subjected to a Kohn-Sham stability analysis to assure that the optimized geometries have a ground state electronic structure (G94 keyword: stable = opt). Subsequently, the electronic structure was studied *via* the atomic charges as calculated from Natural Population Analysis.[39-41]

4.3 Results and Discussion

Geometry optimizations were performed with two distinct starting structures: a *trans* and a *cis* configuration of bis(glycinato)Cu^{II}·2 H_2O (Figure 4.1). Given the significantly increased computational demands of calculations using larger basis sets, a stepwise increase of basis

sets was used to investigate at which level an optimal compromise between accuracy (*i.e.*, full geometry convergence) and efficiency could be obtained.

4.3.1.1 Geometry *Trans complex*

Optimization of the *trans* complex at the 3-21G(d,p) level within C_i symmetry yields a chair-like structure, whereas the structure optimized without symmetry constraints has a distorted symmetry characterized by the bending of one nitrogen atom, N(2), out of the plane defined by Cu, N(1), O(1) and O(2) (Figure 4.1, in which the N(2) is drawn in the plane). The C_1 structure is more stable by 8.27 kcal·mol^{-1} (see Table 4-I for more detailed information regarding the geometry and energies). Vibrational frequency calculations show that the C_1 complex represents a minimum, whereas the C_i complex is a first order saddle point (ν_{imag} = *i*147.23 cm^{-1}). To see whether the distorted symmetry of this coordination complex is real rather than basis set-dependent artifacts, the complexes were also calculated with larger basis sets.

Table 4-I. Total energies (in Hartree) and selected distances *r* (in Å) of *trans* $Cu^{II}(gly)_2(H_2O)_2$ as optimized using unrestricted B3LYP computations with a variety of basis sets.

Entry	Basis set	S[a]	Total Energy	Cu-N(1)	Cu-N(2)	Cu-O(1)	Cu-O(2)	Cu-O_{W1}	Cu-O_{W2}
1	3-21G(d,p)	C_1	-2349.3854568	1.962	1.942	1.926	1.941	3.151	2.013
2	3-21G(d,p)	C_i	-2349.3722711	1.934	1.934	1.907	1.907	2.438	2.438
3	Mixed **I**	C_1	-2361.0874365	1.998	1.998	1.906	1.906	3.547	3.547
4	6-311G (d,p)	C_1	-2361.3182024	2.006	2.006	1.917	1.917	3.540	3.541
5	Mixed **II**	C_1	-2361.3246293	2.024	2.024	1.916	1.916	3.521	3.512
6	6-311+G(d,p)	C_1	-2361.3764998	2.035	2.035	1.932	1.932	3.562	3.562
7	Mixed **IV**	C_1	-917.0220993	2.046	2.046	1.946	1.946	3.560	3.561
8	Mixed **V**	C_1	-917.3371528	2.033	2.033	1.933	1.933	3.571	3.566

[a] S = Symmetry

The most significant result of the computations with basis set Mixed **I** (see Theoretical Methods) and larger basis sets is that full optimization in C_1 symmetry yields a structure, which is essentially identical to that obtained by optimization within C_i symmetry constraints:

bond lengths, bond angles and torsion angles are virtually identical.[3] This strongly suggests that with basis sets from Mixed **I** onwards the potential energy surface of this complex has no strongly symmetry-distorted minimum.

It is noteworthy that the water molecules shift from their coordinating axial position towards a non-coordinating position in the plane defined by Cu^{II}, N(1), N(2), O(1) and O(2), *i.e.*, during the optimization process using basis set Mixed **I** they move from the first to the second metal coordination sphere (Figures 4.1 and 4.2). The water molecule fits between the amino functionality of one glycinate and the carboxylate group of the other glycinate, and can thus form two strong hydrogen bonds: one between a hydrogen atom of the water molecule and an oxygen atom of the carboxylate [r(O-H···O) = 2.713 Å; ∠ O-H···O = 151.7°], the other between the oxygen atom of the water molecule and a hydrogen atom of the amino group [r(N-H···O) = 2.826 Å; ∠ N-H···O = 153.3°]. The formation of these hydrogen bonds is apparently more favorable than the interaction of the water molecule with Cu^{II}, leading to an equatorial position of the water molecules. Only the addition of two more water molecules leads to a hexa-coordinated copper ion. The changes in coordination geometry around Cu^{II} due to variations in the number of coordinating water molecules are described in the chapter 5.

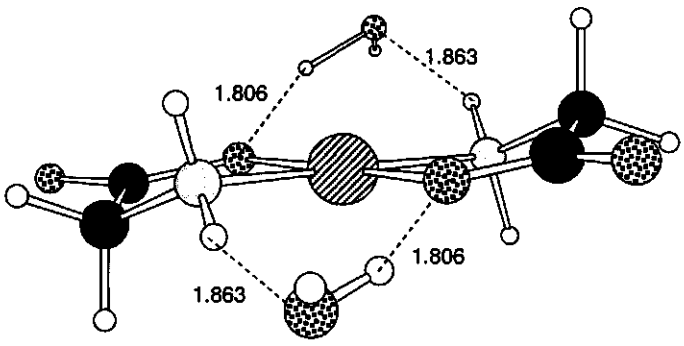

Figure 4.2. B3LYP/6-311+G(d,p)-optimized structure of *trans*-$Cu^{II}(gly)_2(H_2O)_2$ in C_i symmetry with selected geometrical features.

All optimizations with Mixed **I** and larger basis sets result in similar C_i structures. The bond lengths converge, albeit only slowly, with larger basis sets. For example, r(Cu-N(1,2)) = 1.998 Å with Mixed **I**, and this value increases gradually to 2.035 Å with the largest basis set [6-311+G(d,p)] used in the optimizations (entries 3 and 8 in Table 4-I). A similar gradual

[3] Therefore, only the structures optimized without symmetry constraints will be discussed.

increase is observed for r(Cu-O(1)): from 1.906 Å with Mixed **I** to 1.932 Å with 6-311+G(d,p). Such small differences are to be expected with the variety of basis sets used, and raise the question about their chemical significance. In order to find out whether these differences in bond lengths result in significantly different energies, the two geometries – obtained with the largest basis sets used for optimizations, Mixed **II** and 6-311+G(d,p) – are compared with each other by performing single point calculations on the two best potential energy surfaces (PES) [*i.e.*, single point calculations with the 6-311+G(d,p) and Mixed **III** basis sets]. Energy differences are computed of < 0.01 kcal·mol^{-1} between B3LYP/Mixed **III**//B3LYP/Mixed **II** and B3LYP/Mixed **III**//B3LYP/6-311+G(d,p), and of 0.32 kcal·mol^{-1} between B3LYP/6-311+G(d,p)// /B3LYP/Mixed **II** and B3LYP/6-311+G(d,p), in favor of the latter. In other words: the geometrical differences obtained from optimizations with our highest level computations do only correspond to very small energy differences. These small energy differences show that the PES is very flat around this minimum. Furthermore, the nearly constant energy difference suggests that convergence with respect to the geometry has been reached, and thus B3LYP/6-311+G(d,p) computations are of a sufficiently high level for the optimization of such complexes.

The use of the all-electron basis set 6-311+G(d,p) for copper does, however, place stringent computational constraints. Furthermore, no relativistic effects are taken into account, while these have been reported to influence the geometry of Cu^{I}-ethylene complexes [29]. Therefore, a comparison has been made in the optimization of bis(glycinato)Cu^{II} ·2 H_2O between ECPs with and without relativistic effects and the 6-311+G(d,p) all-electron basis set for copper. The application of Mixed **IV** (no relativistic effects) or Mixed **V** (relativistic effects included for Cu^{II}) yields geometries close to that obtained using 6-311+G(d,p) (Table 4-I, entry 6 *vs.* entry 7 or 8, respectively). The Cu^{II}-O(1,2) and Cu^{II}-N(1,2) bond lengths obtained with the ECPs deviate slightly (< 0.02 Å) and this leads only to a marginal increase in energy (< 0.01 kcal·mol^{-1}) on the 6-311+G(d,p) potential energy surface (PES) as compared to the geometry obtained with 6-311+G(d,p). From these data it can be concluded that 1) ECPs provide a good alternative for all-electron basis sets for Cu in the geometry optimization of the *trans*-bis(glycinato)Cu^{II} · 2 H_2O complex, and 2) that in contrast with the results of Hertwig *et al.* for Cu^{I}-alkene complexes, the incorporation of relativistic effects on Cu^{II} has only a minor effect on the final geometry of *trans*-bis(glycinato)Cu^{II} · 2 H_2O.

4.3.1.2 Geometry *Cis complex*

Like the *trans*-bis(glycinato)$Cu^{II} \cdot 2\ H_2O$ complex the *cis* complex has been optimized starting from two geometries: without symmetry (C_1) and with C_s symmetry[4] (a mirror plane through the oxygen atoms of the water molecules and the copper ion; the five-membered Cu-glycinate ring not being flat). These optimizations [3-21G(d,p) basis set] yield two different structures in which the copper complex is nearly tetrahedral (picture not shown; for geometrical details see Table 4-II). Since the geometry of the *trans* complex [C_1 symmetry, 3-21G(d,p)] drastically changed with the use of larger basis sets for the geometry optimization, both structures obtained for the *cis* complex with basis set 3-21G(d,p) were subsequently optimized with larger basis sets. Again with Mixed **I** [*i.e.*, C, H, N, O = 6-31G(d,p) and Cu = 6-311G(f)] a major change in geometry is observed: in both complexes one glycinate rotates back almost 90 degrees, returning again to a structure in which the copper complex is nearly square planar (Figure 4.3). Although large changes in geometry are observed for both the structure originally of C_1 and originally of C_s symmetry, they do not converge to the same geometry: a boat-like and a chair-like structure are obtained, respectively. The latter structure is more stable by 1.23 to 1.56 kcal·mol^{-1} (depending on the basis set used) since it has no hydrogen atoms that experience eclipsing H-H interactions like the boat-like structure (Figure 4.3a).

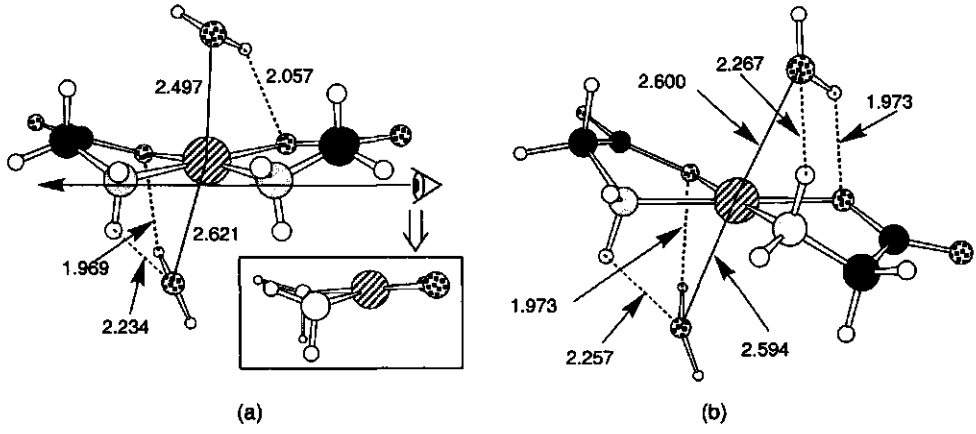

Figure 4.3. B3LYP/Mixed **I**-optimized structures of *cis*-$Cu^{II}(gly)_2(H_2O)_2$: (a) boat-like structure; (b) chair-like structure, together with selected geometrical features.

[4] The geometry was optimized without symmetry constraints since convergence problems were encountered during the optimization within C_s symmetry.

Although the boat-like structure is found at all levels up to Mixed **II**, it transforms into the *trans* geometry with the largest basis set used [6-311+G(d,p)][5] and is also absent in the ECP computation with Mixed **IV**. This boat-like structure will therefore not be discussed any further.

The two coordinating water molecules in the chair-like *cis* complex are at almost equal distances from the copper ion: 2.930 Å and 2.881 Å (Table 4-II, entry 9). Equalization of the Cu-O_w distances [compare the geometry obtained with 3-21G(d,p) and 6-311+G(d,p)] is also observed for the *trans* complex. However, in the latter case the water molecules moved away from their axial position towards the square plane to form two strong hydrogen bonds with the amino acids. In the *cis* complex the water molecules stay at their original axial position, which is probably caused by the fact that now per water molecule only one such strong hydrogen bond to an amino acid can be formed, which makes the axial interaction of Cu-O_w more beneficial. This results in a Cu-O_w bond length that is almost 0.7 Å smaller in the *cis* complex than in the *trans* complex.

Table 4-II. Total energies (in Hartree) and selected distances (r) (in Å) of *cis*-bis(glycinato)$Cu^{II} \cdot 2$ H_2O as optimized using unrestricted B3LYP computations with a variety of basis sets.

Entry	Basis set	S [a]	Total Energy	Cu-N(1)	Cu-N(2)	Cu-O(1)	Cu-O(2)	Cu-O_{w1}	Cu-O_{w2}
1	3-21G(d,p)	C_1	-2349.3793076	1.937	1.994	1.898	1.958	3.021	2.020
2	3-21G(d,p)	C_s	-2349.3841648	1.933	1.933	1.866	1.865	2.716	2.716
3	Mixed **I**	'boat'	-2361.0600642	2.031	2.030	1.924	1.940	2.621	2.497
4	Mixed **I**	'chair'	-2361.0625537	2.025	2.024	1.929	1.929	2.600	2.594
5	6-311G(d,p)	'boat'	-2361.2907830	2.041	2.040	1.936	1.954	2.573	2.518
6	6-311G(d,p)	'chair'	-2361.2929857	2.036	2.036	1.945	1.945	2.555	2.553
7	Mixed **II**	'boat'	-2361.2917500	2.069	2.034	1.909	1.975	2.870	2.496
8	Mixed **II**	'chair'	-2361.2937083	2.046	2.044	1.933	1.934	2.823	2.793
9	6-311+G(d,p)	'chair'	-2361.3471900	2.057	2.057	1.945	1.945	2.930	2.881
10	Mixed **IV**	'chair'	-916.9937485	2.072	2.072	1.969	1.969	2.692	2.696
11	Mixed **V**	'chair'	-917.3079035	2.058	2.058	1.950	1.950	2.741	2.740

[a] S = Symmetry

[5] This transformation takes about 2700 hours CPU time on a SGI R8000 processor.

The optimization of the chair-like structure generally yields longer Cu-N(1,2) and Cu-O(1,2) bonds with larger basis sets: the Cu-N(1/2) bond lengths increases from 2.024/2.025 Å (Mixed **I**) to 2.057 Å [(6-311+G(d,p)], while the Cu-O(1,2) bond increases from 1.929 Å (Mixed **I**) to 1.945 Å [6-311+G(d,p)]. Just as in the case of the *trans* complex, single point calculations were performed with the best two geometries [obtained with Mixed **II** and 6-311+G(d,p)] on the two best potential energy surfaces [Mixed **III** and 6-311+G(d,p)] to investigate whether such bond enlargements lead to significantly different potential energies. These computations: B3LYP/Mixed **III**//B3LYP/Mixed **II** and B3LYP/Mixed **III**//B3LYP/ 6-311+G(d,p) yield a difference of 0.18 kcal·mol^{-1} in favor of the latter, and a difference of 0.37 kcal·mol^{-1} between B3LYP/6-311+G(d,p)//B3LYP/Mixed **II** and B3LYP/6-311+G(d,p), in favor of the latter. Use of Mixed **IV** (no relativistic effects) *vs.* 6-311+G(d,p) leads to a small elongation of the Cu-N(1,2) and Cu-O(1,2) bond lengths and a small shortening of r(Cu-O_w) is observed. However, this hardly affects the potential energy, as can be concluded from the energy difference of only 0.29 kcal·mol^{-1} between B3LYP/6-311+G(d,p)/ /B3LYP/Mixed **IV** and B3LYP/6-311+G(d,p) in favor of the latter. Similar single point calculations performed on the (Mixed **V**)-optimized structure with 6-311+G(d,p) show a very small increase in energy: < 0.01 kcal·mol^{-1}.

These small energy differences show again that the PES is very flat around this minimum[6] and the nearly constant energy difference suggests that convergence with respect to the minimum-energy geometry has been reached. The computations with ECPs yield virtually the same minima as with the all-electron basis set 6-311+G(d,p). Additionally, it can be concluded that the inclusion of relativistic effects on Cu^{II} gives rise to small geometrical changes of bis(glycinato)Cu^{II} ·2 H_2O (Δr < 0.02 Å), in contrast with the larger geometrical changes computed for Cu^{I}-ethylene complexes.[29] The influence of relativistic effects on the total energy is negligible as well. Since the ECP calculations substantially reduce the CPU time (about a factor 1.5 for systems of this size), the use of ECPs in Cu^{II} computations on such large systems is recommended.

4.3.2 Environmental effects

The energy difference of 18.39 kcal·mol^{-1} between the *trans* and the *cis* isomers in favor of the former strongly suggests that the *trans* structure is the only isomer present at room

[6] This is additionally supported by the fact that during the early stages of the optimization the convergence criteria concerning the maximum force and root mean square force are already met, whereas the maximum displacement and root mean square displacement are still very large.

temperature. However, this gas-phase number may not be representative for experiments in aqueous solutions. Therefore, two single point B3LYP/6-311+G(d,p) calculations were performed in which the dielectric effects of an aqueous environment are simulated using a self-consistent reaction field approach, SCIPCM. These computations yield an energy difference that is decreased to 10.15 kcal·mol^{-1}. This decrease in energy difference prompted us to do a full geometry optimization in this dielectric medium for the *cis* isomer. Importantly, in such medium the energy of the thus optimized *cis* isomer does not drop below the energy of the single point calculation of the *trans* isomer (in its gas-phase geometry). Therefore, the *trans* isomer will be the most stable isomer in aqueous solutions as well, in agreement with differential scanning calorimetry experiments.[42] Both these data strongly suggests that the *trans* isomer is the major occurring isomer and that probably the *trans* isomer was investigated in the EXAFS study on Cu^{II}-glycinate complexes in aqueous solutions.[4]

4.3.3 NPA Charges

Atomic charges using the Natural Population Analysis (NPA) procedure were computed to investigate the electronic structure of the optimized structures. Firstly, the basis set dependence is investigated by comparison of the charges obtained with Mixed **I** and those with B3LYP/6-311+G(d,p)//B3LYP/Mixed **I**. Secondly, the effect of geometrical changes of the complexes is studied by comparison of the charges in the geometries obtained with Mixed **I** and 6-311+G(d,p). The NPA charges were calculated for the amino acid N and O atoms coordinating to Cu^{II} [N(1), N(2), O(1) and O(2); Figure 4.1] and for Cu^{II} itself for both the *trans* and the *cis* complexes (Table 4-III).

The basis set dependence is negligible for Cu^{II} and for the oxygen atoms, but the NPA charges on N(1) and N(2) (Table 4-III, entries 2 and 3) show a slight basis set dependence: a difference of 0.087 is observed between the charges calculated for the optimized structure obtained with Mixed **I** (-0.985), the smallest basis set in this study, and that computed using the largest basis set used, *i.e.*, B3LYP/6-311+G(d,p)//B3LYP/Mixed **I** (-0.898). A similar basis set dependence is observed for the *cis* chair-like complex (Table 4-III, entries 7 and 8): -0.981 (Mixed **I**) and -0.887 (6-311+G(d,p)//Mixed **I**). Apparently, going from a double-ζ basis set (Mixed **I**) to a triple-ζ basis set with the addition of diffuse functions has, surprisingly, more effect on the nitrogen atom than on the oxygen atom, since the charges on the latter are more or less unaffected (-0.867 *vs.* -0.883, Table 4-III, entries 4 and 5).

Table 4-III. Selected NPA charges of *trans* and *cis*-bis(glycinato)Cu^{II} ·2 H_2O (C_1 symmetry).

Entry	Atom	Mixed I	6-311+G(d,p) / Mixed I	6-311G(d,p)	6-311+G (d,p)	Mixed IV	Mixed V
trans							
1	Cu	1.320	1.290	1.334	1.291	1.276	1.294
2	N(1)	-0.985	-0.898	-0.915	-0.891	-0.892	-0.893
3	N(2)	-0.985	-0.898	-0.915	-0.891	-0.892	-0.893
4	O(1)	-0.867	-0.883	-0.881	-0.879	-0.875	-0.881
5	O(2)	-0.867	-0.883	-0.881	-0.879	-0.875	-0.881
cis							
6	Cu	1.372	1.329	1.392	1.306	1.315	1.319
7	N(1)	-0.981	-0.887	-0.907	-0.891	-0.892	-0.893
8	N(2)	-0.981	-0.887	-0.907	-0.892	-0.892	-0.893
9	O(1)	-0.836	-0.838	-0.846	-0.833	-0.828	-0.837
10	O(2)	-0.836	-0.838	-0.846	-0.833	-0.828	-0.837

The comparison of the NPA charges calculated with 6-311G(d,p) and the larger 6-311+G(d,p) basis yields very similar charges for Cu^{II}, N and O in both the centrosymmetric *trans* structure and the chair-like *cis* structure. This suggests that basis set saturation has nearly been reached for the description of the electronic structure of the optimized geometries.

The effect of the increase in Cu-N(1,2) and Cu-O(1,2) bond lengths is investigated by comparing the NPA charges of the *trans* complex optimized with Mixed **I**, and as optimized with 6-311+G(d,p). In both cases the electronic structure is calculated with the same [6-311+G(d,p)] basis set to eliminate basis set dependencies. For Cu^{II}, N and O only minor changes in the NPA charges are calculated: 1.290 *vs.* 1.291, -0.898 *vs.* -0.891, and -0.867 *vs.* -0.879, respectively. This suggests that the small increases in the Cu-N(1,2) and Cu-O(1,2) bond lengths that are observed with increasing basis sets are not reflected on the NPA charges. A similar trend can be seen with the chair-like structure: calculations with increasing basis sets generally result in a slight increase in the Cu-N(1,2) and Cu-O(1,2) bond lengths, but this has almost no effect on the NPA charges. Comparison of the data obtained *via* B3LYP/6-311+G(d,p) single point calculations for the geometries resulting from the use

of Mixed I and 6-311+G(d,p) yields differences of -0.023, 0.004 and 0.005 for Cu^{II}, N(1) and O(1), respectively (Table 4-III, entries 6, 7 and 9). From these observations it can be concluded that the small geometrical changes due to elongation of the Cu-N(1,2) and Cu-O(1,2) bonds do not have any significant effect on the electronic structure as observed *via* the NPA charges on Cu^{II}, nitrogen and oxygen.

The use of both relativistic and non-relativistic ECPs (columns 6, 7 and 8) yields almost exactly the same NPA charges as use of 6-311+G(d,p): all deviations are ≤ 1 %. Consequently, the use of ECPs does not affect the NPA charges, and these ECP basis sets are therefore a very good alternative for the larger 6-311+G(d,p) basis set.

4.4 Conclusions

Geometry optimizations on *cis* and *trans*-bis(glycinato)$Cu^{II} \cdot 2\ H_2O$ were performed with B3LYP density functional theory and a variety of basis sets. Optimizations should at least be performed with the all-electron basis set 6-311+G(d,p), or with the effective core potential LanL2DZ for Cu^{II} in combination with the 6-311+G(d,p) basis set for the elements C, N, O and H. This yields two minima: a *trans* centrosymmetric geometry and a *cis* chair-like geometry; it should be noted that spurious minima were found with smaller basis sets. In contrast to a previous study on Cu^{I}-alkene complexes, the effects of the incorporation of relativistic effects in the basis set of Cu (RCEP basis set) were found to be small: the resulting geometries are not significantly different from those obtained with a non-relativistic ECP (LanL2DZ) or the 6-311+G(d,p) basis set.

The final geometries are strongly influenced by the number of hydrogen bonds formed: each of the two coordinating water molecules can form two hydrogen bonds in the centrosymmetric structure, and only one hydrogen bond in the *cis* complex. The *trans* isomer is in the gas phase calculated to be *ca.* 18 kcal·mol^{-1} more stable than the *cis* isomer, and *ca.* 10 kcal·mol^{-1} more stable in a dielectric medium with $\varepsilon = 78.3$ (to mimic the dielectric effects of water). This suggests that, in line with experiments, the *trans* structure is in aqueous solution more stable than the *cis* isomer.

Comparative studies with increasing basis sets of the energy and charge distribution (NPA charges) of the optimized geometries show that basis set saturation has been nearly reached with 6-311+G(d,p). The highly efficient ECPs for Cu yield virtually the same geometries, energies and NPA charges as the bigger 6-311+G(d,p) basis set. To investigate the wide variety of experimentally observed structures of bis(amino acid)Cu^{II} complexes with DFT

methods such as B3LYP, the application of an ECP (LanL2DZ) for Cu is therefore recommended.

References & Notes

[1] For a list of examples see in F. Wiesemann, S. Teipel, B. Krebs and U. Höweler, *Inorg. Chem.*, 1994, **33**, 1891-1898 ref. 15.

[2] S. Hirota, K. Hayamizu, M. Endo, T. Hibino, T. Takabe, T. Kohzuma, O. J. Yamauchi, *J. Am. Chem. Soc.* **1998**, *120*, 8177-8183.

[3] K. M. Mackay, R. A. Mackay. In *Introduction to Modern Inorganic Chemistry*, 4 ed.; Blackie: Glasgow, 1989, pp 238.

[4] P. D. Angelo, E. Bottari, M. R. Festa, H. F. Nolting, N. V. Pavel, *Inorg. Chem.* **1998**, *102*, 3114-3122.

[5] J. Savolovic, K. Rasmussen, *Inorg. Chem.* **1995**, *34*, 1221-1232.

[6] B. P. Hay, *Coord. Chem. Rev.* **1993**, *126*, 177-236.

[7] R. D. Hancock, *Prog. Inorg. Chem.* **1989**, *37*, 187-291.

[8] P. V. Bernardt, P. Comba, *Inorg. Chem.* **1992**, *31*, 2638-2644.

[9] P. Comba, *Coord. Chem. Rev.* **1993**, *123*, 1-48.

[10] P. Comba, T. W. Hambley. In *Molecular Modeling of Inorganic Compounds*; VCH: Weinheim, 1995, pp 188-191.

[11] F. Wiesemann, S. Teipel, B. Krebs, U. Höweler, *Inorg. Chem.* **1994**, *33*, 1891-1898.

[12] C. R. Landis, D. M. Root, T. Cleveland. Molecular Mechanics Force Fields for Modeling Inorganic and Organometallic Compounds; VCH: New York, 1995; Vol. VI; pp 73-148.

[13] L. Roderiquez-Santiago, M. Sierka, V. Branchadell, M. Sodupe, J. Sauer, *J. Am. Chem. Soc.* **1998**, *120*, 1545-1551.

[14] M. C. Holthausen, M. Mohr, W. Koch, *Chem. Phys. Lett.* **1995**, *240*, 245-252.

[15] M. C. Holthausen, C. Heinemann, H. H. Cornehl, W. Koch, H. Schwarz, *J. Chem. Phys.* **1995**, *102*, 4931-4941.

[16] S. Niu, M. B. Hall, *J. Phys. Chem. A* **1997**, *101*, 1360-1365.

[17] M. N. Glukhovtsev, B. R. D., C. J. Nagel, *J. Phys. Chem. A* **1997**, *101*, 316-323.

[18] M. Pavlov, M. R. A. Blomberg, P. E. M. Siegbahn, R. Wesendrup, C. Heinemann, H. Schwarz, *J. Phys. Chem. A* **1997**, *101*, 1567-1579.

[19] A. Luna, B. Amekraz, J. Tortajada, *Chem. Phys. Lett.* **1997**, *266*, 31-37.

[20] I. Cacelli, D. W. Keogh, R. Poli, A. Rizzo, *J. Phys. Chem. A* **1997**, *101*, 9801-9812.

[21] E. Ruiz, P. Alemany, S. Alvarez, J. Cano, *J. Am. Chem. Soc.* **1997**, *119*, 1297-1303.

[22] A. C. Scheiner, J. Baker, J. W. Andzelm, *J. Comp. Chem.* **1997**, *18*, 775-795.

[23] C. L. Gatlin, F. Turecek, T. Vaiser, *J. Mass Spectrom.* **1995**, *30*, 1605-1616.

[24] U. Ryde, M. H. M. Olsson, K. Pierloot, B. O. Roos, *J. Mol. Biol.* **1996**, *261*, 586-596.

[25] K. Pierloot, J. O. A. De Kerpel, U. Ryde, B. O. Roos, *J. Am. Chem. Soc.* **1997**, *119*, 218-226.

[26] K. Pierloot, J. O. A. De Kerpel, U. Ryde, M. H. M. Olsson, B. O. Roos, *J. Am. Chem. Soc.* **1998**, *120*, 13156-13166.

[27] A. Schäfer, H. Horn, R. Ahlrichs, *J. Chem. Phys.* **1992**, *97*, 2571-2577.

[28] M. Flock, K. Pierloot, *J. Phys. Chem. A* **1999**, *103*, 95-102.

[29] R. H. Hertwig, W. Koch, D. Schröder, H. Schwarz, J. Hrusák, P. Schwerdtfeger, *J. Phys. Chem.* **1996**, *100*, 12253-12260.

[30] Gaussian 94, Revision D.4, M. J. Frisch, G. W. Trucks, H. B. Schlegel, P. M. W. Gill, B. G. Johnson, M. A. Robb, J. R. Cheeseman, T. Keith, G. A. Petersson, J. A. Montgomery, K. Raghavachari, M. A. Al-Laham, V. G. Zakrzewski, J. V. F. Ortiz, J. B., J. Cioslowski, B. B. Stefanov, A. Nanayakkara, M. Challacombe, C. Y. Peng, P. Y. Ayala, W. Chen, M. W. Wong, J. L. Andres, E. S. Replogle, R. Gomperts, R. L. Martin, D. J. Fox, J. S. Binkley, D. J. Defrees, J. Baker, J. P. Stewart, M. Head-Gordon, C. Gonzalez, J. A. Pople, Gaussian, Inc., Pittsburgh PA, 1995.

[31] A. D. Becke, *J. Chem. Phys.* **1993**, *98*, 5648-5652.

[32] C. Lee, W. Yang, R. G. Parr, *Phys. Rev. B* **1988**, *37*, 785-789.

[33] P. J. Stephens, F. J. Devlin, C. F. Chabalowski, M. J. Frisch, *J. Phys. Chem.* **1994**, *98*, 11623-11627.

[34] This basis set was obtained from the Extensible Computational Chemistry Environment Basis Set Database, Version 1.0, as developed and distributed by the Molecular Science Computing Facility, Environmental and Molecular Sciences Laboratory which is part of the Pacific Northwest Laboratory, P.O. Box 999, Richland, Washington 99352, USA. URL: http://wserv1.dl.ac.uk:800/emsl_pnl/basisform.html

[35] M. J. Frisch, J. A. Pople, B. J. S., *J. Chem. Phys.* **1984**, *80*, 3265-3269.

[36] P. J. Hay, W. R. Wadt, *J. Chem. Phys.* **1985**, *82*, 270-283.

[37] W. J. Stevens, M. Krauss, H. Basch, P. G. Jasien, *Can. J. Chem.* **1992**, *70*, 612-630.

[38] J. B. Foresman, T. A. Keith, K. B. Wiberg, J. Snoonian, M. J. Frisch, *J. Phys. Chem.* **1996**, *100*, 16098-16104.

[39] A. E. Reed, L. A. Curtiss, F. Weinhold, *Chem. Rev.* **1988**, *88*, 899-926.

[40] NBO, 4.0, E. D. Glendening, J. K. Badenhoop, A. E. Reed, J. E. Carpenter, F. Weinhold, Theoretical Chemistry Institute, University of Wisconsin, Madison, WI, 1996.

[41] A. E. Reed, R. B. Weinstock, F. A. Weinhold, *J. Chem. Phys.* **1985**, *83*, 735-746.

[42] B. W. Delf, R. D. Gillard, P. O'Brien, *J. Chem. Soc., Dalton Trans.* **1979**, 1301-1305.

Appendix 4.1 Introduction to Density Functional Theory

For a molecular system the total energy is found by solving the well-known Schrödinger equation:[1]

$$\hat{\mathbf{H}}\Psi = E\Psi \qquad \text{(A4.1-1)}$$

The total electronic energy E of a chemical system can be written as the sum of (a) the kinetic energy, (b) the classical nucleus-electron Coulomb interactions, and (c) the classical Coulomb electron-electron interaction. However, the classical electron-electron interaction incorrectly assumes that electrons move independently in their own field: electrons will try to avoid each other as a consequence of their mutual coulomb repulsion (expressed in the correlation energy). In addition also a purely quantum mechanical phenomenon is at work. As a consequence of the Pauli exclusion principle - which implies that no two electrons can occupy the same state - electrons with parallel spins must keep apart (expressed in the exchange energy).[2,3]

The expressions to calculate the classical electrostatic interactions are common to all quantum mechanical methods. However, the formulae used to calculate the kinetic, exchange and correlation energy are different and can be distinguished by the use of orbitals ψ_i (Hartree-Fock-based theories) and by electron density ρ (Thomas-Fermi theories).

A year after the Schrödinger paper, Thomas[4] and Fermi[5] derived a kinetic energy formula, which requires only the wavefunctions of a particle in a box. When their formula was applied to atoms and molecules, it yielded energies that were roughly 10% smaller than those obtained by Hartree using the orbital-based formula.[6] The derivation of their formula marked the birth of density functional theory for it was the first occasion on which it was shown that a non-electrostatic energy term can be expressed directly in terms of the density, without using the wavefunction. This functional[1] was improved by Von Weizsacker in 1935 and he introduced the 'original' gradient-corrected density functional.[7]

In 1951 Slater came up with the revolutionary idea to combine orbital-based and density functional theory.[8] He used the orbital-based theory expression for the kinetic energy of Hartree and the exchange functional of Dirac.[9] This 'new' Hartree-Dirac theory yielded

[1] A functional maps a function into a number. An example is the area under a curve, which is a functional of the function that defines the curve between two points.

energies that were better than with either theory. In 1964 Hohenberg and Kohn[2] proved that each of the contributions to the total energy can be expressed as a functional of the total electron energy, *e.g.* in the form of the Thomas-Fermi scheme.[10] The basic statement of the first Hohenberg-Kohn (HK) theorem is that the energy and all other electronic properties of the ground state are uniquely determined by its charge density $\rho(\mathbf{r})$. In other words, the total energy of a system in its ground state is a functional of that system's electronic density, and that any density distribution other than the true density will necessarily lead to a higher energy.[11] Thus instead of working with a complex $3N$-dimensional wavefunction describing the behavior of each electron in an N-electron system, 'only' the simple three-dimensional energy functional $E[\rho(\mathbf{r})]$ has to be minimized. Unfortunately, the exact nature of the energy functional is unknown, and approximate DFT methods need to be applied. Kohn and Sham (KS) offered a practical approach to perform DFT calculations.[12] In this KS approach, the unknown Hohenberg-Kohn energy functional, $E[\rho(\mathbf{r})]$, is partitioned in the following manner:

$$E[\rho(\mathbf{r})] = U[\rho(\mathbf{r})] + T[\rho(\mathbf{r})] + E_{xc}[\rho(\mathbf{r})] \qquad \text{(A4.1-2)}$$

$U[\rho(\mathbf{r})]$ is the classical electrostatic energy of nucleus-electron and electron-electron:

$$U[\rho(\mathbf{r})] = -\sum_A \int \frac{Z_A \rho(\mathbf{r})}{|\mathbf{r} - \mathbf{R}_A|} d\mathbf{r} + \frac{1}{2} \iint \frac{\rho(\mathbf{r}) - \rho(\mathbf{r}')}{|\mathbf{r} - \mathbf{r}'|} d\mathbf{r} d\mathbf{r}' \qquad \text{(A4.1-3)}$$

$T[\rho(\mathbf{r})]$ is the kinetic energy of a system of non-interacting electrons with the same density, $\rho(\mathbf{r})$, as the real system of interacting electrons. This seems to introduce a severe error, but corrections for the difference between $T[\rho(\mathbf{r})]$ and the true electronic kinetic energy of a system are included in $E_{xc}[\rho(\mathbf{r})]$.

Following Kohn and Sham, $\rho(\mathbf{r})$ of an N-electron system is expressed as the sum of the square moduli of singly occupied, orthonormal KS molecular orbitals:

$$\rho(\mathbf{r}) = \rho_\alpha(\mathbf{r}) + \rho_\beta(\mathbf{r}) = \sum_i^{N^\alpha} \left|\psi_i^\alpha(\mathbf{r})\right|^2 + \sum_i^{N^\beta} \left|\psi_i^\beta(\mathbf{r})\right|^2 \qquad \text{(A4.1-4)}$$

And now the kinetic energy can be defined:

$$T[\rho(\mathbf{r})] = \sum_i^{N^{\alpha,\beta}} \int \psi_i^{\alpha,\beta}(\mathbf{r}) \frac{-\nabla^2}{2} \psi_i^{\alpha,\beta}(\mathbf{r}) d\mathbf{r} \qquad \text{(A4.1-5)}$$

[2] In 1998 Walter Kohn received the Nobel prize for his development in Density Functional Theories. The prize was equally shared with John A. Pople (for his development of computational methods in quantum chemistry).

The exchange-correlation potential V_{XC}, combines all non-classical exchange and correlation interactions plus the effect of non-classical electron interaction on the kinetic energy that has been neglected in the term $T[\rho(\mathbf{r})]$. V_{XC} is defined as the functional derivative of the exchange-correlation energy with respect to the density.

$$V_{XC} = \frac{\partial E_{XC}[\rho(\mathbf{r})]}{\partial \rho} \tag{A4.1-6}$$

Finally, recalling the fact that the energy functional is minimized by the true ground state density, $\partial E[\rho(\mathbf{r})]/\partial\rho(\mathbf{r}) = 0$, and that the final functional must be stationary with respect to any variation in either of the spin densities, *i.e.*

$$\frac{\partial E[\rho(\mathbf{r})]}{\partial \rho^{\alpha}(\mathbf{r})} = \frac{\partial E[\rho(\mathbf{r})]}{\partial \rho^{\beta}(\mathbf{r})} = 0 \tag{A4.I-7}$$

this yields the one electron Kohn-Sham equation, for performing practical DFT calculations:

$$\hat{\mathbf{H}}_{KS}^{\alpha,\beta}\psi_i^{\alpha,\beta}(\mathbf{r}) = \left(-\frac{1}{2}\nabla^2 - \sum_A \frac{Z_A}{|\mathbf{r} - \mathbf{r}_A|} + \int \frac{\rho^{\alpha,\beta}(\mathbf{r})}{|\mathbf{r} - \mathbf{r}'|} d\mathbf{r}' + \frac{\partial E_{XC}[\rho(\mathbf{r})]}{\partial \rho^{\alpha,\beta}(\mathbf{r})} \right) \psi_i^{\alpha,\beta}(\mathbf{r}) = \varepsilon_i \psi_i(\mathbf{r}) \tag{A4.1-8}$$

With an initial guess at the total spin densities, $\rho^{\alpha}(\mathbf{r})$ and $\rho^{\beta}(\mathbf{r})$, the KS equations are constructed and solved, and the resulting set of KS spin-orbitals, $\{\psi_i^{\alpha,\beta}\}$, are then used to generate new guesses of $\rho^{\alpha}(\mathbf{r})$ and $\rho^{\beta}(\mathbf{r})$. This procedure is repeated until self-consistency is achieved, so the densities and KS orbitals are regenerated.

If the true exchange-correlation energy functional, $E_{xc}[\rho(\mathbf{r})]$, was known, this scheme would yield the true ground state density, and in turn, exact values for all ground state properties. But this is exactly the catch in DFT: no one knows the correct functional $E_{xc}[\rho(\mathbf{r})]$ for atoms and molecules [13]. It thus seems that no progress is made, since $E[\rho(\mathbf{r})]$ (Eq. A4.1-2) was also unknown. However, simple approximations to $E_{xc}[\rho(\mathbf{r})]$ yield already fairly accurate results.

The reason of the dilemma of not knowing the exact explicit form of $E_{xc}[\rho(\mathbf{r})]$ can be traced back to the inhomogenity of the charge distribution in molecular systems. The most obvious simplification is to neglect this by assuming a charge density that is constant or only very slowly varying with position. In this model, $E_{xc}[\rho(\mathbf{r})]$ can be expressed as a function of the exchange-correlation energy per particle, $\varepsilon_{XC}(\rho)$ and the single-particle density $\rho(\mathbf{r})$. This defines the local (spin) density approximation (LDA). To remedy some of the deficiencies inherent in the LDA scheme, some additional functionals have been introduced which

consider the gradient of the charge density, $\nabla\rho(\mathbf{r})$. The development of gradient or non-local exchange functionals is dominated by the contributions of Becke.[14,15] Non-local correlation functionals have been proposed by Perdew (P);[16] Lee, Yang, and Parr (LYP)[17] and Perdew and Yang (PY).[18]

The main error of the LDA approach originates from the improper description of exchange interactions, which can be cured to some extent by gradient corrections. Becke suggested a new approach for improving this situation by mixing 'exact' HF exchange with DFT exchange and correlation energies. These hybrid functionals achieve a highly improved accuracy. The semi-empirical weight factors assigned to the functional components are obtained from a fit to well-established experimental values. The most commonly used functional of this type, the 3-parameter functional due to Becke (B3), consists of the following mixture incorporating also non-local corrections.[19]

$$E_{XC} = 0.2E_X^{HF} + 0.8E_X^{LDA} + 0.72E_X^{B} + 1.0E_C^{LDA} + 0.81E_C^{NL} \qquad \text{(A4.1-9)}$$

The implementation of this functional usually allows different gradient-corrected functionals to be used for E_C^{NL}; the B3LYP functional as implemented in the Gaussian 94 suite of programs,[20] slightly differs form Becke's original formulation.[21]

Applicability of DFT to transition metal systems

Several systematic studies have shown that various implementations of DFT in the form of the LDA, its non-local extensions, and hybrid methods yield binding or atomization energies, equilibrium geometries, vibrational frequencies, and other properties of compounds containing main group elements that are superior to HF results when compared with experimental values.[14,19,22,23]

Because of their more complex, often open shell electronic structure, the question must be raised whether DFT are likewise suitable for transition metal systems. The difficulties in describing such systems stem mainly from electron exchange and correlation and the fact that many systems are not well described by a single Slater determinant. The exchange energy is described exactly in HF methods and the correlation problem solved approximately; in DFT both contributions are implicitly included in the exchange-correlation energy functional, albeit in an approximate manner. This can cause large errors in the total energies, but since only energy differences are in most cases of interest, these errors cancel to a larger extent. However, in transition metal compounds the electronic structure often drastically changes *e.g.*

upon bond-breaking, which can result in substantial errors, especially for open shell situations like Cu^{II}. Wavefunction-based strategies are facing similar difficulties in such situations, although this often occurs to a smaller extent.[24]

The fact that Hohenberg-Kohn theorem applies only to ground states and that a many-electron wavefunction is not defined in DFT, makes it difficult to assign a particular state symmetry. The only practical way out known so far is to take the Slater determinant built from the Kohn-Sham (KS) orbitals, which actually represents the wavefunction for the non-interacting system, and use this as if it were the actual wavefunction of the real interacting system. Similarly, in an open shell situation the unrestricted variant of the KS formalism is often used. As in unrestricted HF theory an $\langle S^2 \rangle$ expectation value can be computed from the KS Slater determinant. It turns out that spin contamination in DFT is much less of a problem than in the corresponding unrestricted HF case. However, it is an unsolved question what relevance this expectation value has for the unknown wavefunction of the real system.

In spite of all the above-mentioned disadvantages, DFT has a major advantage over HF methods, which makes it a very attractive technique.[25] The efficiency of DFT is manifested in the formal N^3 scaling of the computational demand with the number of basis sets,[3] N, whereas the computational demand of HF-methods with similar accuracy scale at least with the fifth power of N.

References

[1] E. Schrödinger, *Ann. Physik* **1926**, *79*, 361-376.

[2] J. Coomer. DFT for beginners. http://newton.ex.ac.uk/people/coomer/dft_intro.html.

[3] P. W. Atkins, R. S. Friedman. In *Molecular Quantum Mechanics*; Oxford University Press: Oxford, 1997, pp 218-221.

[4] L. H. Thomas, *Proc. Camb. Phil. Soc.* **1927**, *23*, 542-548.

[5] E. Fermi, *Accad. Lincei* **1927**, *6*, 602-607.

[6] P. M. W. Gill. Density Functional Theory (DFT), Hartree–Fock (HF) and the Self-consistent Field. In *Encyclopedia of Computational Chemistry*; P. von Ragué Schleyer, P. R. Schreiner, N. L. Allinger, T. Clark, J. Gasteiger, P. Kollman, H. F. Schaefer III, Eds.; J. Wiley & Sons: Chichester, 1998; pp 675-689.

[7] C. F. Von Weizsacker, *Z. Physik* **1935**, *96*, 431-458.

[8] J. C. Slater, *Phys. Rev.* **1951**, *81*, 385-390.

[9] P. A. M. Dirac, *Proc. Camb. Phil. Soc.* **1930**, *26*, 376-385.

[10] P. Hohenberg, W. Kohn, *Phys. Rev. B* **1964**, *136*, 864-871.

[3] For a brief description of basis sets see Chapter 4, Appendix II.

[11] A. St-Amant. Density Functional Methods in Biomolecular Modeling. In *Reviews in Computational Chemistry*; VCH: New York, 1996; Vol. 7; pp 217-259.

[12] W. Kohn, L. J. Sham, *Phys. Rev. A* **1965**, *140*, 1133-1138.

[13] W. Koch, R. H. Hertwig. Density Functional Theory Applications to Transition Metal Problems. In *Encyclopedia of Computational Chemistry*; P. von Ragué Schleyer, P. R. Schreiner, N. L. Allinger, T. Clark, J. Gasteiger, P. Kollman, H. F. Schaefer III, Eds.; J. Wiley & Sons: Chichester, 1998; Vol. 1; pp 689-700.

[14] A. D. Becke, *Int. J. Quantum Chem.* **1983**, *23*, 1915-1922.

[15] A. D. Becke, *Phys. Rev. A* **1988**, *38*, 3098-3100.

[16] J. P. Perdew, *Phys. Rev. B* **1986**, *33*, 8822-8824.

[17] C. Lee, W. Yang, R. G. Parr, *Phys. Rev. B* **1988**, *37*, 785-789.

[18] J. P. Perdew, Y. Wang, *Phys. Rev. B* **1992**, *45*, 13244-13249.

[19] A. D. Becke, *J. Chem. Phys.* **1993**, *98*, 5648-5652.

[20] Gaussian 94, Revision D.4, M. J. Frisch, G. W. Trucks, H. B. Schlegel, P. M. W. Gill, B. G. Johnson, M. A. Robb, J. R. Cheeseman, T. Keith, G. A. Petersson, J. A. Montgomery, K. Raghavachari, M. A. Al-Laham, V. G. Zakrzewski, J. V. F. Ortiz, J. B., J. Cioslowski, B. B. Stefanov, A. Nanayakkara, M. Challacombe, C. Y. Peng, P. Y. Ayala, W. Chen, M. W. Wong, J. L. Andres, E. S. Replogle, R. Gomperts, R. L. Martin, D. J. Fox, J. S. Binkley, D. J. Defrees, J. Baker, J. P. Stewart, M. Head-Gordon, C. Gonzalez, J. A. Pople, Gaussian, Inc., Pittsburgh PA, 1995.

[21] P. J. Stephens, F. J. Devlin, C. F. Chabalowski, M. J. Frisch, *J. Phys. Chem.* **1994**, *98*, 11623-11627.

[22] T. Ziegler, *Chem. Rev.* **1991**, *91*, 651-667.

[23] R. H. Hertwig, W. Koch, *J. Comp. Chem.* **1995**, *16*, 576-585.

[24] V. Hrouda, P. Cársky, M. Ingr, Z. Chval, G. N. Sastry, T. Bally, *J. Phys. Chem. A* **1998**, *102*, 9297-9307.

[25] S. Niu, M. B. Hall, *Chem. Rev.* **2000**, *100*, 353-406.

Appendix 4.2 Basis sets

In Appendix 4.1 it was described how the exact Hamiltonian can be approached. However, there is also a molecular wavefunction needed to solve the Schrödinger equation (Eq. A4.1-1) in order to calculate the energy of an atomic or a molecular system. The set of one-electron wavefunctions used to build molecular orbital wavefunctions is called the basis set. Although any basis set that sufficiently spans the space of electron distribution could be used, the concept of Molecular Orbitals as Linear Combinations of Atomic Orbitals (LCAO) by Mulliken in 1935 suggests a very natural set of basis functions: atomic orbital-type functions centered on each nucleus.[1] Early on, the Slater Type Orbitals (STOs) were used as basis functions due to their similarity to atomic orbitals of the hydrogen atom.

$$\phi_{n\ell m}(r,\theta,\phi) = N \cdot R_n(r) \cdot Y_{\ell m}(\phi,\theta) \qquad R_n(r) = r^{n-1} e^{-\zeta r} \tag{A4.2-1}$$

where N is a normalization constant and ζ is called the 'exponent'. The r, θ, and ϕ are spherical coordinates, and $Y_{\ell m}$ is the angular momentum part to describe the shape; n, ℓ, and m are the principal, angular momentum and magnetic quantum numbers, respectively. The radial part of such orbitals is an exponentially decaying function. Basis orbitals of this type are called Slater-type orbitals (STO). For practical calculations they have the disadvantage that evaluation of integrals involving such functions is time-consuming. Therefore, to accelerate computations,[1] these orbitals are approximated by a linear combination of Gaussian basis functions;[2] the radial part (R_n) is replaced by:

$$R_n(r) = e^{-\alpha r^2} \tag{A4.2-2}$$

The so-called minimal basis sets have one basis function per two inner shell electrons and one basis function for each valence atomic orbital. For example, for second-row elements there are in total 5 basis functions resembling the 1s, 2s, $2p_x$, $2p_y$, $2p_z$ atomic orbitals. To increase the flexibility of the SCF wavefunction one can increase the number of basis functions per atomic orbital. In a double-ζ basis set there are two functions for each atomic orbital: one which is closer to the nucleus, the other allowing for electron density to move away from the

[1] Even if one uses 10 Gaussian type functions to represent an STO, one still calculates the integrals much faster than if the original STOs are used.

[2] Sometimes these functions are called Gaussian Type Orbitals (GTOs). This is a misnomer, since they are not really orbitals: they are simply functions. Nowadays they are frequently called Gaussian primitives.

nucleus. For second-row elements this gives 1s, 1s', 2s, 2s', 2px, 2px', 2py, 2py', 2pz, 2pz' basis functions.

Since valence orbitals of atoms are more affected by forming a bond than the inner (core) orbitals, more basis functions should be assigned to describe valence orbitals. This prompted the development of split-valence basis sets. Split-valence basis sets use two (or more) basis functions for each valence atomic orbital, but only one function for each inner-shell (core) atomic orbital. Some well-known examples of split-valence double-ζ basis sets are 3-21G, 6-31G and an example of a split-valence triple-ζ basis set is 6-311G.[3]

The next step in improving the basis set is the augmentation of polarization functions. When atomic orbitals are mixed to form molecular orbitals the symmetry of the atomic orbital is lowered. This is best accomplished by adding basis functions of higher angular momentum quantum number (Figure A4.2-1).

Figure A4.2-1. The spherical 1s orbital on hydrogen is mixed in an orbital with p symmetry. The positive lobe at one side increases the value of the orbital while the negative lobe at the other side decreases the orbital. The orbital has overall 'moved' sideways: it has been polarized.

For example, the basis set 6-31G(3df,pd) adds 3 *d*-type functions and 1 *f*-type function to atoms second and third row elements and one *p*-type and one *d*-type function to H and He.

In some cases the normal basis functions are not adequate. This is particularly the case in excited states, in anions, or atoms with lone pairs where the electronic density is more spread. Such stretched-out densities are described by so-called diffuse basis functions, and they are denoted with a '+' sign.

It was known for a long time that core (inner) orbitals are in most cases not affected significantly by changes in chemical bonding.[2] This prompted the development of Effective Core Potential (ECP) approaches,[3] which allow treatment of inner shell electrons as if they were some averaged potential rather than actual particles. The core potentials are usually specified for shells that are filled. For the rest of the electrons, *i.e.*, valence electrons, special

[3] For example, in a 6-311G basis set for oxygen there are 13 basis functions and 26 primitive Gaussian functions: the core 1s orbital is described by 1 basis function (*i.e.* 6 primitive Gaussian functions are contracted to one basis function), plus 3 functions for each of the valence 2s and $2p_{x,y,z}$ orbitals (the first function is a contraction of 3 primitives).

basis functions are needed that are optimized for use with a specific ECP.[4-10] ECPs are not orbitals but modifications of a hamiltonian, and as such they are very efficiently calculated. Relativistic effects, which are crucial to describe the heavier atoms well, are relatively easily incorporated into ECPs, whereas all-electron relativistic computations are very time-consuming. Consequently, ECPs simplify calculations and at the same time make them more accurate as compared to all-electron non-relativistic computations.

References

[1] R. S. Mulliken, *J. Chem. Phys.* **1935**, *3*, 375-378.

[2] J. K. Labanowski. Simplified Introduction to ab initio basis sets. Terms and Notation. http://www.chem.utas.edu.au/staff/yatesb/honours/modules/mod5/jan_basis.html.

[3] T. R. Cundari, M. T. Benson, M. L. Lutz, S. O. Sommerer. Effective Core Potential Approaches to the Chemistry of the Heavier Elements; VCH: New York, 1996; Vol. 8; pp 145-202.

[4] D. Andrae, U. Haussermann, M. Dolg, H. Stoll, H. Preuss, *Theor. Chim. Acta* **1991**, *78*, 247-266.

[5] P. Durand, J.-C. Barthelat, *Theor. Chim. Acta* **1975**, *38*, 283-302.

[6] P. J. Hay, W. R. Wadt, *J. Chem. Phys.* **1985**, *82*, 270-283.

[7] M. M. Hurley, L. F. Pacios, P. A. Christiansen, R. B. Ross, W. C. Ermler, *J. Chem. Phys.* **1986**, *84*, 6840-6853.

[8] L. F. Pacios, P. A. Christiansen, *J. Chem. Phys.* **1985**, *82*, 2664-2671.

[9] W. J. Stevens, H. Basch, M. Krauss, *J. Chem. Phys.* **1984**, *81*, 6026-6033.

[10] W. R. Wadt, P. J. Hay, *J. Chem. Phys.* **1985**, *82*, 284-298.

Chapter

Hydrated Bis(glycinato)Cu^{II} Complexes as studied by the B3LYP Functional. On the Problems of Accurate Molecular Mechanics Computations

A slightly modified version of this chapter has been submitted for publication in the Journal of Physical Chemistry A.

Abstract

Geometry optimizations were performed on bis(glycinato)$Cu^{II} \cdot n\ H_2O$ ($n = 0 - 4$) complexes using B3LYP density functional calculations. The resulting geometries strongly depend on the number of hydrogen bonds formed between the coordinating water molecules and the amino and carboxylate functionalities, as formation of such hydrogen bonds competes with axial $Cu^{II} \cdots OH_2$ interactions. The trans isomer is computed to be more stable than the corresponding cis isomer, independent of the number of coordinating water molecules.

The electronic structure, as obtained from natural population analysis charges for Cu^{II} and directly coordinated O and N atoms, is nearly independent of the cis/trans isomerism and variation in the number of coordinating water molecules. This is in sharp contrast to the electrostatic potential-derived (ESP) charges calculated with the well-known methods CHELPG, Merz-Singh-Kollman, and the Restrained ElectroStatic Potential model.

No uniform set of ESP charges could thus be derived for this set of complexes, as would be required for the parameterization in molecular mechanics. Therefore, it is recommended that bis(amino acid)Cu^{II} complexes, which are too large for a complete quantum chemical approach, are described with QM/MM methods in which the coordination sphere is calculated by quantum mechanics and the other parts by molecular mechanics.

5.1 Introduction

The micelle-enhanced ultrafiltration technique, as described in Chapter 2, has been proven to be very promising for obtaining enantiomer-enriched amino acid solutions. With this technique operational enantioselectivities are measured of up to 14.[1] For different amino acids the measured enantioselectivities vary over a wide range, which is likely caused by differences in the coordination geometry and intramolecular amino acid-amino acid interactions in the complex. This suggests that the geometry around Cu^{II} in such complexes is dependent on the type and size of the ligands, which will influence the measured enantioselectivities. It is known that with a fixed set of ligands significant variations in the geometry can exist. This is for example encountered in enzymes for the Cu-coordination by cysteine and methionine.[2]

Hence, an accurate model is needed to quantitatively describe the interactions between Cu^{II} and (amino acid) ligands, which determine the geometry around copper in experimental systems. Computational approaches provide an attractive manner to obtain information about the geometry and electronic structures of such Cu^{II} systems.[3-10] To describe large transition metal complexes, molecular mechanics (MM) is an appealing tool, since it is relatively fast, while alternative *ab initio* methods of sufficiently high accuracy frequently require impractically large computer resources. Numerous force fields for transition metal complexes have therefore been developed.[11-18] For the parameterization increasing amounts of X-ray and quantum chemical data are used, and precisely these efforts show that it is still difficult to obtain a parameter set that can accurately describe the wide variety of experimentally observed Cu^{II} complexes, even for a small set of ligands as occurring in the case of bis(amino acid)Cu^{II} complexes.[18]

Even density functional calculations with Becke's B88 exchange functional[19] and correlation functional of Vosko *et al.*[20] in combination with a Double Numerical Polarization basis set[21] are not sufficiently precise to obtain the relative stabilities of ternary diastereomeric bis(amino acid)Cu^{II} complexes.[22] Recently, we have shown that at least basis sets of triple-ζ quality augmented with diffuse and polarization functions, like 6-311+G(d,p), together with the better performing B3LYP functional are required for an accurate description of $Cu^{II}(gly)_2(H_2O)_2$ complexes,[23] whereas smaller basis sets yield spurious minima on the potential energy surface.

In that same study the atomic charges of these complexes were also investigated by the use two distinct methods: (a) natural population analysis (NPA),[24,25] an orbital-based method to investigate the electronic structure of the complexes, and (b) charges derived from the

electrostatic potential. Since atomic charges cannot unambiguously be determined, neither by experiments nor by quantum mechanical calculations, many methods for the computation of these charges have been suggested for various purposes.[26] Charges have also been derived from experimental observables such as electron densities of X-ray diffraction,[27,28] or ionization potentials, electron affinities and atomic radii.[29] However, most techniques derive atomic charges from quantum mechanical computations.[30]

Electrostatic potential-derived (ESP) charges are frequently used in the set of parameters of force fields like Amber and CHARMM to calculate the (inter) molecular interactions.[31,32] Such empirical methods are based on the assumption that a uniform set of atomic parameters can be used for the description of a wide variety of coordination complexes. Hence, for accurate molecular mechanics calculations on transition metal complexes (near-)constant atomic charges for both the metal and coordinating ligands with a variety of geometrical structures would be highly preferable. Recently, Hæffner *et al.* have successfully used such an approach for the parameterization of copper(I)-olefin systems.[31]

The most widely used method for the computation of ESP charges is to derive them from a least-squares fit to the electrostatic potential,[30] which can be sampled in different ways as is the case in *e.g.* CHELPG,[33] or the method of Merz-Singh-Kollman (MKS).[34,35] More recently, Bayly *et al.* introduced for this purpose the restrained electrostatic potential (RESP) model.[36] The main improvements of this model with respect to CHELPG and MKS lie in a better transferability of the charges between functional groups in related molecules, a decreased dependence of the computed charges with changes in the conformation of a molecule, and a better simulation of intramolecular interactions.

Our own preliminary ESP charge-calculations on *trans* and *cis*-$Cu^{II}(gly)_2(H_2O)_2$ using both CHELPG and MKS yielded clearly non-uniform charges on the *cis* and the *trans* isomer.[23] This might partially be caused by the difference in coordination of the two water molecules. In the *cis* complex two axially coordinating water molecules are present, whereas in the *trans* isomer they lie in the equatorial coordination plane. Hence, the question arises, whether the differences in atomic charges between *cis* and *trans* complexes are primarily caused by the *cis/trans* effect, or whether the water molecules have a major influence as well. In the first case, parameterization of bis(amino acid)Cu^{II} complexes would just require different parameter sets for *cis* and *trans* isomers, but in the second case any generally applied parameterization for empirical computations inevitably contains inaccuracies, thereby hampering MM and molecular dynamics studies using empirical force fields. In this chapter these questions will be answered by a detailed study of the geometry and electronic structure

of the *cis* and *trans* isomers of hydrated $Cu^{II}(gly)_2$ complexes (schematically depicted in Figure 5.1) in which the number of coordinating water molecules is varied from 0 to 4. Specifically, the issue will be addressed to which degree coordination by water prefers an axial or equatorial position in these complexes. In addition, the ESP charges of these complexes have been investigated by the use of the CHELPG, MKS, and RESP methods.

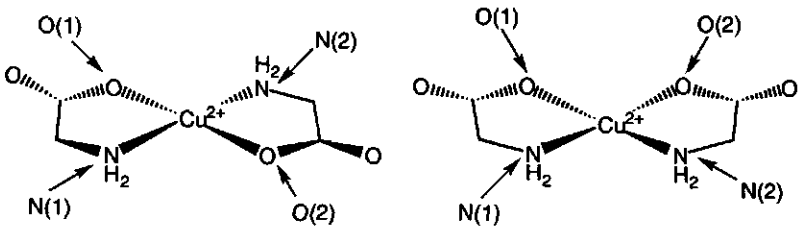

Figure 5.1. *Schematic representation of trans-*$Cu^{II}(gly)_2$ *(left) and cis-*$Cu^{II}(gly)_2$ *(right) with nomenclature N(1), N(2), O(1) and O(2) to designate specific atoms (see text).*

5.2 Theoretical Methods

All computations, unless mentioned otherwise, were performed using the Gaussian 94 suite of programs,[37] with the unrestricted B3LYP method as implemented in there.[38-40] The expectation value of $\langle S^2 \rangle$ for the complexes under study was smaller than 0.755 in all cases, and thus in good agreement with the theoretical value of 0.75 expected for a doublet system. All calculations were performed with a mixed basis set: C, H, N, O = 6-311+G(d,p) and Cu = LanL2DZ, which was previously shown to yield the best combination of accuracy and computational speed for this type of complexes.[23] Furthermore, it was concluded that relativistic effects do not have a notable effect on the final geometries, and are therefore not included in the basis sets.[23]

In this study, it is not our objective to minutely explore all minima on the multidimensional potential energy surfaces of the $Cu^{II}(gly)_2(H_2O)_n$ (n = 0 – 4) complexes. Rather we are interested in the geometrical and concomitant energy differences between the lowest energy structures found, which result from variation in the number of water molecules in the Cu^{II} coordination sphere. Since the energetic difference between different local minima due to changes in the geometry of coordinating water molecules in Cu^{II} complex is usually significant (> 3 kcal·mol^{-1})[41] the discussion is focussed only on the lowest energy structures found. To diminish the chances of ending up in a local minimum several different starting

structures were used. All geometry optimizations were performed without any symmetry constraints. A number of the mentioned stationary points was subjected to a vibrational frequency analysis to confirm that the optimized structures indeed represent a minimum on the potential energy surface.[23] Inclusion of the zero point energy did not affect the relative energies of the *cis* and *trans* complexes (< 0.2 kcal·mol^{-1}), and ZPE corrections are thus not taken into consideration in our discussion. This was a useful outcome as such frequency analyses were prohibitively expensive for the largest complexes in this study.

To check that the calculated hydration energy, which results from the stepwise addition of water molecules, is not significantly contaminated by an extra stabilization due to the basis set superposition error (BSSE), counter-poise calculations have been performed for a representative number of complexes. From these calculations the BSSE was estimated to be *ca.* 1.0 – 2.5 kcal·mol^{-1} for the coordinated water molecules with r(Cu-O_w) from 3.5 Å to 2.5 Å, respectively. These corrections are taken into account in the estimation of the water binding energies.

Single point calculations in which an aqueous environment is simulated were performed using the Self-Consistent Isodensity Polarized Continuum Model (SCIPCM) reaction field method,[42] with the dielectric constant ε set at 78.3.

Orbital-based charges were obtained from natural population analysis.[24,25,43] Electrostatic potential-derived charges were computed using the CHELPG[33] and MKS[34,35] schemes. Restrictive ESP (RESP) charges were calculated using the RESP program.[44] Since no value for the ionic radius for Cu^{II} is available in Gaussian 94, a manually added value of 2.0 Å – as recommended by Sigfridsson *et al.*[30] – was used throughout. A potential problem in ESP charge calculations is an insufficient number of grid points per unit area at which the electrostatic potential is sampled. To exclude such errors, Sigfridsson *et al.*[30] recommended to use at least 2000 grid points per atom. Therefore, a 4-fold increase of the number of grid points with respect to the implemented default values was used for the CHELPG scheme [IOp(6/42 = 4)], and a 50-fold increase for the MKS and RESP computations [IOp(6/42 = 50)]. Electrostatic points for the RESP program were generated with Gaussian 94 using the undocumented IOp(6/33 = 2) option.

5.3 Results and Discussion

5.3.1 Geometry

Geometry optimizations of the *trans* and *cis* isomers of $Cu^{II}(gly)_2(H_2O)_n$ complexes were performed with the unrestricted B3LYP method for $n = 0 - 4$ (see Figure 5.1). The lowest energy structures resulting from the geometry optimization of these complexes are depicted in Figure 5.2, together with selected geometrical features. First the geometries of all *trans* isomers will be discussed, then those of the *cis* isomers, and subsequently a comparison between the two will be made, in relation to the relative stability of these isomers.

5.3.1.1 *Trans* complexes.

The optimization of the $Cu^{II}(gly)_2$ complex without coordinating water molecules yields a structure that is essentially of C_i symmetry, in which Cu^{II} is nearly square planar coordinated (Figure 5.2a). Addition of one water molecule (W1) distorts the symmetry, however, Cu^{II} has still a near-square planar coordination (Figure 5.2b). The water molecule nicely fits between the amino functionality of one glycinate and the carboxylate group of the other glycinate. Two strong hydrogen bonds are formed: one between a hydrogen atom of the water molecule and an oxygen atom of the carboxylate [$r(O_{W1}\text{-}H\cdots O) = 2.718$ Å; $\angle\ O_{W1}\text{-}H\cdots O = 150.2°$], the other between the oxygen atom of the water molecule and a hydrogen atom of the amino group [$r(N\text{-}H\cdots O_{W1}) = 2.839$ Å; $\angle\ N\text{-}H\cdots O_{W1} = 143.9°$]. This hydrogen bond formation is also reflected in the bond lengths of the coordinating N and O atoms with Cu. In this complex the r(Cu-N) bond length has become slightly shorter (2.052 → 2.038 Å), while r(Cu-O) has increased (1.924 → 1.944 Å; Table 5-I).

Addition of a second water molecule (W2) again yields a structure with C_i symmetry in which Cu^{II} has a near square planar coordination, and both water molecules lie in the equatorial

Table 5-I. Selected interatomic distances r (Å) of B3LYP-optimized *trans*-$Cu^{II}(gly)_2(H_2O)_n$ complexes.

n H_2O	Cu-N(1)	Cu-N(2)	Cu-O(1)	Cu-O(2)	Cu-O_{W1}	Cu-O_{W2}	Cu-O_{W3}	Cu-O_{W4}
0	2.052	2.052	1.924	1.924	-	-	-	-
1	2.038	2.059	1.925	1.944	3.587	-	-	-
2	2.046	2.046	1.946	1.946	3.560	3.561	-	-
3	2.037	2.057	1.971	1.961	3.408	3.589	2.468	-
4	2.047	2.047	1.978	1.979	3.434	3.434	2.569	2.569

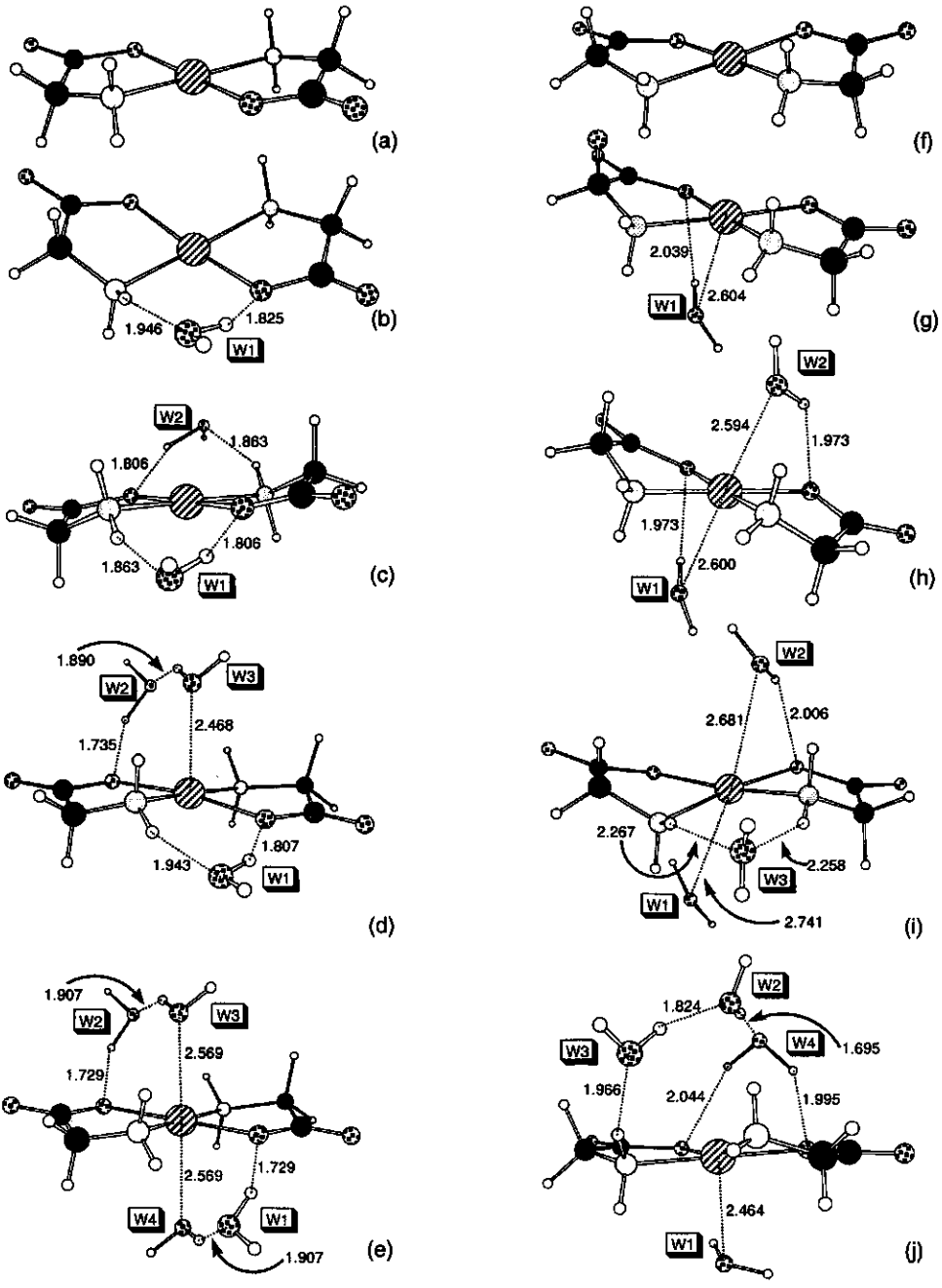

Figure 5.2. Optimized geometries of the *trans* (left) and *cis* (right) isomers of $Cu^{II}(gly)_2(H_2O)_n$ ($n = 0 - 4$) complexes with selected geometrical features.

plane (Figure 5.2c).[45] The water molecules form two strong hydrogen bonds as in *trans* $Cu^{II}(gly)_2(H_2O)$: [$r(O_{W1,2}\text{-}H\cdots O) \approx 2.713$ Å; $\angle O_{W1,2}\text{-}H\cdots O = 151.7°$], and [$r(N\text{-}H\cdots O_{W1,2}) = 2.826$ Å; $\angle N\text{-}H\cdots O_{W1,2} = 153.3°$].

In the complex with three water molecules the third water molecule (W3) occupies the axial site and forms one hydrogen bond with a water molecule in the equatorial coordination plane (Figure 5.2d), and has a relatively strong interaction with the Cu^{II} ion, as can be seen from the shorter bond lengths: $r(Cu\text{-}O_{W3}) = 2.468$ *vs.* $r(Cu\text{-}O_{W1/2}) = 3.408/3.589$ Å (Table 5-I). Water molecule W2 forms two hydrogen bonds, but in contrast with Figure 5.2c, only one with a glycinate molecule and the other with the water molecule that occupies the axial site. This latter hydrogen bond causes water molecule W2 to move out of the plane defined by Cu^{II}, N(1), N(2), O(1) and O(2).

Addition of the fourth water molecule (W4) leads to a more or less octahedral coordination of the Cu^{II} ion: two water molecules are at the axial positions and have relatively strong interactions with Cu^{II}, as can be seen from the relatively short bond lengths $r(Cu\text{-}O_{W3}) \approx r(Cu\text{-}O_{W4}) = 2.569$ Å (Figure 5.2e). The other two water molecules are located near the equatorial position $r(Cu\text{-}O_{W1,2}) = 3.434$ Å. As in the case of *trans*-$Cu^{II}(gly)_2(H_2O)_3$, the 'equatorial' water molecules (W1 and W2) form a hydrogen bond with the oxygen of the carboxylate of the glycinate, and, at the expense of a hydrogen bond with a nitrogen atom, a hydrogen bond with the nearest axial water molecule is formed.

5.3.1.2 *Cis* complexes.

The geometry optimization of the *cis* isomer without coordinating water molecules yields a structure in which Cu^{II} is square planar coordinated and the complex has a chair-like structure (see also Chapter 4, § 4.3.1.2 and Figure 5.2f).

Addition of both the first (W1) and the second (W2) water molecule results in geometries in which the water molecules are axially coordinated to Cu^{II}, yielding a near octahedral coordination of Cu^{II} for *cis*-$Cu^{II}(gly)_2(H_2O)_2$. For *cis*-$Cu^{II}(gly)_2(H_2O)$ a crystal structure is known.[46] In this structure the water molecule also occupies an axial position, whereas an oxygen atom of the carboxylate group of an another bis(glycinato)Cu^{II} complex coordinates to the other axial position. Furthermore, in the crystal structure the water molecule has additional hydrogen bonds with other bis(glycinato)Cu^{II} complexes in the unit cell. Nevertheless, the calculated structure is nearly identical to the bis(glycinato)Cu^{II} monohydrate crystal structure, as can be seen from Figure 5.3 and Table 5-II.

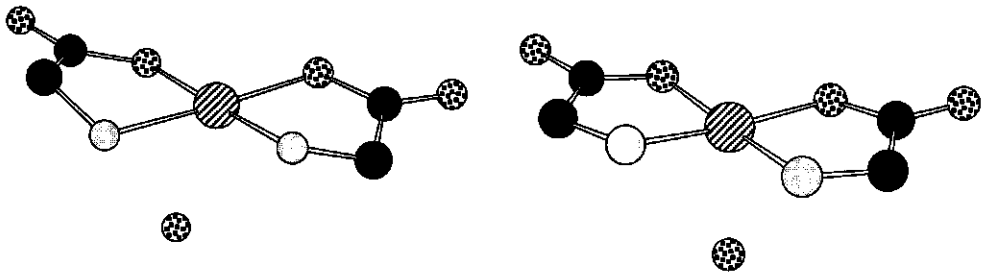

Figure 5.3. Calculated structure (left) and crystal structure (right) of *cis*-$Cu^{II}(gly)_2(H_2O)$ (hydrogen atoms not shown).

In the *cis* complex only one strong hydrogen bond per water molecule can be formed with the amino acid, which makes the axial Cu-$O_{W1,2}$ interaction energetically more attractive. This is in contrast to the corresponding *trans* structures in which the water molecules (W1 and W2) are in equatorial positions and form two strong hydrogen bonds (Figures 5.2g and 5.2h). The interatomic distances between the coordinating water molecules and the Cu^{II} ion in the *cis* $Cu^{II}(gly)_2(H_2O)$ complex are r(Cu-O_{W1}) = 2.692 Å and r(Cu-O_{W2}) = 2.696 Å, which are close to the distances of the axially coordinated water molecules in the *trans*-$Cu^{II}(gly)_2(H_2O)_4$ complex r(Cu-$O_{W3,4}$) = 2.569 Å. Note that both water molecules in the *cis*-$Cu^{II}(gly)_2(H_2O)_2$ complex point with their hydrogen atoms in the same direction due to hydrogen bond interactions with the carboxylate functionalities. This contrasts with the *trans* $Cu^{II}(gly)_2(H_2O)_4$ complex, in which the axial coordinated water molecules (W3 and W4) point their hydrogen bonds in opposite directions (Figure 5.2e).

Table 5-II. Selected interatomic distances r (in Å) of B3LYP-optimized *cis*-$Cu^{II}(gly)_2(H_2O)_n$ complexes.

n H_2O	Cu-N(1)	Cu-N(2)	Cu-O(1)	Cu-O(2)	Cu-O_{W1}	Cu-O_{W2}	Cu-O_{W3}	Cu-O_{W4}
0	2.095	2.095	1.932	1.932	-	-	-	-
1	2.081	2.087	1.967	1.938	2.604	-	-	-
1[a]	1.984	2.021	1.957	1.946	2.404			
2	2.072	2.072	1.969	1.969	2.692	2.696	-	-
3	2.057	2.058	1.977	1.976	2.681	2.741	4.072	-
4	2.055	2.072	1.988	1.978	3.415	2.464	3.660	3.141

[a] Experimental value from bis(glycinato)Cu^{II} monohydrate crystal Ref [46].

In the *cis* complex with three water molecules, the third water molecule (W3) is in an equatorial position and not coordinated to Cu^{II}, $r(Cu\text{-}O_{W3})$ = 4.072 Å. The water molecule is orientated in such a way that both lone pairs of the oxygen atom are pointing towards a hydrogen atom of the two amino groups. This strongly suggests that this water molecule is involved in two hydrogen bonds and explains the relatively long distances (~2.26 Å) between the oxygen of the water molecule and the hydrogen atoms of the amino groups (Figure 5.2i). Other characteristics of these hydrogen bonds are $r(O_{W3}\cdots H\text{-}N(1))$ = 3.169 Å; $\angle O_{W3}\cdots H\text{-}N(1)$ = 147.0° and $r(O_{W3}\cdots H\text{-}N(2))$ = 3.167 Å; $\angle O_{W3}\cdots H\text{-}N(2)$ = 148.0°.

Optimization of the *cis* complex with four water molecules does not yield an octahedral structure like the corresponding *trans* isomer (Figure 5.2j). Although the fourth water molecule (W4) was initially placed at the free equatorial position between the oxygen atom of the two carboxylate groups, after the optimization three water molecules (W2, W3 and W4) are located above the coordination plane defined by Cu^{II}, N(1), O(1) and O(2), and W1 is located below this plane. The water molecules W2, W3 and W4 form hydrogen bonds among themselves and with one amine group and the carboxylate groups. Because of these hydrogen bonds, the interaction of the axially coordinated water molecule (W2) with Cu^{II} is weakened, as can be concluded from the long bond length $r(Cu\text{-}O_{W2})$ = 3.415 Å (Table 5-II). Due to the hydrogen-bonded network Cu^{II} is not square planar coordinated: N(2) is bent out of the plane defined by Cu, N(1), O(1) and O(2). Furthermore, water molecule W1 can now approach the Cu^{II} ion more closely [$r(Cu^{II}\text{-}O_{W1})$ = 2.464 Å] than in the *cis* complex with 3 H_2O [$r(Cu^{II}\text{-}O_{W1})$ = 2.741 Å].

From the discussion of these 10 geometries (Figure 5.2a – 5.2j) it is clear that hydrogen bond formation has a major influence on the geometry of hydrated bis(amino acid)Cu^{II} complexes. In addition it is obvious that axial coordination of the water molecules is not as attractive as equatorial binding, or complexation to coordinating water molecules. This is in line with recent finding of Bérces *et al.*,[41] and will be discussed in more detail later (*vide infra*).

5.3.1.3 Comparison of *cis* and *trans* isomers.

Since we are specifically interested in the relative energy between the *cis* and *trans* isomers in relation to our MEUF experiments performed in water, calculations with a fully solvated complex would be ideal. However, such an approach is currently computationally impracticable at this level of theory. On the other hand, treatment of the water molecules present in the first and second coordination spheres of the Cu^{II} ion is computational possible

and relevant, since these water molecules have a large influence on the overall geometry of bis(glycinato)Cu^{II} complexes as can be seen from the large geometrical differences described above. These large structural variations between complexes with a varying number of coordinating water molecules lead to two questions: 1) what is the extra stabilization offered by each additionally coordinating water molecule?, and 2) to which degree does the addition of extra water molecules affect the relative stability of *cis* and *trans* isomers.

For all investigated complexes $n = 0 - 4$ the *trans* complex is more stable than the corresponding *cis* complex, as indicated in Table 5-III by the negative values for ΔE. The energy difference between *cis* and *trans* isomers increases from $n = 0$ to $n = 3$, but decreases strongly for $n = 4$. The precise value of ΔE is largely determined by two factors: a) the energetics for the complexes with $n = 0$, caused by the repulsive N-N and O-O interactions that occur to a greater extent in all *cis* isomers, and b) the number of hydrogen bonds that is formed.

In the *trans* complexes all the coordinating water molecules can form either two strong hydrogen bonds per water molecule, or one hydrogen bond and a (strong) interaction with the Cu^{II} ion. In contrast, in the corresponding *cis* complexes there is only one such hydrogen bond per water molecule. In *cis*-$Cu^{II}(gly)_2(H_2O)_3$, the water molecules mostly form weak hydrogen bonds, which results in the large ΔE value as compared to *trans*-$Cu^{II}(gly)_2(H_2O)_3$ of -20.98 kcal·mol^{-1}. However, in *cis*-$Cu^{II}(gly)_2(H_2O)_4$ the three water molecules on top of the complex form strong hydrogen bonds with each other, thereby stabilizing the complex, which results in a relatively small energy difference.

Table 5-III. Total energies (in Hartree) of *trans* and *cis*-$Cu^{II}(gly)_2(H_2O)_n$ complexes, their relative stability ΔE (kcal·mol^{-1}), and the stabilization energy of each additional water molecule (kcal·mol^{-1}).

n H_2O	E_{trans}	E_{cis}	ΔE^a	Stabilization[b] per H_2O	
				trans	*cis*
0	-764.060545	-764.039221	-13.38	-	-
1	-840.540944	-840.516974	-15.04	-12.8	-9.6
2	-917.022099	-916.993749	-17.79	-13.2	-9.5
3	-993.498072	-993.464639	-20.98	-8.5	-7.3
4	-1069.971001	-1069.956478	-9.11	-6.5	-20.0

[a] $\Delta E = E_{trans} - E_{cis}$ [b] BSSE-corrected stabilization energy (defined as $E_n - E_{n-1} - E_w - (BSSE_{n-1} - BSSE_n)$; E_w[B3LYP/6-311+G(d,p)]= -76.4584631 Hartree).

To investigate the energetic effects of coordinating water molecules, the stepwise gain in energy, or hydration energy, was calculated from $\Delta E_{hydr.} = E_n - E_{n-1} - E_w$ (in which E_n is the energy of the complex with n water molecules; E_{n-1} the complex with $n-1$ water molecules and E_w the SCF energy of a water molecule). However, if a coordinated water molecule is relatively close to atoms of the $Cu^{II}(gly)_2$ complex, *e.g.*, when a relatively short Cu-O_W distance is present, basis functions from $Cu^{II}(gly)_2$ can help to compensate for the basis set incompleteness of the coordinating water molecule (and *vice versa*). Therefore, the energy of, *e.g.*, $Cu^{II}(gly)_2(H_2O)$ can be artificially lowered, and thus the stabilization energy is overestimated.[47] This effect, known as the basis set superposition error (BSSE), has to be taken into account. The BSSE has been estimated using Counter Poise calculations, and the BSSE-corrected stabilization energies are presented in Table 5-III.

Addition of the first water molecule stabilizes the *trans* complex more than the *cis* complex. This is caused by the formation of two hydrogen bonds per water molecule, whereas in the *cis* complex only one hydrogen bond is formed, in combination with an axial Cu^{II}-O_{W1} interaction. Recently, in a quantum mechanical study on the solvation of Cu^{II} it was found that water molecules prefer equatorial hydrogen-bonded positions in Cu^{II} water clusters by 5 to 8.5 kcal·mol^{-1} as compared to the axial coordination position, in which water coordinates directly to Cu^{II}.[41] However, this energy difference is probably overestimated, since no BSSE corrections were applied, while these are likely bigger for equatorial than axial position due to the smaller Cu-O distance. Our study shows that equatorial coordination yields only 3 to 4 kcal·mol^{-1} more stabilization than axial coordination, as can be calculated from the difference in stabilization energy between the *trans* and *cis* isomers for the first two water molecules. However, there is still a preference for equatorial positions, as can be seen from the $n = 2$ complex.

The stabilization energies for the third (-8.5 kcal·mol^{-1}) and the fourth (-6.5 kcal·mol^{-1}) water molecules in the *trans* complexes are significantly smaller than for the first (-12.8 kcal·mol^{-1}) and second (-13.2 kcal·mol^{-1}) water molecules. This is caused by the fact that these water molecules coordinate at the axial positions where they only form one hydrogen bond. Moreover, the hydrogen bond is formed with the water molecule that was positioned at the equatorial site for $n = 1$ and 2. This latter water molecule is now lifted from the equatorial plane to form a hydrogen bond with an axial water molecule, but as a result its hydrogen bond to an amino acid is broken.

In the *cis* complex, the third water molecule has only relatively weak interactions with the rest of the complex and yields a hydration energy of -7.3 kcal·mol^{-1}, while the fourth water

molecule gives the highest stabilization energy of -20.0 kcal·mol^{-1}. This large stabilization is the result of the formation of three hydrogen bonds formed between the three water molecules on top of the $n = 4$ *cis* complex. Despite this large stabilization, the $n = 4$ *trans* complex still is more stable than the $n = 4$ *cis* complex (-9.11 kcal·mol^{-1}). From the data presented in Table 5-III two things can be concluded: 1) irrespective of the degree of solvation by water the *trans* structure is more stable than the *cis* isomer which is in line with experiments,[48] and 2) hydrogen bond formation dominates the relative stability of the complexes (*cis* and *trans*, n = 0 – 4).

5.3.2 Atomic Charges

For molecular mechanics and molecular dynamics computations it would be desirable to derive one uniform set of atomic charges to parameterize both *cis* and *trans* complexes with a varying number of coordinating water molecules. However, two uniform sets for a separate treatment of *cis* and *trans* complexes would, in principle, also be acceptable, as long as these would cover the wide variety of experimentally observed types of coordination around Cu^{II}. Hence, the ESP charges of Cu^{II} and directly coordinated atoms [N(1), N(2), O(1) and O(2); Figure 5.1] are of specific interest here. These ESP charges, computed with the CHELPG, MKS and RESP methods, are compared to the orbital-based NPA charges. All charges, except the RESP charges, were also calculated in a simulated aqueous medium using the SCIPCM model. Such a set of ESP charges would be of practical use, since most experimental (amino acid)Cu^{II} systems are studied in an aqueous medium. The charges obtained from the SCIPCM model and from the *in vacuo* calculations are nearly identical. Only the NPA and CHELPG charges of O(1) differ to some degree *in vacuo* and in the water-like medium, as is depicted in Figure 5.4. Therefore, it can be concluded that the NPA, CHELPG and MKS charges are nearly medium independent, and consequently only the *in vacuo* charges will be considered in the discussion below.

The charges of Cu^{II}, N(1), N(2), O(1) and O(2) are presented in Table 5-IV, and a selection thereof is graphically displayed in Figure 5.5.

From the NPA charges three conclusions can be drawn. First, the calculated charges *in vacuo* and in a water-like medium (not shown) are virtually the same, suggesting that the polarity of the medium does not affect the electron distribution within the complex significantly. Second, *cis/trans* isomerism also hardly affects these charges: the largest difference is 0.058 e^- for O(1) between *cis* 0 H_2O and *trans* 0 H_2O; Figure 5.4a and Table 5-IV. Third, variation

of the number of coordinating water molecules does not result in a significant variation in the NPA charges of Cu^{II} or any of the coordinated N or O atoms: the largest difference is 0.096 e^- for O(1) between *cis* 0 H_2O and *cis* 4 H_2O. Overall, the electronic structure around copper of all complexes under investigation is thus nearly constant despite the significant changes in geometry between the *cis* and *trans* complexes with $n = 0 - 4$.

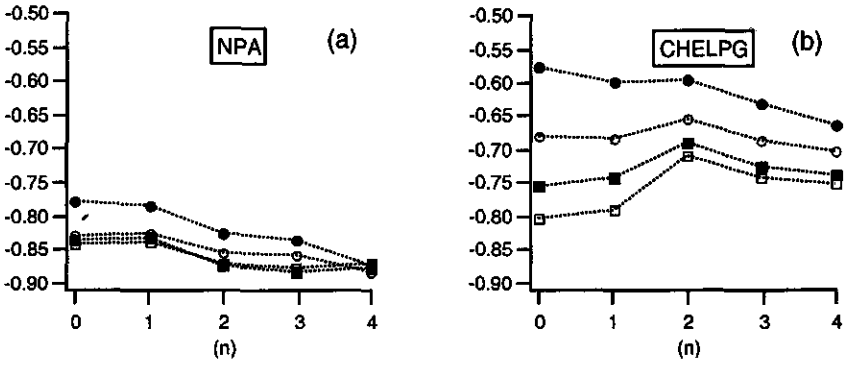

Figure 5.4. Atomic charges of O(1) using NPA and CHELPG methods. X-axis: number of coordinating water molecules, Y-axis: atomic charge/e⁻. Legend: ○ (*cis*, water); □ (*trans*, water); ● (*cis, in vacuo*); ■ (*trans, in vacuo*). Note that the dotted line connecting the data points has no physical meaning.

This constancy in electronic structures is, however, not reflected on the ESP charges (Figure 5.5 and Table 5-IV). For example, the CHELPG- and MKS-charge increases on Cu^{II} are 0.221 e^- and 0.342 e^-, respectively, in going from $n = 3$ to $n = 4$ in the *trans* complex. In contrast, the corresponding NPA charges do not change by more than 0.036 e^-. The large change in ESP values can be explained by the fact that for the complex with $n = 3$ one side of the complex is more or less open. As a result, the sampling points needed for the calculation of the ESP charges are at that side closer to Cu^{II} than in the complex with $n = 4$. This effect is absent in the NPA charges, since in this method the charges are calculated on basis of the orbital coefficients, and no sampling points are used, but it is intrinsically inevitable for ESP charge determination from grids of the electrostatic potential. The ESP charges for nitrogen show even more pronounced variations (Figure 5.5). A significant charge difference is computed between the *cis* and *trans* complex (~ 0.3 e^-, CHELPG). Furthermore, within both sets of *cis* and *trans* complexes, the computed ESP charges depend on the number of water

Table 5-IV. Atomic charges for selected atoms calculated using natural population analysis and the ESP methods: CHELPG, MKS and RESP.

		Cis				*Trans*			
n H_2O	**Atom**	**NPA**	**CHELPG**	**MKS**	**RESP**	**NPA**	**CHELPG**	**MKS**	**RESP**
0	Cu	1.257	0.595	0.556	0.553	1.268	0.579	0.655	0.653
	N(1)	-0.893	-0.504	-0.384	-0.381	-0.877	-0.169	-0.190	-0.189
	N(2)	-0.893	-0.504	-0.384	-0.381	-0.877	-0.169	-0.190	-0.189
	O(1)	-0.778	-0.577	-0.579	-0.578	-0.836	-0.756	-0.784	0.783
	O(2)	-0.778	-0.577	-0.579	-0.578	-0.836	-0.756	-0.784	-0.783
1	Cu	1.292	0.583	0.555	0.552	1.269	0.536	0.585	0.583
	N(1)	-0.889	-0.430	-0.291	-0.288	-0.891	-0.164	-0.212	-0.209
	N(2)	-0.895	-0.496	-0.372	-0.368	-0.879	-0.146	-0.156	-0.156
	O(1)	-0.785	-0.599	-0.603	-0.602	-0.832	-0.742	-0.765	-0.764
	O(2)	-0.820	-0.582	-0.590	-0.589	-0.876	-0.677	-0.681	-0.679
2	Cu	1.315	0.565	0.551	0.547	1.276	0.538	0.524	0.520
	N(1)	-0.892	-0.426	-0.288	-0.284	-0.892	-0.098	-0.063	-0.061
	N(2)	-0.892	-0.421	-0.289	-0.286	-0.892	-0.099	-0.064	-0.062
	O(1)	-0.828	-0.596	-0.607	-0.606	-0.875	-0.690	-0.679	-0.675
	O(2)	-0.828	-0.597	-0.607	-0.606	-0.875	-0.691	-0.680	-0.676
3	Cu	1.310	0.580	0.678	0.672	1.324	0.487	0.519	0.515
	N(1)	-0.897	-0.321	-0.183	-0.175	-0.890	0.045	0.005	0.004
	N(2)	-0.896	-0.318	-0.191	-0.183	-0.888	-0.096	-0.049	-0.050
	O(1)	-0.836	-0.632	-0.681	-0.679	-0.883	-0.725	-0.739	-0.736
	O(2)	-0.836	-0.635	-0.681	-0.679	-0.869	-0.611	-0.610	-0.606
4	Cu	1.309	0.645	0.680	0.673	1.360	0.708	0.861	0.830
	N(1)	-0.904	-0.313	-0.223	-0.216	-0.889	-0.031	-0.013	0.057
	N(2)	-0.898	-0.419	-0.282	-0.275	-0.889	-0.032	-0.015	0.054
	O(1)	-0.874	-0.665	-0.707	-0.705	-0.876	-0.739	-0.779	-0.789
	O(2)	-0.851	-0.676	-0.715	-0.713	-0.876	-0.739	-0.778	-0.788

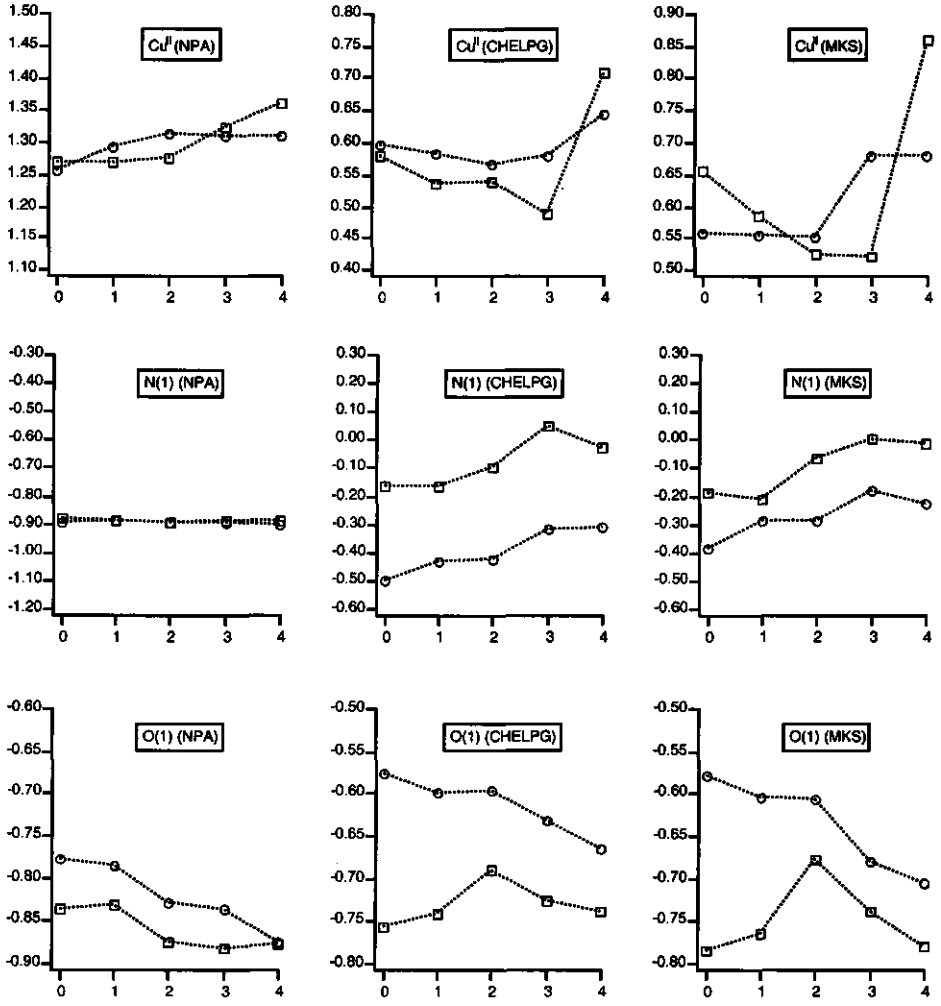

Figure 5.5. Atomic charges of the atoms Cu^{II}, N(1) and O(1), using NPA, CHELPG and Merz-Singh-Kollman (MKS) methods. X-axis: number of coordinating water molecules, Y-axis: atomic charge/e^-. Legend: O *cis*; □ *trans*. Note that the dotted line connecting the data points has no physical meaning.

molecules. For example, the CHELPG charge on N(1) in the *trans* complex changes even sign, in going from 0 H_2O (-0.169 e^-) to 3 H_2O (+0.045 e^-), and similar change takes place for the MKS charge, in going from 1 H_2O (-0.212 e^-) to 4 H_2O (+0.005 e^-). No evidence for such profound changes in the electronic structure of the complexes is found in the corresponding NPA charges.

Finally, the ESP charges of the amino acid oxygen atoms that are coordinated to the Cu^{II} ion are close to the charges based on NPA (Figure 5.5). The NPA charges are again almost unaffected by the geometrical changes occurring in going from $n = 0$ to $n = 4$; the largest being 0.096 e^-. In sharp contrast, the ESP charges show again a significant dependence on the geometry: both *cis/trans* isomerism and a varying number of water molecules yield changes up to 0.205 e^-. In addition, there are significant differences, up to ~0.1 e^-, in the CHELPG charges calculated *in vacuo* and those calculated in a water-like medium (Figure 5.4b).

The ESP charges calculated with the modified CHELPG, MKS and RESP methods are roughly the same. The more recently developed RESP model does not perform better than the older CHELPG or MKS methods for the complexes investigated.

Since the electronic structure, as studied by NPA charges, is hardly affected by variation of the number of coordinating water molecules, or *cis/trans* isomerism, the significant changes in the ESP charges are rather unexpected. It thus seems that calculated variations in ESP charges are due to fundamental limitations in the way these charges are obtained, indicating that the methods to derive these ESP charges are inferior to the NPA method. It might therefore be tempting to use the NPA charges for the parameterization in molecular mechanics (MM) calculations. Such an approach was recently applied by Sabolovic *et al.*[18] to parameterize the Coulomb interactions in their force field. However, such electrostatic interactions are, per definition, better calculated from the ESP charges, since these charges are calculated from the electrostatic potential.

Nevertheless, the lack of a set of uniform ESP charges would require different parameter sets for the *cis* and *trans* complexes studied. Even the derivation of an accurate parameter set for either *cis* or *trans* complexes will likely be troublesome, given the effects of variation of the number of coordinating water molecules on the computed ESP charges. Although these variations in atomic charges may not be exceptionally large as compared to 'normal' organic compounds, for which accurate MM calculations can be performed, MM calculations on complexes like bis(amino acid)Cu^{II} are seriously hampered. The errors in the geometries in organic compounds due to variations in the ESP atomic charges can be repaired by corrections in the bond length, bond angle terms *etc.* of the MM hamiltonian. However, such corrections are hardly possible for ionic species that (mainly) interact by non-bonded electrostatic interactions in a wide variety of coordination geometries. For accurate calculations on bis(amino acid)Cu^{II} complexes that are too large for a fully quantum chemical treatment, QM/MM methods are therefore recommended.[49-51] In such methods, the metal ion and its direct surroundings should be described by quantum mechanical methods like the

ones used in this study. On the other hand, the parts of the complex that are not directly involved in the coordination to copper can then be described by the molecular mechanics parameters developed for protein modeling.[52-57] Since molecular mechanics has been widely shown to provide accurate geometries for such non-coordinating atoms, QM/MM will likely provide a fruitful and computationally manageable approach to such large transition metal ion containing systems.

5.4 Conclusions

B3LYP computations on $Cu^{II}(gly)_2(H_2O)_n$ (n = 0, 1, 2, 3, 4) complexes show that hydrogen bond formation by the coordinating water molecules dominates the overall shape of these complexes. The *trans* isomer is computed to be more stable than the corresponding *cis* isomer for the whole range of $n = 0 - 4$, and therefore likely to be the dominant isomer in experimental systems such as the MEUF system. The magnitude of this energy difference is determined by two factors: a) the intrinsic dipolar repulsion between coordinating amino acid O and N atoms, and b) the number of hydrogen bonds formed by the coordinating water molecules.

From the calculated NPA charges it is deduced that geometrical changes such as *cis/trans* isomerism, and the number of coordinating water molecules affect the electronic structure only to a minor degree. Despite this observation, the ESP charges –derived from the CHELPG method, the Merz-Singh-Kollman scheme or the restrained electrostatic potential model– show significant geometry-dependent variations. As a result, no single set of ESP charges from these methods can be derived for the description of either *cis* or *trans*-bis(amino acid)Cu^{II} complexes, thereby hampering accurate parameterizations for molecular mechanics. Since the coordination sphere can be accurately described using quantum chemical techniques,[3,6,58-60] for Cu^{II} amino acids complexes that are too large for a completely quantum chemical approach QM/MM calculations probably offer the best compromise between chemical accuracy and computational limitations. Such an approach will, in general, be preferable for *any* transition metal complex that shows significant variations in ESP charges within the set of experimentally observed variations in geometry for that type of complex.

Acknowledgment. The Dutch National Computer Facilities Foundation (project SC-500) is thanked for the funding to use supercomputing facilities, and Ms. E. Sigfridsson and Dr. U. Ryde (Lund University) are acknowledged for valuable comments.

Notes & References

[1] T. J. M. De Bruin, A. T. M. Marcelis, H. Zuilhof, L. M. Rodenburg, H. A. G. Niederländer, A. Koudijs, P. E. M. Overdevest, A. Van der Padt, E. J. R. Sudhölter, *Chirality* - submitted (Chapter 2).

[2] K. Pierloot, J. O. A. De Kerpel, U. Ryde, M. H. M. Olsson, B. O. Roos, *J. Am. Chem. Soc.* **1998**, *120*, 13156-13166.

[3] J. Bertrán, L. Rodríguez-Santiago, M. Sodupe, *J. Phys. Chem. B* **1999**, *103*, 2310-2317.

[4] T. Lind, P. E. M. Siegbahn, R. H. Crabtree, *J. Phys. Chem. B* **1999**, *103*, 1193-1202.

[5] C. L. Gatlin, F. Turecek, T. Vaiser, *J. Mass Spectrom.* **1995**, *30*, 1605-1616.

[6] K. Pierloot, J. O. A. De Kerpel, U. Ryde, B. O. Roos, *J. Am. Chem. Soc.* **1997**, *119*, 218-226.

[7] J. O. A. De Kerpel, K. Pierloot, U. Ryde, B. O. Roos, *J. Phys. Chem. B* **1998**, *102*, 4638-4647.

[8] A. Bérces, *Inorg. Chem.* **1997**, *36*, 4831-4837.

[9] K. Tanaka, H. Johansen, *Int. J. Quantum Chem.* **1997**, *64*, 453-458.

[10] C. J. Calzado, J. F. Sanz, *J. Am. Chem. Soc.* **1998**, *120*, 1051-1061.

[11] M. Zimmer, *Chem. Rev.* **1995**, *95*, 2629-2649.

[12] J. Savolovic, K. Rasmussen, *Inorg. Chem.* **1995**, *34*, 1221-1232.

[13] V. J. Burton, R. J. Deeth, C. M. Kemp, P. J. Gilbert, *J. Am. Chem. Soc.* **1995**, *117*, 8407-8415.

[14] B. P. Hay, *Coord. Chem. Rev.* **1993**, *126*, 177-236.

[15] P. V. Bernardt, P. Comba, *Inorg. Chem.* **1992**, *31*, 2638-2644.

[16] F. Wiesemann, S. Teipel, B. Krebs, U. Höweler, *Inorg. Chem.* **1994**, *33*, 1891-1898.

[17] P. Comba, T. W. Hambly. In *Molecular Modeling of Inorganic Compounds*; VCH: Weinheim, 1995, pp 124.

[18] J. Sabolovic, K. R. Liedl, *Inorg. Chem.* **1999**, *38*, 2764-2774, and references cited.

[19] A. D. Becke, *Phys. Rev. A* **1988**, *38*, 3098-3100.

[20] S. H. Vosko, L. Wilk, M. Nusair, *Can. J. Phys.* **1980**, *58*, 1200-1211.

[21] B. Delley, *J. Chem. Phys.* **1990**, *92*, 508-517.

[22] Z. Chilmonczyk, H. Ksycinska, J. Cybulski, M. Rydzewski, A. Les, *Chirality* **1998**, *10*, 821-830.

[23] T. J. M. De Bruin, A. T. M. Marcelis, H. Zuilhof, E. J. R. Sudhölter, *Phys. Chem. Chem. Phys.* **1999**, *1*, 4157-4163 (Chapter 4).

[24] A. E. Reed, R. B. Weinstock, F. A. Weinhold, *J. Chem. Phys.* **1985**, *83*, 735-746.

[25] A. E. Reed, L. A. Curtiss, F. Weinhold, *Chem. Rev.* **1988**, *88*, 899-926.

[26] S. M. Bachrach. Population Analysis and Electron Densities from Quantum Mechanics. In *Reviews in Computational Chemistry*; VCH: New York, 1995; Vol. 5; pp 171-227.

[27] D. Pearlman, S.-H. Kim, *J. Mol. Biol.* **1990**, *211*, 171-187.

[28] P. Coppens, *Annu. Rev. Phys. Chem.* **1992**, *43*, 663-692.

[29] A. K. Rappé, W. A. Goddard III, *J. Phys. Chem.* **1991**, *95*, 3358-3363.

[30] E. Sigfridsson, U. Ryde, *J. Comp. Chem.* **1998**, *19*, 377-395.

[31] F. Hæffner, T. Brinck, M. Haeberlein, C. Moberg, *J. Mol. Struct. (Theochem)* **1997**, *397*, 39-50.

[32] K. B. Wiberg, P. R. Rablen, *J. Comp. Chem.* **1993**, *14*, 1504-1518.

[33] C. M. Breneman, K. B. Wiberg, *J. Comp. Chem.* **1990**, *11*, 361-373.

[34] B. H. Besler, K. M. Merz, P. A. Kollman, *J. Comp. Chem.* **1990**, *11*, 431-439.

[35] U. C. Singh, P. A. Kollman, *J. Comp. Chem.* **1984**, *5*, 129-145.

[36] C. I. Bayly, P. Cieplak, W. D. Cornell, P. A. Kollman, *J. Phys. Chem.* **1993**, *97*, 10269-10280.

[37] Gaussian 94, Revision D.4, M. J. Frisch, G. W. Trucks, H. B. Schlegel, P. M. W. Gill, B. G. Johnson, M. A. Robb, J. R. Cheeseman, T. Keith, G. A. Petersson, J. A. Montgomery, K. Raghavachari, M. A. Al-Laham, V. G. Zakrzewski, J. V. F. Ortiz, J. B., J. Cioslowski, B. B. Stefanov, A. Nanayakkara, M. Challacombe, C. Y. Peng, P. Y. Ayala, W. Chen, M. W. Wong, J. L. Andres, E. S. Replogle, R. Gomperts, R. L. Martin, D. J. Fox, J. S. Binkley, D. J. Defrees, J. Baker, J. P. Stewart, M. Head-Gordon, C. Gonzalez, J. A. Pople, Gaussian, Inc., Pittsburgh PA, 1995.

[38] A. D. Becke, *J. Chem. Phys.* **1993**, *98*, 5648-5652.

[39] C. Lee, W. Yang, R. G. Parr, *Phys. Rev. B* **1988**, *37*, 785-789.

[40] P. J. Stephens, F. J. Devlin, C. F. Chabalowski, M. J. Frisch, *J. Phys. Chem.* **1994**, *98*, 11623-11627.

[41] A. Bérces, T. Nukada, P. Margl, T. Ziegler, *J. Phys. Chem. A* **1999**, *103*, 9693-9701.

[42] J. B. Foresman, T. A. Keith, K. B. Wiberg, J. Snoonian, M. J. Frisch, *J. Phys. Chem.* **1996**, *100*, 16098-16104.

[43] NBO, 4.0, E. D. Glendening, J. K. Badenhoop, A. E. Reed, J. E. Carpenter, F. Weinhold, Theoretical Chemistry Institute, University of Wisconsin, Madison, WI, 1996.

[44] Downloaded from the URL: http://www.amber.ucsf.edu/amber/

[45] Note that the structure with two axial water molecules does not represent a minimum on the potential energy surface: optimization of this geometry yields two equatorial hydrogen bond-forming water molecules, which clearly points to their favorable position, see also Chapter 4.

[46] H. C. Freeman, M. R. Snow, I. Nitta, K. Tomita, *Acta Crystallogr.* **1964**, *17*, 1463-1470.

[47] F. Jensen. In *Introduction to Computational Chemistry*; John Wiley & Sons: Chichester, 1994, pp 172-173.

[48] B. W. Delf, R. D. Gillard, P. O'Brien, *J. Chem. Soc., Dalton Trans.* **1979**, 1301-1305.

[49] J. Gao. Methods and Applications of Combined Quantum Mechanical and Molecular Mechanical Potentials. In *Reviews in Computational Chemistry*; VCH: New York, 1996; Vol. 7; pp 119-185.

[50] J. Åqvist, A. Warshel, *Chem. Rev.* **1993**, *93*, 2523-2544.

[51] S. Antonczak, G. Monard, M. F. Ruiz-López, J.-L. Rivail, *J. Am. Chem. Soc.* **1998**, *120*, 8825-8833.

[52] A. D. MacKerell Jr., D. Bashford, M. Bellott, R. L. Dunbrack Jr., J. D. Evanseck, M. J. Field, S. Fischer, J. Gao, H. Guo, S. Ha, D. Joseph-McCarthy, L. Kuchnir, K. Kuczera, F. T. K. Lau, C. Mattos, S. Michnick, T. Ngo, D. T. Nguyen, B. Prodhom, W. E. Reiher III, B. Roux, M. Schlenkrich, J. C. Smith, R. Stote, J. Straub, M. Watanabe, J. Wiórkiewicz-Kuczera, D. Yin, M. Karplus, *J. Phys. Chem. B* **1998**, *102*, 3586-3616.

[53] W. D. Cornell, P. Cieplak, C. I. Bayly, I. R. Gould, K. M. Merz Jr, D. M. Ferguson, D. C. Spellmeyer, T. Fox, J. W. Caldwell, P. A. Kollman, *J. Am. Chem. Soc.* **1995**, *117*, 5179-5197.

[54] S. J. Weiner, P. A. Kollman, D. A. Case, U. C. Singh, C. Ghio, G. Alagona, S. Profeta Jr., P. Weiner, *J. Am. Chem. Soc.* **1984**, *106*, 765-784.

[55] J. R. Maple, M. J. Hwang, K. J. Jalkanen, T. P. Stockfisch, A. T. Hagler, *J. Comp. Chem.* **1998**, *19*, 430-458.

[56] F. Mohamadi, N. G. J. Richards, W. C. Guida, R. Liskamp, M. Lipton, C. Caufield, G. Chang, T. Hendrickson, W. C. Still, *J. Comp. Chem.* **1990**, *11*, 440-467.

[57] S. L. Mayo, B. D. Olafson, W. A. Goddard III, *J. Phys. Chem.* **1990**, *94*, 8897-8909.

[58] M. C. Holthausen, M. Mohr, W. Koch, *Chem. Phys. Lett.* **1995**, *240*, 245-252.

[59] U. Ryde, M. H. M. Olsson, K. Pierloot, B. O. Roos, *J. Mol. Biol.* **1996**, *261*, 586-596.

[60] J. L. C. Thomas, C. W. Bauschlicher Jr., M. B. Hall, *J. Phys. Chem. A* **1997**, *101*, 8530-8539.

Chapter

General Discussion, Conclusions and Perspectives

6.1. Introduction

A system has been developed to produce enantio-pure amino acids by means of ultrafiltration of micelles. In this study, a microheterogeneous medium has been used that consists of non-ionic surfactants and an enantioselective selector. The studied chiral selectors are amino acid derivatives that can form ternary chelate complexes with a Cu^{II} ion and a D- or L-amino acid (racemic mixture). The enantioselectivity of the chiral selector molecules is related to the difference in stability of the two possible diastereomeric complexes. During filtration the unbound enantiomers pass the membrane, whereas the membrane is unpenetrable for the micelles, including chiral selectors and bound enantiomers. Two aspects of this system need to be distinguished: the affinity of the selector to bind an enantiomer (K), and the chiral recognition or enantioselectivity of the selector for the enantiomers (α). From a study of the affinity of the selector for phenylalanine it was concluded that the binding can be described with Langmuir isotherms, from which follows that the operational enantioselectivity (α_{op}) is equal to the intrinsic enantioselectivity ($= K_D/K_L$).[1]

High operational enantioselectivities have been measured with several racemic amino acids, up to 14.5 for phenylglycine. Hence, it can be concluded that the principle of chiral separation using MEUF works. In addition it has been shown that the enantioselectivities are dependent on the nature of the amino acids used, chiral selectors, and microheterogeneous media used. Several methods have been applied to help understand the molecular interactions between the selector and the enantiomers in order to optimize the separation process: (i) MEUF, (ii) isothermal titration calorimetry and (iii) quantum mechanical techniques.

6.2. Micelle-Enhanced Ultrafiltration system

i) Substrate. High enantioselectivities have been obtained for several amino acids in a microheterogeneous medium, consisting of the non-ionic surfactant NNP-10 and cholesteryl-L-glutamate as selector. However, experiments with different racemic amino acids have shown that the measured enantioselectivity is highly dependent on the hydrophobicity of the amino acid. Only within a certain window of hydrophobicity the racemic amino acids can be separated. Outside this range there is an unfavorable partitioning of the substrate over micelle and aqueous bulk, *i.e.*, the more hydrophobic amino acids dissolve non-selectively in the micelle, whereas the more hydrophilic amino acids prefer the aqueous bulk. Therefore, a modification of the amino acid can be required, if the hydrophobicity is outside the indicated range. In the strongly related separation technique chiral ligand exchange chromatography

(CLEC), such an unfavorable partitioning seems to be a smaller dilemma, since a change of the polarity of the mobile phase can at least partly circumvent this problem. Such a change in polarity is difficult to realize in the MEUF system if micelles are used as microheterogeneous medium. However, if the micelles are exchanged for polymers or dendrimers, to which the chiral selector can be attached, the polarity of the solvent can (partly) be adjusted to prevent unfavorable partitioning. Although the MEUF system may have some drawbacks as compared to CLEC, the scale-up of CLEC seems to be less straightforward than the scale-up of the MEUF system. On the other hand, the more preparative-orientated MEUF system should not be viewed as a competitor or a substitute of the more analytically-orientated CLEC, but as an augmentation within the separation techniques. For example, CLEC can be used to roughly scan some racemates and to test if a racemate might get be separated by MEUF, since HPLC runs are considerably less time-consuming. Many of the amino acid-derived selectors that are used to separate amino acids in CLEC, can also distinguish between the two enantiomers of other racemic mixtures like α-hydroxy acids. It is recommended that attempts will be undertaken to separate such compounds by MEUF (with cholesteryl L-glutamate) as well, thereby considerably expanding the applicability of MEUF.

ii) Selector. From the MEUF experiments with the cholesteryl glutamate selectors it was concluded that the chiral recognition cannot solely be ascribed to the glutamate head group, since inversion of the chirality of the glutamic acid part does not yield to the reciprocal operational enantioselectivity. Furthermore, the operational enantioselectivity of 1.6 measured for phenylalanine with cholesteryl DL-glutamate also points to an influence of the cholesteryl group on the measured enantioselectivity. The isothermal titration experiments also suggest that there might be an influence of the cholesteryl anchor. Hence, there are indications that the chirality of the cholesteryl group enhances the enantioselectivity. From this point of view, cholesteryl L-glutamate is a very attractive selector. However, the selectors like cholesteryl L-glutamate, cholesteryl DL-glutamate and cholesteryl D-glutamate, have also some negative properties. The solubility in the investigated microhetereogeneous media is rather low (up to ~3 mM), and the procedure to dissolve the selector is precarious and time-consuming. Consequently, either a change of the microhetereogeneous medium is necessary (*vide infra*), or the solubility of selector should be improved when the system is scaled up. For example, exchanging the cholesteryl anchor with an anchor that has smaller packing forces in the solid phase will increase the solubility. However, an anchor that has a rigid structure will have a positive influence on the enantioselectivity, and if the anchor itself also contains one or more chiral centers, this could even further enhance the

enantioselectivity. Steroids with a curved structure meet these conditions. In this case one can think of steroids in which rings A and B are *cis* fused, giving the molecule a more bent structure, as in lithocholic acid.

The MEUF set-up has the flexibility to change the selector and/or microheterogeneous medium in an easy fashion, and thus any selector used in HPLC or CLEC to separate enantiomers can in principle be used in the MEUF system.

iii) Microheterogeneous medium. The influence of the micelles on the enantioselectivity has been studied as well. In addition to NNP-10 used in our studies, two sets of commercially available surfactants, Tween® and Brij®, have been tested by Overdevest *et al.* (Scheme 6.1).[2] Increasing operational enantioselectivities were measured for phenylalanine and cholesteryl L-glutamate as selector at pH 11 with decreasing alkyl lengths of these micelle-forming surfactants. However, this trend was not observed in a series of 1,2-*O*-dioctadecyl-*rac*-glycerol ether surfactants containing a polydisperse non-ionic monomethyl polyoxyethylene glycol $(MPEG)_n$ head group.[3] Operational enantioselectivities for phenylalanine and cholesteryl L-glutamate as selector at pH 11 were measured of α_{op} = 3.4 ±0.6, 6.4 ±1.3 and 1.9 ±0.3, in which the number of oxyethylene units of the surfactant was varied from n = 14, 16 and 21, respectively.[4]

Scheme 6.1

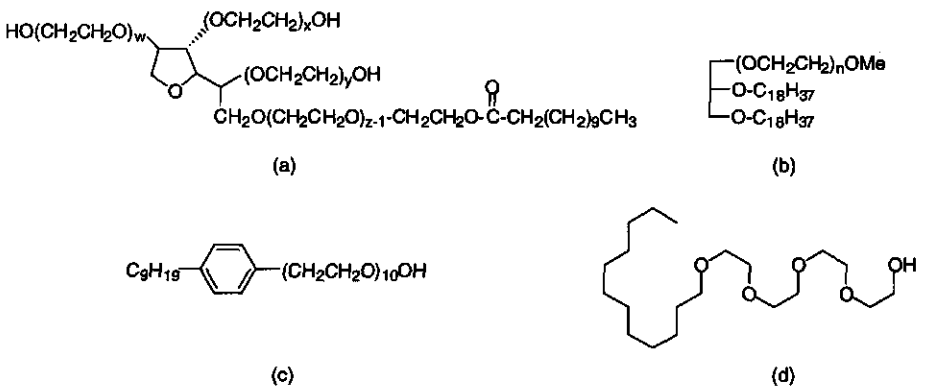

(a) Tween 20 (w + x + y + z = 20); (b) 1,2 dioctadecyl-*rac*-glycerol ether; (c) NNP-10; (d) Brij 30.

The difference in observed trends in measured enantioselectivities between the two types of surfactants may lie in the different nature of these surfactants. The 1,2-di-octadecyl-*rac*-glycerol ether surfactants have two hydrophobic alkyl chains, and can form vesicles, whereas the Tween® and Brij® surfactants have only a single hydrophobic tail. It is therefore not

unlikely that the two types of surfactant form different types of aggregates. The variation in measured enantioselectivities indicate that both the size of the surfactant and the nature of the surfactant seem to influence the formation of the diastereomeric complex. However, up to now it is unclear how the structure of microhetereogeneous medium influences the enantioselectivity and further research is needed.

Although in this investigation mainly the non-ionic surfactant NNP-10 has been used, this surfactant is not recommended if the MEUF system is scaled up to pilot plant scale. Firstly, the solubilities of the cholesteryl glutamate selectors in this medium is rather low (*vide supra*), and secondly, the loss of surfactant in each filtration step would be too large due the critical micelle concentration (~0.005 mM). A cheap microheterogeneous medium that has no or a low critical micelle concentration, like polymerized micelles or polymers, and is biodegradable, is more preferred.

6.3 Isothermal Titration Calorimetry

The ITC experiments have shown a striking resemblance with the MEUF experiments. In both types of experiments an enantioselectivity (K_D/K_L) larger than 1.0 is measured for the same amino acids. Additionally, the enantioselectivities measured with ITC qualitatively closely follow, those obtained with MEUF, *i.e.*, for the α's obtained with ITC the order is PheGly > Phe > Leu > Val ≥ Ala ≥ Ser and the order obtained with MEUF is PheGly > Phe > Leu > Val ≈ Ala ≈ Ser. The origin of the enantioselectivity measured with ITC for the different amino acids, is probably found in the size of R-group of the amino acid, since an increase in α is found with increasing alkyl chain of the R-group, and also enantioselectivities significantly larger than 1.0 are measured for phenylalanine and phenylglycine. This is in line with the MEUF experiments, although isoleucine, which has almost the same size of R-group as leucine, shows a significantly smaller enantioselectivity than leucine in MEUF. Isoleucine has not been measured with ITC, but research on the influence of isomerism, like β-branching, in the R-group of the amino acid on the enantioselectivity with ITC would be interesting.

The enantioselectivities measured with MEUF are significantly larger than with ITC for the different amino acid substrates. Both the absence of reciprocal enantioselectivities upon inversion of the chirality of the glutamate headgroup, and the significantly larger than 1.0 enantioselectivity for cholesteryl DL-glutamate strongly suggest an influence of the cholesteryl anchor on the enantioselectivity in the MEUF experiments. However, this

influence is less obvious from ITC measurements, since reciprocal enantioselectivities are found, and there are only indications for a small enantioselectivity with cholesteryl DL-glutamate. Therefore, a model has been drawn up to explain this discrepancy. This model states that recognition initially occurs at the glutamate headgroup of the selector. On a longer time scale, which cannot be measured with ITC, the influence of a supramolecular rearrangement of the chiral complex in the micellar environment becomes more pronounced, resulting in larger enantioselectivities.

With ITC experiments also information has been obtained about the thermodynamics of the formation of the diastereomeric complex. The experiments have pointed out that the diastereomeric complex formation is endothermic, and thus that the complexation is an entropically favored process. This has been interpreted as a release of water molecules from the cholesteryl L-glutamate:Cu^{II} complex upon binding of the substrate. Upon going from the hydrophilic aqueous bulk into the relatively hydrophobic micelle the titrated amino acid will probably lose some of its coordinated water molecules. Since this is an energy consuming process, this can explain the measured endothermic effect and the increase of the entropy of this complexation reaction.

In conclusion, ITC has proven to be an accurate method to measure enantioselectivities. Furthermore, it can provide essential information on the thermodynamics of the formation of the diastereomeric complexes. This method can be used to scan relatively fast whether a racemic substrate can be separated in MEUF. However, MEUF experiments are still needed for the exact operational enantioselectivities and to optimize the process parameters of the MEUF system.

6.4 Quantum mechanical methods

The measured variation in the enantioselectivities ($1 < \alpha_{op} \leq 14.5$) for the different amino acids points to an influence of the substituents of the amino acids on the stability of the coordination compound due to different amino acid-amino acid interactions. This suggests that the geometry around Cu^{II} ion in such complexes is influenced by the type and size of the substrate. Due to fundamental limitations, the computationally fast and therefore attractive molecular mechanics technique could not be applied to investigate the bis(amino acid)Cu^{II} diastereomeric complexes. Instead, computationally intensive, quantum mechanical methods were needed, and such an approach consequently required that the diastereomeric bis(amino acid)Cu^{II} complex had to be simplified. The geometric and electronic structures of

bis(glycinato)Cu^{II}·n H_2O (n = 0 – 4) complexes were investigated by the relatively fast, but accurate B3LYP density functional. Already this smallest bis(amino acid)Cu^{II} complex displayed a variety of geometries, and showed that an accurate description thereof demanded the use of a large all-electron basis sets, like 6-311+G(d,p). Three conclusions stand out here: (i) hydrogen bond formation strongly influences the final geometry; (ii) the *trans* complex is more stable than the corresponding *cis* complex; (iii) no uniform set of electrostatic-derived atomic charges can be derived for both the *cis* and *trans* complexes with varying number of coordinating water molecules. Such a uniform set is essential for performing accurate molecular mechanics, especially for ionic compounds that have strong ionic-ionic non-bonded interactions. Hence, to describe large bis(amino acid)Cu^{II} complexes, a combination of quantum mechanical and molecular mechanics (QM/MM) calculations seems to be the only way out. In such computations the metal ion and the atoms present in first and second coordination sphere of Cu^{II} are described quantum mechanically, whereas other parts are described by molecular mechanics. Such an approach will, in general be preferable to describe systems containing transition metal ions that show significant variations in ESP charges within the set of experimentally observed variations in geometry. It is expected that this method can be used to ultimately compute and predict enantioselectivity.

6.5 Process Engineering Aspects

Up till now, the enantioselectivity and a number of factors that influence the chiral recognition have been approached from a molecular level point of view. However, for a successful application of MEUF in large-scale enantiomer separation, knowledge of the factors that affect the process engineering is of great importance as well. Overdevest has extensively investigated some of these aspects, and the conclusions are concisely reported.[5] It was found that the binding of phenylalanine to cholesteryl L-glutamate could be described with Langmuir isotherms. Calculations, using these Langmuir isotherms, have shown that a high enantioselectivity alone is not sufficient to acquire both enantiomers in optically pure form.[1] A deficiency of selector molecules leads to enantio-enriched micelles due to the competitive nature of the complexation, but the enantiomeric excess in the aqueous bulk phase is relatively small. Consequently, to reach 99$^+$% separation of a racemic mixture, a multi-stage separation process is required. However, for multi-stage separation regeneration of the saturated micelles is required, *i.e.*, decomplexation of the bound enantiomers. Ultrafiltration experiments have shown that decomplexation can be accomplished by a

decrease in pH; dilution or increased temperatures hardly have any effect. Therefore, the complexation has been studied from pH 11 to 6, and it has been found that the enantioselectivity increases upon decreasing pH, but there is concomitant decrease in affinity which ends in no complexation at pH 6. Nevertheless, the difference in pH between complexation and decomplexation should be minimized, in order to avoid unwanted large salt production in multiple separation cycles.

This multi-step separation system is operated in a counter-current mode, analogous to conventional extraction and distillation processes. Here, the enantioselective micellar phase flows in opposite direction of the water phase, and in each stage an ultrafiltration membrane separates the micellar phase from the micelle-free aqueous phase (Figure 6.1).

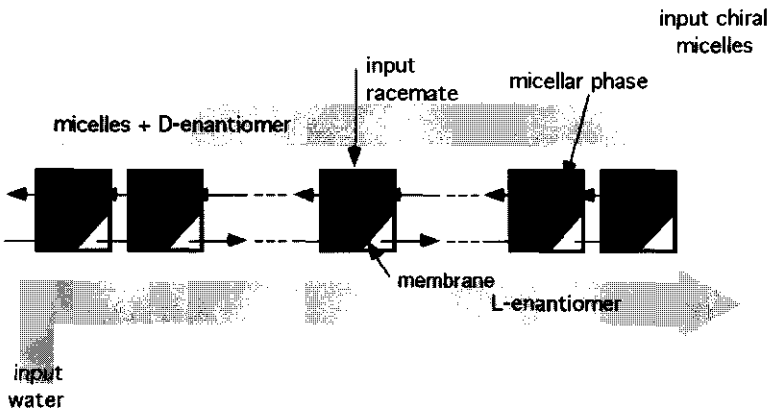

Figure 6.1. Counter-current process to reach 99⁺% separation of the racemic mixture.

The cascaded UF system under development consists of n stages. Straightforward multi-component Langmuir isotherms can be used to predict the bound and unbound D,L-Phe concentrations in each UF stage at equilibrium.[1] The (de)complexation kinetics was measured to appoint the minimal residence time in each stage. The (de)complexation kinetics was described by a Linear Driving Force (LDF) model, and it was found that the complexation rate constants ($k_{D,L}$) are in the order of $3 \cdot 10^{-4}$ s^{-1} and the decomplexation rate constants ($k'_{D,L}$) are in the order of 10^{-6} s^{-1}. Fortunately, decomplexation of the L-Phe is induced by simultaneous complexation of the D-Phe. This exchange phenomenon has been modeled by a second order LDF term based on both the bound L-concentration and the unbound D-concentration. In addition to the isotherms and the LDF model the separation model is completed by mass balances over each stage. With this separation model the performance of a cascaded separation system could be calculated, given the enantioselectivity

and affinity of the enantioselective micelles for the two enantiomers. This model was successfully validated by experiments using a cascaded system of 5 stages operated in a counter-current mode. To enhance the feasibility of a separation system at preparative scale, model calculations using the validated model have indicated that (i) improvement of the quality of the chiral selector to discriminate between enantiomers (from α = 1.1 to 10), drastically reduces the number of stages to reach 99+% separation. However, this influence sharply diminishes upon further improvement of the chiral selector ($\alpha > 10$); (ii) the selector concentration should be in the same order of magnitude as the enantiomer feed concentration; (iii) the affinity (K) of the chiral selector to bind an enantiomer times the feed concentration of the racemic mixture should be approximately three ($K \cdot C_{feed} = 3$).

In conclusion it can be said that ultrafiltration of microheterogeneous media containing chiral selectors for the separation of enantiomers in cascaded systems utilizes the advantages of chromatographic and distillation processes. That is, preferential binding under mild conditions and counter-current flow of both the micellar phase and the bulk phase through the apparatus. These benefits, in combination with the high enantioselectivities that substantially reduce the number of stages in a multiple stage process, provide this separation technique a solid basis for further development for the large-scale resolution of enantiomers.

References

[1] P. E. M. Overdevest, J. T. F. Keurentjes, A. Van der Padt, K. Van 't Riet, *Colloids Surf., A* **2000**, *163*, 209 - 224.

[2] P. E. M. Overdevest, A. Van der Padt, *Chemtech* **1999**, *29(12)*, December, 17-27.

[3] M. J. Lawrence, S. M. Lawerence, S. Chauhan, D. J. Barlow, *Chem. Phys. Lipids* **1996**, *82*, 89-100.

[4] T. J. M. de Bruin, A. Koudijs, A. T. M. Marcelis, H. Zuilhof, E. J. R. Sudhölter, Unpublished results.

[5] P. E. M. Overdevest, *Ph.D. Thesis*, Wageningen University, Wageningen, 2000.

Summary

The need for enantio-pure compounds is growing as can for example be seen from the increasing annual sales in the pharmaceutical industry. In Chapter 1 several methods are mentioned that can be used in order to obtain enantio-pure compounds. In this research project a separation system has been investigated that can potentially be used for large-scale enantioseparations. This system, based on micelle-enhanced ultrafiltration (MEUF), combines high permeate flows with the possibility to separate low molecular weight components depending on their affinity for the micelle. The pore size of the ultrafiltration membrane is small enough to retain the micelles, but sufficiently large to pass all other unbound aqueous solutes.

The chirality is introduced by chiral selectors, which are dissolved in micelles that are formed by non-ionic surfactants. The studied chiral selectors are hydrophobic amino acid derivatives, which form chiral-metal complexes with Cu^{II} ions, and this complex is used for the selective binding of one of the enantiomers of a dilute racemic amino acid solution. The enantioselectivity is related to the energy difference between the two possible ternary diastereomeric complexes. Separation of the enantiomers can be accomplished since the unbound enantiomers pass the membrane after filtration, whereas the micelles, including chiral selectors and bound enantiomers, are retained. The effectiveness of the separation system is quantified by the operational enantioselectivity, which is equal to the quotient of the equilibrium constants for the formation of the diastereomeric complexes (K_D/K_L), and this is equal to the distribution of the D-enantiomer over micellar phase and aqueous bulk divided by the distribution of L-enantiomer over micellar phase and aqueous bulk.

For the racemic α-amino acids phenylalanine, phenylglycine, *O*-methyltyrosine, isoleucine and leucine good separations were obtained using cholesteryl L-glutamate and Cu^{II} ions as chiral selector, with an operational enantioselectivity (α_{op}) of up to 14.5 for phenylglycine. From a wide set of substrates, including four β-amino acids, it was concluded that the performance of this system is determined by two factors: the hydrophobicity of the racemic amino acid, which results in a partitioning of the racemic amino acid over micelle and aqueous solution, and the stability of the diastereomeric complex formed upon binding of the amino acid with the chiral selector.

The chiral hydrophobic cholesteryl anchor of the chiral selector also plays an active role in the recognition process, since inversion of the chirality of the glutamate does not yield the

reciprocal enantioselectivities. However, if the cholesteryl group is replaced by a non-chiral alkyl chain, reciprocal operational enantioselectivities are found with enantiomeric glutamate selectors (Chapter 2).

In Chapter 3 the use of isothermal titration calorimetry for determining enantioselectivity is described. To a system containing non-ionic micelles, Cu^{II} ions and cholesteryl glutamate as chiral selector, either the D- or L-amino acid was titrated. These experiments, which are faster to perform than the corresponding ultrafiltration experiments, give a good qualitative resemblance with the MEUF experiments, and moreover provide detailed information about the thermodynamics of the complexation reactions. The binding of the amino acid to the chiral-metal complex is an entropically driven process, which is interpreted as the release of coordinating water molecules upon complexation of the titrated amino acid. The highest enantioselectivities (K_D/K_L) were measured for the amino acids with relatively bulky R-groups: phenylalanine (1.24) and phenylglycine (1.26), while an increase in enantioselectivity to 1.21 was measured upon increasing the size of the R-group in the amino acids alanine to leucine. For serine no enantioselectivity was measured. Comparison of the ITC and MEUF results show two important differences: (i) the enantioselectivities measured with MEUF are significantly larger, (ii) reciprocal enantioselectivities are measured with ITC for phenylalanine upon inversion of the chirality of the glutamate headgroup of the chiral selector, whereas this is not observed with MEUF experiments. This indicates that the time scale, which is the main difference in the experimental set-up, influences the overall measured enantioselectivity. Probably, the recognition process initially takes place at the glutamate headgroup, whereas on a longer time scale, which is outside measuring range of ITC, the influence of the cholesteryl anchor becomes more pronounced resulting in larger enantioselectivities.

The variation in enantioselectivity for different types of amino acids measured both with MEUF and ITC point to differences in the geometry of the diastereomeric complexes of the different amino acids. Therefore, a theoretical study has been performed to obtain information about the geometry and electronic structure of the diastereomeric complexes (Chapter 4). The computationally fast molecular mechanics approach could not be applied due to parameterization problems for the description of electronic effects such as Jahn Teller distortions and other 'non-bonded' interactions (*vide infra*). Therefore, the more computationally demanding quantum mechanical density functional theory was used. However, this also requires a simplified description of the diastereomeric complex to the non-chiral bis(glycinato)Cu^{II} model complex. First a basis set study was performed in order to

obtain reliable results with the B3LYP functional for the $Cu^{II}(gly)_2(H_2O)_2$ complexes. The geometry and the electronic structure as studied by Natural Population Analysis (NPA) were probed with various basis sets. It turned out that geometry optimizations should at least be performed with the all-electron basis set 6-311+G(d,p) or with C, H, N, O = 6-311+G(d,p) and an effective core potential (LanL2DZ) for Cu^{II}. Further increase in size of the basis set hardly affected the geometry or electronic structure, whereas spurious minima on the potential energy surfaces were found with smaller basis sets. Two real minima were found: a *trans* configurated complex of C_i symmetry, and a *cis* configurated complex with C_1 symmetry. *In vacuo* the *trans* structure is more stable by 18 kcal·mol^{-1}, which reduces to 10 kcal·mol^{-1} in a dielectric medium representing water as modeled by a polarizable continuum model.

Since the C, H, N, O = 6-311+G(d,p) and Cu = LanL2DZ basis set offered the best balance in accuracy and computation time, this set was used to explore the geometries and the electronic structures of $Cu^{II}(gly)_2(H_2O)_n$ (n = 0 – 4) complexes (Chapter 5). It was found that the optimized geometries strongly depend on the number of hydrogen bonds formed between the coordinating water molecules and the amino and carboxylate functionalities, as formation of such hydrogen bonds competes with axial $Cu^{II}\cdots OH_2$ interactions. The *trans* isomer is computed to be more stable than the corresponding *cis* isomer, independent of the number of coordinating water molecules. This suggests that probably also in chiral separation system the *trans* configuration will be the dominant isomer.

The electronic structure as obtained from NPA charges on Cu^{II} and directly coordinated O and N atoms is nearly independent of the *cis/trans* isomerism and variation in the number of coordinating water molecules. This is in sharp contrast to the electrostatic potential-derived (ESP) charges obtained by the often-used ESP methods: CHELPG, Merz-Singh-Kollman, and the Restrained ElectroStatic Potential model. No uniform set of ESP charges could thus be derived for this set of complexes, as would be required for the parameterization to accurately describe the Coulomb interactions in molecular mechanics programs. Therefore, it is recommended to describe bis(amino acid)Cu^{II} complexes that are too large for a complete quantum chemical approach with QM/MM methods. In such calculations the coordination sphere around the Cu^{II} ion is described by quantum mechanics and the other parts by molecular mechanics.

The research described in this thesis shows promising results for the enantioseparation of amino acids using micelle-enhanced ultrafiltration, and these provide a solid basis to investigate the application of this technique on a large-scale. Also the results from techniques

like ITC and quantum mechanical calculations to investigate the (chiral) copper(II) amino acid complexes encourage further research.

Samenvatting

De behoefte aan optisch zuivere verbindingen neemt sterk toe, zoals bijvoorbeeld te zien is aan de jaarlijks groeiende omzet van deze verbindingen in de farmaceutische industrie. In Hoofdstuk 1 worden diverse methoden genoemd die gebruikt kunnen worden om optisch zuivere verbindingen te produceren. In dit onderzoek is een scheidingsmethode onderzocht, die gebaseerd is op micellaire ultrafiltratie en in potentie op grote schaal kan worden toegepast. De poriegrootte van het membraan is klein genoeg om aggregaten als micellen tegen te houden, maar groot genoeg om verbindingen of aggregaten met een molecuulgewicht kleiner dan 5000 Dalton te laten passeren. Op grond van de affiniteit voor de micellen kunnen verbindingen met een klein molecuulgewicht door het membraan worden tegengehouden.

Door chirale selectoren in de micellen op te lossen, welke door niet-ionische zeepmoleculen zijn gevormd, wordt chiraliteit in het systeem geïntroduceerd. De bestudeerde chirale selectoren zijn aminozuurderivaten met een hydrofoob anker, die complexen kunnen vormen met koper(II)-ionen. Deze chirale kopercomplexen worden op hun beurt gebruikt voor de preferente binding van één van de twee enantiomeren van een racemisch mengsel. De enantioselectiviteit wordt door het verschil in energie tussen de twee mogelijke diastereomere complexen bepaald. Scheiding van de enantiomeren wordt uiteindelijk bewerkstelligd doordat na filtratie de ongebonden enantiomeren in het filtraat terecht komen, terwijl de enantiomeren die wel affiniteit hebben voor de micellen achterblijven. De effectiviteit van het systeem wordt door de operationele enantioselectiviteit gekwantificeerd en is gedefinieerd als het quotiënt van de verdeling van de D-enantiomeer over de micellaire fase en waterfase, en de verdeling van de L-enantiomeer over micellaire fase en waterfase. Dit is weer gelijk aan het quotiënt van de evenwichtsconstanten (K_D/K_L) voor de vorming van diastereomere complexen.

De selector cholesteryl L-glutamaat vertoonde, in combinatie met Cu^{II}-ionen, goede operationele enantioselectiviteiten voor de racemische α-aminozuren fenylalanine, *O*-methyltyrosine, isoleucine, leucine en voor fenylglycine. Voor de laatste verbinding werd zelfs een operationele enantioselectiviteit van 14.5 gemeten. Uit een aanzienlijke serie van geteste substraten, welke ook vier β-aminozuren bevatte, werd geconcludeerd dat de mate van scheiding door twee factoren wordt bepaald: (i) de hydrofobiciteit van het racemische aminozuur dat tot een zekere niet-selectieve verdeling van het aminozuur over micel en

waterfase leidt, en (ii) de stabiliteit van het gevormde diastereomere complex gevormd tussen chirale selector en racemisch aminozuur.

Ook het chirale hydrofobe cholesterylanker van de chirale selector blijkt een belangrijke rol in het chirale herkenningsproces te spelen. Inversie van de chiraliteit van de glutamaat-kopgroep leidt namelijk niet tot de verwachte reciproque enantioselectiviteit. Wanneer de cholesteryl-groep echter door een achirale alkylketen wordt vervangen, worden wel reciproque enantioselectiviteiten waargenomen (Hoofdstuk 2).

In Hoofdstuk 3 zijn enantioselectiviteitsexperimenten met behulp van isotherme titratie-calorimetrie (ITC) beschreven. Dit is mogelijk door aan een systeem met niet-ionische micellen waarin de chirale selector cholesteryl glutamaat is opgelost en waarin ook Cu^{II}-ionen aanwezig zijn, de D- dan wel de L-enantiomeer van een aminozuur te titreren. Uit de ITC experimenten volgt dat de binding van het getitreerde aminozuur aan het chirale kopercomplex een door entropie gedreven proces is. Dit kan geïnterpreteerd worden als het vrijkomen van gebonden watermoleculen op het moment dat het getitreerde aminozuur aan het chirale kopercomplex bindt. De grootste enantioselectiviteiten (K_D/K_L) werden voor de aminozuren gemeten met een relatief grote R-groep: fenylalanine (1.24) en fenylglycine (1.26), terwijl een toename in enantioselectiviteit tot 1.21 werd gemeten naarmate de alkylgroep van het aminozuur groter werd, zoals in de serie van alanine – valine – leucine. Voor serine werd geen selectiviteit gemeten. De ITC-experimenten tonen kwalitatief goede overeenkomsten met de corresponderende ultrafiltratie-experimenten, maar er zijn ook twee belangrijke verschillen: (i) de met ultrafiltratie gemeten enantioselectiviteiten zijn significant groter; (ii) als de chiraliteit van de glutamaat-kopgroep wordt geïnverteerd wordt met ITC een reciproque enantioselectiviteit voor fenylalanine gemeten, terwijl dat bij de ultrafiltratie experimenten niet het geval is. Dit kan erop duiden dat de tijdschaal een belangrijke rol speelt. Dat is namelijk één van de voornaamste verschillen tussen beide experimenten. Vermoedelijk vindt de chirale herkenning in eerste instantie plaats aan de glutamaat-kopgroep; op langere tijdschaal, wat buiten het meetbereik van ITC valt, speelt het cholesterylanker een actieve rol in het herkenningsproces dat leidt tot een toename in de gemeten enantioselectiviteit.

De variatie in enantioselectiviteit gemeten met ultrafiltratie en ITC voor de verschillende aminozuren, duidt op verschillen in de geometrie van de diastereomere complexen. Om meer inzicht te krijgen in zowel de geometrie als de elektronische structuur van de diastereomere koper(II)complexen is er een theoretische studie uitgevoerd (Hoofdstuk 4). De relatief snelle moleculaire mechanica (MM) rekenmethode kon niet gebruikt worden, omdat elektronische

effecten ten gevolge van bijvoorbeeld Jahn-Teller-verstoringen en ook andere effecten momenteel nauwelijks geparameteriseerd kunnen worden. In plaats daarvan werd de – vanuit rekenkundig oogpunt – veeleisender quantummechanische dichtheidsfunctionaal theorie (DFT) toegepast. Dit vereiste echter een vereenvoudiging van het diastereomere complex tot het achirale bis(glycinato)koper(II) complex. Eerst werd een basissetstudie gedaan om zo de juiste balans tussen rekensnelheid en precisie te vinden. Hiertoe werden diverse basissets en de B3LYP functionaal gebruikt voor de beschrijving van zowel de geometrische als de elektronische structuur van *cis*- en *trans*-$Cu^{II}(gly)_2(H_2O)_2$ complexen. De elektronische structuur werd bestudeerd aan de hand van de ladingen die volgen uit 'Natural Population Analysis' (NPA). Uit de basissetstudie volgde dat de geometrische en elektronische structuur goed beschreven wordt met de 6-311+G(d,p) basisset, of met C, H, N, O = 6-311+G(d,p) en een 'effective core potential' LanL2DZ voor Cu^{II}. Met kleinere basissets werden valse minima op het potentiële energieoppervlak gevonden. Twee echte minima werden gevonden behorende bij een complex met een *trans*-configuratie en C_i symmetrie, en één met een *cis*-configuratie en C_1 symmetrie. De *trans*-structuur is *in vacuo* 18 kcal·mol^{-1} stabieler dan de *cis*-structuur, dit verschil reduceert tot 10 kcal·mol^{-1} in een diëlektrisch medium dat representatief is voor water en gemodelleerd is met behulp van een 'polarizable continuum model'.

Daar de basisset C, H, N, O = 6-311+G(d,p) en Cu = LanL2DZ de beste verhouding tussen precisie en snelheid opleverde is deze basisset, in combinatie met de B3LYP functionaal, gebruikt om de geometrische en elektronische structuren van diverse $Cu^{II}(gly)_2(H_2O)_n$ ($n = 0 - 4$) complexen te bestuderen (Hoofdstuk 5). De geoptimaliseerde geometrieën blijken sterk afhankelijk te zijn van het aantal waterstofbruggen dat tussen de gecoördineerde watermoleculen en de amino- en carboxylaat-functionaliteiten gevormd kan worden. Deze waterstofbruggen concurreren met de axiale $Cu^{II}\cdots OH_2$-interacties. De *trans*-isomeer is stabieler dan de corresponderende *cis*-isomeer, onafhankelijk van het aantal gecoördineerde watermoleculen. Dit betekent dat vermoedelijk ook in het chirale scheidingsproces de *trans*-configuratie de dominante isomeer is.

De met NPA-ladingen bestudeerde elektronische structuur is onafhankelijk van *cis/trans*-isomerie en variatie in het aantal gecoördineerde watermoleculen voor Cu^{II} en de direct gecoördineerde O en N atomen. De 'electrostatic potential-derived' (ESP) ladingen, berekend met de veel gebruikte methoden CHELPG, Merz-Singh-Kollman, en het Restrained ElectroStatic Potential model, zijn dat duidelijk niet. Dergelijke ladingen worden gebruikt om de Coulombinteracties te berekenen in moleculaire mechanica berekeningen. Daar er dus

voor de bestudeerde bis(aminozuur)koper(II) complexen geen uniforme set van ESP-ladingen kon worden verkregen, wat de parameterisering voor MM berekeningen bemoeilijkt, worden voor dergelijke complexen QM/MM-berekeningen aanbevolen. Dit betekent dat het Cu^{II}-ion, inclusief de direct gecoördineerde atomen, quantummechanisch worden beschreven, terwijl de overige delen met moleculaire mechanica beschreven worden.

Het hier beschreven onderzoek laat veelbelovende resultaten zien voor de scheiding van aminozuren enantiomeren met behulp van micellaire ultrafiltratie en deze resultaten leveren een goede uitgangspositie voor verder onderzoek en toepassing van het systeem op een preparatieve schaal. Ook de gebruikte technieken, ITC en quantummechanische berekeningen, voor onderzoek aan (chirale) koper(II)-aminozuurcomplexen, laten bemoedigende resultaten zien, en verder onderzoek wordt dan ook zeer aanbevolen.

Curriculum Vitae

Theodorus Jozef Maria de Bruin werd op 27 april 1971 te Utrecht geboren. In 1989 werd het V.W.O. diploma aan het Niels Stensen College behaald. In datzelfde jaar werd met de studie Scheikunde aan de Universiteit Utrecht begonnen. Een jaar later werd het propedeutisch examen afgelegd. Na twee Klein Bijvakken: Fysica en Chemie van Materialen (Prof. dr. G. Blasse) en NMR Spectroscopie (Prof. dr. R. Boelens), en een onderzoeksspecialisatie in de Fysisch-Organische Chemie (Prof. dr. L. W. Jenneskens), waarin gewerkt werd aan gefunctionaliseerde oligo(cyclohexylidenen), werd in 1995 het doctoraalexamen behaald. Van juni 1995 tot juni 1999 was hij als onderzoeker in opleiding werkzaam bij het Laboratorium voor Organische Chemie aan de Universiteit Wageningen alwaar hij onder leiding van Prof. dr. E. J. R. Sudhölter het in dit proefschrift beschreven onderzoek heeft uitgevoerd. Per 1 juli 2000 zal hij als postdoctoraal medewerker aan de Université de Joseph Fourier te Grenoble werkzaam zijn.

List of Publications

T. J. M. de Bruin, A. T. M. Marcelis, H. Zuilhof, E. J. R. Sudhölter, Geometry and electronic structure of bis-(glycinato)-Cu^{II}·2 H_2O complexes as studied by density functional B3LYP computations, *Phys. Chem. Chem. Phys.* **1999**, *1*, 4157-4163.

T. J. M. de Bruin, A. T. M. Marcelis, H. Zuilhof, L. M. Rodenburg, H. A. G. Niederländer, A. Koudijs, P. E. M. Overdevest, A. van der Padt, E. J. R. Sudhölter, Separation of Amino Acid Enantiomers by Micelle-Enhanced Ultrafiltration, *Chirality* - accepted.

T. J. M. de Bruin, A. T. M. Marcelis, H. Zuilhof, E. J. R. Sudhölter, Geometry and Electronic Structure of Hydrated Bis(glycinato)Cu^{II} Complexes as Studied by Density Functional B3LYP Computations. On the problems of molecular mechanics, *J. Phys. Chem. A* - submitted.

T. J. M. de Bruin, A. T. M. Marcelis, H. Zuilhof, E. J. R. Sudhölter, Enantioselectivity Measurements of Copper(II) Amino Acid Complexes Using Isothermal Titration Calorimetry, *Langmuir* - submitted

Other publications

T. J. M. de Bruin, M. Wiegel, G. J. Dirksen, G. Blasse, Luminescence of Li_2ZrTeO_6, *J. Solid State Chem.* **1993**, *107*, 397-400.

M. Wiegel, M. H. J. Emond, T. J. M. de Bruin, G. Blasse, Non-linear optical Porperties and Luminescence of solid Solutions of $Li_{1-x}(Nb,Ta)_{1-x}W_xO_3$, *Chem. Mater.* **1994**, *6*, 973-976.

F. J. Hoogesteger, D. M. Grove, L. W. Jenneskens, T. J. M. de Bruin, B. A. J. Jansen, Oligo(cyclohexylidene) oximes and derivatives as probe molecules for long-range substituent effects on ^{13}C NMR chemical shifts, *J. Chem. Soc., Perkin Trans. 2* **1996**, 2327-2334.

F. J. Hoogesteger, J. M. Kroon, J. L. W., E. J. R. Sudhölter, T. J. M. de Bruin, J. W. Zwikker, E. ten Grotenhuis, C. H. M. Marée, N. Veldman, S. A., Langmuir-Blodgett Mono- and Multilayers of Rodlike Oligo(cyclohexylidene) Derivatives Bearing an Oxime Headgroup, *Langmuir* **1996**, *12*, 4760-4767.

D. P. Piet, H. M. Willemen, T. J. M. de Bruin, M. C. R. Franssen, J. B. P. A. Wijnberg, Æ. de Groot, Acid- and Enzyme-Catalysed Cyclisation Reactions of (*Z,E*)-1(10),4 Cyclodecadiene Derivatives as Model Systems for Melampolides, *Tetrahedron* **1997**, *53*, 11425-11436.